THESIS FOR THE DEGREE OF DOCTOR OF PHILOSOPHY

Adaptive Finite Element Methods for Div-Curl Problems

Rickard Bergström

CHALMERS | GÖTEBORG UNIVERSITY

Department of Computational Mathematics
Chalmers University of Technology and Göteborg University
Göteborg, Sweden 2002

Adaptive Finite Element Methods for Div-Curl Problems
Rickard Bergström
ISBN 91–7291–191–3

Doktorsavhandlingar vid Chalmers tekniska högskola
Ny serie nr 1873
ISSN 0346-718X

Department of Computational Mathematics
Chalmers University of Technology and Göteborg University
SE-412 96 Göteborg
Sweden
Telephone +46 (0)31 772 1000

Printed in Göteborg, Sweden 2002

Adaptive Finite Element Methods for Div-Curl Problems

Rickard Bergström

Department of Computational Mathematics
Chalmers University of Technology
Göteborg University

Abstract

In this thesis, we develop and apply finite element methods to problems of div-curl type, mainly from applications in electromagnetics. In particular, we focus on least-squares formulations for problems with singularities, edge elements in eddy current computations, and the implementation of the finite element method.

We introduce discontinuous elements in the least-squares finite element method (LSFEM) and enforce continuity and boundary conditions weakly. For this scheme, we prove stability and optimal a priori error estimates for the div-grad and the div-curl problems posed on nonconvex domains. Numerical studies in three dimensions, confirming the theoretical results, are presented. Moreover, combining LSFEM and a Galerkin formulation, a scheme for wave propagation problems with beneficial dispersion properties is proposed.

To efficiently solve eddy current problems, we use tetrahedral and hexahedral edge elements in an ungauged potential formulation combined with adaptive mesh refinement. We also introduce anisotropic mesh refinement to compute the power loss for a hydrogenerator with laminated materials.

A software environment for implementation of finite element methods is developed. It is based on object-oriented programming techniques and combines generality with sufficient efficiency.

Keywords: least-squares finite element method, div-curl problem, adaptivity, computational electromagnetics, nonconforming elements, edge elements, eddy current problems, object-oriented software

This thesis consists of an introduction and the following papers:

Paper I R. Bergström, *Least-Squares Finite Element Methods with Applications in Electromagnetics*, to appear in Math. Models Methods Appl. Sci.

Paper II R. Bergström and M.G. Larson, *Discontinuous/Continuous Least-Squares Finite Element Methods for Elliptic Problems*, submitted.

Paper III R. Bergström and M.G. Larson, *Discontinuous Least-Squares Finite Element Methods for the Div-Curl Problem*, submitted.

Paper IV R. Bergström, M.G. Larson, and K. Samuelsson , *The $\mathcal{LL}^*$ Finite Element Method and Multigrid for the Magnetostatic Problem*, submitted.

Paper V Y.Q. Liu, A. Bondeson, R. Bergström, C. Johnson, M.G. Larson, and K. Samuelsson, *Eddy Current Computations Using Adaptive Grids and Edge Elements*, IEEE Trans. Mag., vol. 38, pp. 449-452, 2002.

Paper VI Y.Q. Liu, A. Bondeson, R. Bergström, M.G. Larson, and K. Samuelsson, *Edge Element Computations of Eddy Currents in Laminated Materials*, submitted.

Paper VII T. Rylander, R. Bergström, M. Levenstam, A. Bondeson, and C. Johnson, *FEM Algorithms for Maxwell's Equations*, Conference Proceedings, EMB 98 - Electromagnetic Computations for Analysis and Design of Complex Systems, November 17-18, 1998, Linköping, Sweden.

Paper VIII R. Bergström and M.G. Larson, *Dispersion Analysis of Galerkin Least Squares Approximations of Maxwell's Equations*, Mathematical and Numerical Aspects of Wave Propagation, Ed: A. Bermúdez, D. Gómez, C. Hazard, P. Joly and J.E. Roberts, SIAM Proceedings, 2000.

Paper IX R. Bergström, *Object Oriented Implementation of a General Finite Element Code*, Technical report.

Contents

Acknowledgements

There are many people that, in different ways, have taken part in my work and made this thesis possible.

To begin with, my advisor Dr. Mats G Larson has given me invaluable encouragement, time, and knowledge during these years. A crucial direction for this work was given by my former advisor Dr. Mårten Levenstam, who shared his experience in practical FEM and interest in simulating and explaining everyday phenomena.

Prof. Claes Johnson, who together with Prof. Kenneth Eriksson, opened my eyes to the world of computational modeling. Moreover, their sparkling enthusiasm is contagious.

Niklas Ericsson has generously shared room, thoughts, ideas and our sofa. Also all other present and former colleagues at Chalmers Finite Element Center Φ have contributed, not only with input on my work, but by creating an enjoyable working environment.

For questions concerning electromagnetics, Prof. Anders Bondeson and the members of his group have willingly tried to give me the answers. Dr. Klas Samuelsson has given invaluable help with different implementation issues. Dr. Arne Wolfbrandt and his coworkers at ABB Corporate Research offered me the opportunity to experience various aspects of computations in industry.

The Swedish Foundation for Strategic Research (SSF) provided the main funding through the National Graduate School in Scientific Computing (NGSSC) and the National Network in Applied Mathematics (NTM).

I also want to thank all my friends for the valuable distraction you offer. And finally, to my family and Johanna, thanks for everything you have given me.

Thank you all!

Rickard Bergström
Göteborg, August 2002

1 Introduction

Physical phenomena described by mathematical models involving the div- and curl-operators arise in many different applications. In this thesis, we focus our attention on applications originating in electromagnetics. Problems of this type can be found in a wide range of applications, including radar and cellular phones, medical applications involving, e.g., cancer treatments, power generation with hydrogenerators or by wind power, and the electricity network to and in our homes.

The physics behind these phenomena was mainly explored during the 19:th century. Faraday and Ampère stated laws that bridged electric currents and magnetism, and in 1864, Maxwell joined the relations into one system of equations, and later also predicted the occurrence of electromagnetic waves.

Despite their simple appearance, div-curl problems are often difficult to treat computationally due to the kernels of the operators and the singularities that occur in nonconvex domains. In the case of Maxwell's equations, the solution also behaves very differently depending on the frequency and application.

As a science, the area of computational electromagnetics (CEM) is thus challenging and relatively new. Wave propagation problems on geometries without curved boundaries can be solved successfully with the FDTD method introduced by Yee in 1966, but it is only recently that problems with general geometries have been successfully solved. In low frequency problems, the geometrical object is often large while there are thin layers that still must be resolved. Therefore, one is in many cases restricted to two dimensional approximations.

1.1 Thesis objectives

The main objectives of this thesis are:

- development of least-squares finite element methods for div-curl problems posed on nontrivial geometries in three spatial dimensions,
- development of existing methods for electromagnetics, mainly low frequency, problems, and
- implementation of an environment for general finite element computations.

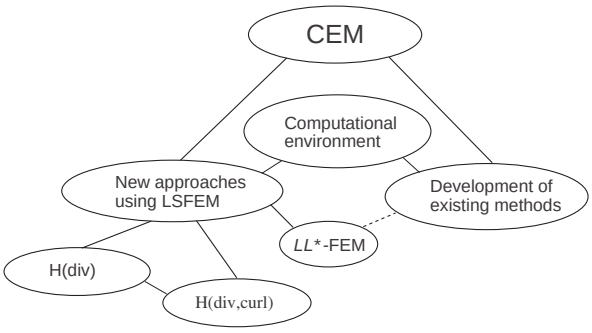

Figure 1: A schematic picture of the components of the thesis.

Previous work on least-squares finite element methods (LSFEM) mainly treats relatively simple geometries, often convex, in two dimensions. The step from two to three dimensions leads to interesting applications, difficulties with the regularity of the solution, and increasing computational complexity. Standard least-squares methods demand high regularity of the solution which leads to serious problems in most applications, for instance, problems posed on domains with corners. Our approach to overcome these obstacles is to weaken the norm in the least-squares functional or enrich the finite element spaces.

In high frequency electromagnetic problems, the edge elements are dominant. However, these elements are not yet as common in the potential formulations used in low frequency applications, nor is adaptivity. Our work is concerned with adaptive methods based on tetrahedral and hexahedral edge elements in the context of eddy current computations in laminated materials.

Throughout the thesis, a wide variety of finite element formulations and elements are used to solve the different applications. We have therefore implemented a flexibly, yet efficient, computational environment for general finite element methods to meet this demand. The software is based on object oriented programming techniques.

1.2 Main results

1.2.1 LSFEM for div-curl problems

- In an interface problem with corners, we use weak enforcement of interface and boundary conditions, and obtain convergence for the

energy with standard LSFEM in numerical computations. We also show this convergence theoretically using duality arguments. (Paper I)

- Optimal convergence on nonconvex domains is proved when introducing discontinuous elements in the least-squares formulation (DLSFEM) and the performance of this scheme is illustrated by computations. (Papers II and III)

- The $\mathcal{LL}^*$-finite element method, i.e. using a dual norm in the least-squares functional but computing in the dual variables, is successfully used for a magnetostatic problem. Also, we derive an a posteriori error estimator which is used for adaptive mesh refinement. (Paper IV)

- Test problems in 3D, motivated by industrial applications, have successfully been solved using these modified least-squares techniques.

- A hybrid scheme, combining Galerkin and least-squares finite element methods, is proposed for wave propagation problems, and its dispersion relation is investigated numerically. (Papers VII and VIII)

1.2.2 Development of existing methods

- Combining edge elements and adaptivity, an efficient method for solving eddy current problems is presented. (Paper V)

- The properties of tetrahedral and hexahedral edge elements in eddy current computations with laminated materials are analyzed and we show that hexahedral elements aligned with the laminations correctly represent the solution. (Paper VI)

- Anisotropic mesh refinement and hexahedral edge elements are combined and used to compute the power loss in a simplified hydrogenerator model in 3D. (Paper VI)

1.2.3 General computational environment

- With object-oriented programming techniques, a general environment for finite element computations has been developed. (Paper IX)

- Several different finite element methods and element types have been implemented demonstrating its generality. (Paper IX)

- The software has been used in a wide range of applications. (Papers I-IX)

1.3 Future directions

As already mentioned, this area of computational science is relatively new and there are many questions to answer. Natural extensions of the work in this thesis include:

- applying LSFEM to more realistic industrial applications,
- incorporating multigrid techniques to solve these problems, and
- developing efficient anisotropic a posteriori estimates for edge elements and mesh refinement algorithms that exploit these estimates.

2 Maxwell's theory for electromagnetic fields

2.1 Maxwell's equations

The system of equations governing all macroscopic electromagnetic phenomena, called Maxwell's equations, takes the form of the following first order system of partial differential equations:

$$\nabla \times E = -\frac{\partial B}{\partial t}, \tag{2.1a}$$

$$\nabla \times H = J + \frac{\partial D}{\partial t}, \tag{2.1b}$$

$$\nabla \cdot D = \rho, \tag{2.1c}$$

$$\nabla \cdot B = 0, \tag{2.1d}$$

in $\mathbf{R}^3$. E and H are the electric and magnetic field intensities respectively, and D and B are the corresponding flux densities, $J = J_{sc} + \sigma E$ is the total current density, J_{sc} is an imposed current density, σ is the electric conductivity, and ρ is the charge density.

In simple materials, the electric and magnetic fields are connected to the fluxes through the following constitutive relations

$$B = \mu H, \tag{2.2a}$$

$$D = \epsilon E, \tag{2.2b}$$

where μ is the magnetic permeability and ϵ is the electric permittivity. Often, one expresses these parameters as $\epsilon = \epsilon_r \, \epsilon_0$ and $\mu = \mu_r \, \mu_0$, where the

index r refers to a relative value and the index 0 is the value in free space, $\mu_0 = 4\pi \times 10^{-7}$ H/m and $\epsilon_0 = \frac{1}{c^2 \mu_0}$ F/m, where c is the speed of light. In the general case of anisotropic media, these parameters are tensors and can be functions of both space and time. They may also depend on the magnetic and electric fields and fluxes, and in lossy media they are complex-valued.

Solutions to (2.1) satisfy the following continuity conditions at material interfaces:

$$[E] \times n = 0, \tag{2.3a}$$
$$[H] \times n = 0, \tag{2.3b}$$
$$[D] \cdot n = 0, \tag{2.3c}$$
$$[B] \cdot n = 0, \tag{2.3d}$$

where $[\cdot]$ denotes the jump across the interface, and n is a unit normal to the surface, stating that the tangential components of E and H are continuous as well as the normal components of D and B. These conditions imply that since $B = \mu H$, the normal component $H \cdot n$ will be discontinuous across an interface of discontinuity of μ. Corresponding relations hold for the other fields. One further observation is that in corners and on edges, where the normal vector abruptly changes direction, these conditions are in conflict leading to a singularity in the solution, see e.g. Costabel and Dauge [26] and Assous *et al.* [4].

In the special case where one material is a perfect conductor or a perfect magnetic wall, which cannot sustain fields, the interface conditions reduce to the following conditions in the other material:

$$E \times n = 0, \tag{2.4a}$$
$$B \cdot n = 0, \tag{2.4b}$$

and

$$H \times n = 0, \tag{2.5a}$$
$$D \cdot n = 0, \tag{2.5b}$$

respectively. For computations on bounded domains, these conditions will also act as boundary conditions.

2.2 The quasi-static approximation

In most low frequency applications one may set $\epsilon = 0$, and thus $D \equiv 0$. This low frequency assumption is applicable when the wave length is larger

than the object we are modeling, see the work of Ammari *et al.* [1] for the validity of this approximation.

We are thus lead to the following so called quasi-static form, or eddy currents model, of Maxwell's equations:

$$\nabla \times E = -\frac{\partial B}{\partial t}, \tag{2.6a}$$

$$\nabla \times H = J, \tag{2.6b}$$

$$\nabla \cdot B = 0, \tag{2.6c}$$

where as before, $J = J_{sc} + \sigma E$ and $B = \mu H$. The interface conditions (2.3) reduce to

$$[E] \times n = 0, \tag{2.7a}$$

$$[H] \times n = 0, \tag{2.7b}$$

$$[B] \cdot n = 0. \tag{2.7c}$$

However, since $\nabla \cdot J = 0$ by (2.6b), we have the additional interface condition,

$$[J] \cdot n = 0. \tag{2.8}$$

2.2.1 The time-harmonic quasi-static equations

Assuming a harmonic time dependence of the form $e^{j\omega t}$, we obtain the following time harmonic analog to (2.6):

$$\nabla \times E = -j\omega B, \tag{2.9a}$$

$$\nabla \times H = J, \tag{2.9b}$$

$$\nabla \cdot B = 0. \tag{2.9c}$$

In this case, we work with complex-valued fields even in lossless media. The elimination of the time dependency can of course be performed also on the full system (2.1).

2.3 The static equations

In the static case, with no time variation, the equations decouple into an electrostatic system

$$\nabla \times E = 0, \tag{2.10a}$$

$$\nabla \cdot D = \rho, \tag{2.10b}$$

and a magnetostatic system

$$\nabla \times H = J, \tag{2.11a}$$
$$\nabla \cdot B = 0. \tag{2.11b}$$

Equations (2.10) is normally modeled by introducing a scalar electric potential which results in a Poisson problem for this potential. The magnetostatic problem (2.11) is not as easily treated. It appears as a special case of the quasi-static applications and includes the complication of magnetic materials, leading to discontinuities and singularities in the field variables. Also here one normally introduces a potential which becomes a vector potential for the magnetic flux. This formulation is considered in Section 3.2.

2.4 Examples of applications

2.4.1 Wave propagation problems

In high frequency problems, one often wants to solve a wave propagation problem in the time domain. This may be the case when computing the characteristics of a microwave antenna or trying to minimize the radar cross section of an aircraft. Equations (2.1) are rewritten as a second order equation, similar to the ordinary wave equation, as described in Section 3.1. A complication in this type of simulations, is that the computational complexity increases rapidly with the physical dimensions of the object. This is due to the fact that the mesh needs to resolve the wave length which may be considerably smaller than the object.

2.4.2 Eddy current problems

In the construction of a hydrogenerator, typically working at low frequencies ($f \leq 200$ Hz), one wants to reduce power loss from eddy currents induced by the magnetic fields. To compute this loss, the quasi-static equations need to be solved, often in laminated highly anisotropic materials. Another complication is that the eddy currents are concentrated to thin layers at the surface of conductors in the generator, layers that thus must be resolved by the mesh.

3 Computational methods for electromagnetic problems

Traditionally, finite element methods have not been applied directly to the first order form as written in (2.1). Instead the problem has been rewritten as a second order problem, either by eliminating one of the fields, or by introducing scalar and vector potentials. Which approach to choose depends on the frequency range in question: eliminating the magnetic field and using a second order curl-curl equation for E is normally used for wave propagation problems, while different potentials have been used in low frequency, e.g. eddy current, computations.

3.1 Second order formulation in E

One can derive second order equations for both the electric and the magnetic fields. Which one to choose depends on the application, and in some problems it can be interesting to use both [14]. To get an equation for the E-field, which is often used in e.g. radar computations, equation (2.1a) is used to eliminate H from equation (2.1b). We get the following basic second order equation for the electric field:

$$\nabla \times \mu^{-1} \nabla \times E + \epsilon \frac{\partial^2 E}{\partial t^2} = 0. \tag{3.1}$$

A Galerkin method for this problem leads to the weak form

$$(\mu^{-1} \nabla \times E^n, \nabla \times V) + (\beta E^n, V) = f(V), \tag{3.2}$$

where E^n denotes the approximate solution for the next time step, β includes the time step, and f depends on the approximate solutions on the previous time steps.

3.2 Potential formulations

There are several ways to express the electric and magnetic fields as derivatives of different potentials [9][34][51]. To exemplify the techniques, we demonstrate the version used in Paper V for time-harmonic eddy current computations.

In conducting regions, where no source currents are present, the divergence of the magnetic flux density vanishes, and we can introduce a magnetic vector potential A defined as $\nabla \times A = B$. Further, we use an electric scalar potential V which together with equation (2.1a) and the definition of the

vector potential yields $E = -j\omega A - \nabla V$. Inserting these expressions into equation (2.1b), we arrive at

$$\nabla \times \mu^{-1} \nabla \times A + \sigma \left(j\omega A + \nabla V \right) = 0. \tag{3.3}$$

In general also a gauge or divergence constraint is added to ensure uniqueness of the potentials involved. We note that this problem leads to a weak form similar to (3.2) and some results in the literature is valid for both formulations.

In the coil region, the current density is specified and we do not need to introduce the electric potential. Instead, we solve

$$\nabla \times \mu^{-1} \nabla \times A = J_s. \tag{3.4}$$

In simply connected regions where the current density vanishes, we may simplify further by only solving for a magnetic scalar potential ψ, such that $H = \nabla \psi$. We then solve only the Laplace problem

$$\nabla \cdot \mu \nabla \psi = 0. \tag{3.5}$$

3.3 Kernels, spurious solutions, and gauge conditions

The form of Maxwell's equations, with two curl equations defining the fields, leads in some cases to problems with non-unique solutions due to the kernel of the curl-operator. In the full formulation, the divergence conditions (2.1c)-(2.1d) yields uniqueness but in many numerical schemes these equations are considered superfluous and are excluded. In potential formulations, they are implicitly included which makes the fields unique while the potentials remain non-unique.

In field computations, this leads to the occurrence of spurious modes, non-physical static or low frequency solutions that violate the divergence conditions. See Jiang *et al.* [33] or Bossavit [13] for more information on the history and analysis of this complication. In potential computations, spurious solutions do not occur, but the non-uniqueness may still cause numerical difficulties.

The most common way to circumvent these numerical problems, is to apply a penalty ,or gauge condition, on the divergence of the magnetic vector potential A [9]. The most common types are the Coulumb gauge, forcing the condition $\nabla \cdot A = 0$, and the Lorentz gauge, $\nabla \cdot A = -\sigma \mu V$. In field computations, a Coulumb-type gauge on the field may be applied [46].

3.4 Element types for CEM

The question on which type of elements to choose for the finite element computations is a topic of large interest. When using potential formulations, continuous node based elements have most often been used. The drawbacks are the loss of one order in accuracy since one differentiation of the solution is needed to express the actual fields, and the need for a gauge condition in order to avoid spurious solutions. There are however classes of problems where node based formulation fails [8]. In wave propagation problems, node based schemes have not been used due to the occurrence of spurious solutions and the poor dispersion properties of the schemes. Instead, one has used explicit finite difference (FDTD) methods [53], which however do not allow local mesh refinement or curved geometries.

Today, the focus is instead on curl-conforming edge elements. These elements have degrees of freedom associated with moments over edges and faces and were introduced by Whitney and extended and popularized by Nédélec in 1980 [45]. For the lowest order elements, the unknowns are vectors aligned with the edges of the geometrical elements, see also Section 7.2. The practical advantages when using these elements include that spurious solutions do not occur and boundary and interface conditions are naturally implemented since the tangential continuity of the elements fits with the problem.

For eddy current computations, the use of edge elements is still fairly new, and main questions involve how to treat the kernel of the curl-curl operator with respect to solvability [8] and the application of efficient iterative solver techniques such as multigrid algorithms [3][6][30]. In wave propagation problems these elements are more established [54]. The main difficulty arising here, is the problem with not being able to lump the mass matrices, thereby ruling out the use of explicit time stepping schemes [37]. Areas of research are thus curl-conforming elements that can be lumped [35], and the use of hybrid schemes, coupled to FDTD [49][53].

4 Development of established methods in CEM

4.1 Edge elements for eddy current computations

In low frequency computations, the edge elements have not yet reached the same popularity as in wave propagation problem. Still, the properties of these elements are desirable also in these applications. Since edge elements lack continuity in the normal direction, it is not feasible to use the gauges

described in Section 3.3, involving the divergence of the fields. Therefore, the system matrix becomes singular, and the solvability of this discrete algebraic system becomes a crucial issue [8].

In cooperation with Bondeson and Liu in the Department of electromagnetics at Chalmers, we have performed eddy current computations on a simplified model of a hydrogenerator using an ungauged formulation with an orthogonalization process to assure solvability, i.e., we solve a Poisson problem in order to clean the load vector from components that are not in the discrete solution space and thus make it orthogonal to the kernel of the curl-operator. The key to this procedure is the characterization of the discrete kernel as gradients of standard polynomial elements. This work is described in Paper V.

Further, we found that in laminated materials, it is difficult to achieve accurate results using lowest order tetrahedral elements. Also for hexahedral elements not aligned with the laminations, similar difficulties occur. This is since these elements are not able to represent the solution, as explained in Paper VI. In this paper, we also use anisotropically refined hexahedral edge elements to restore optimal convergence order for the finite element method.

4.2 Galerkin least-squares method for wave propagation problems

The main motivation for not using nodal elements in high frequency computations is the possible occurrence of spurious solutions. In a wave propagation problem, where we, e.g., send a wave towards an object and measure the reflection, spurious solutions can be seen at corners and details in the geometry and they vary rapidly in space but are typically of low frequency.

However, using the Lee-Madsen formulation of the first order system [38] [40], see Paper VIII, we have performed numerical experiments in two and three dimensions that indicate that these spurious solutions can be avoided by means of local mesh refinement.

Another reported drawback is that the phase error in this formulation has the same sign independent of the direction of propagation of the wave relative to the element [42]. According to Wu and Lee [52], it is desirable if the phase errors have different sign in different directions since on unstructured grids, this property is believed to lead to cancellation of the phase errors.

Noting that a least-squares formulation of the Maxwell equations [44] gives phase errors with opposite sign compared with the Lee-Madsen formu-

lation, we propose a combined scheme: find $U = [E, H] \in \mathcal{V}$, such that

$$(1-\alpha)A_G(U,\overline{U}) + \alpha A_{LS}(U,\overline{U}) = 0 \quad \text{for all } \overline{U} \in \mathcal{V}, \tag{4.1}$$

where $\alpha \in [0,1]$ is a parameter, $A_G(\cdot,\cdot)$ is the bilinear form associated with the standard Galerkin method, and $A_{LS}(\cdot,\cdot)$ is the bilinear form associated with the least-squares method.

A numerical dispersion analysis shows that with $\alpha \approx 0.4$, we get a scheme with varying sign of the phase error and the region with small error is larger compared to each of the methods, as well as compared to using formulation (3.2) and edge elements [42]. Furthermore, the problem with spurious solution is not present in the least-squares method and thus nor in the combined scheme.

5 Least-squares finite element method

Finite element methods based on least-squares techniques (LSFEM) were first applied on electromagnetic problems by Jiang *et al.* [33][32]. Since LSFEM can be applied to over determined systems and is preferably applied to a first order system, the method is suitable to apply directly to Maxwell's equations in the form of (2.1). We thus avoid the loss in accuracy of the potential methods as well as the occurrence of spurious solutions. Discontinuities in material parameters must however be handled by discontinuous elements [23][47]. However, we have found that the high regularity requirements for the standard formulation of LSFEM hinders simulation of realistic applications.

In this section we describe in some detail the basic principles of the least-squares finite element method. We start with a general first order problem, derive the least-squares functional and the weak form, and comment on extensions of the functional to include the weak treatment of boundary conditions and constitutive relations. Finally, we state the a priori error estimates that are standard in the least-squares methodology. In the next section we discuss different ways suggested to relax the regularity requirements.

5.1 A general first order problem

Consider the following first order boundary value problem:

$$\mathcal{L}u = f \quad \text{in } \Omega, \tag{5.1a}$$

$$\mathcal{B}u = g \quad \text{on } \Gamma, \tag{5.1b}$$

where Ω is a bounded domain in $\mathbf{R}^3$ with boundary Γ. Here u is a vector of m unknowns, $\mathcal{L}$ is a linear differential operator of the form

$$\mathcal{L}u = \sum_{i=1}^{3} A_i \frac{\partial u}{\partial x_i} + A_0 u, \tag{5.2}$$

and $\mathcal{B}$ is an algebraic boundary operator of the form

$$\mathcal{B}u = Bu, \tag{5.3}$$

where A_i and B are matrices with variable coefficients of type $m \times m$ and $n \times m$ respectively, where $n \leq m$. These coefficient matrices are assumed to be bounded.

Furthermore, we assume that problem (5.1) has a unique solution, u.

5.2 The least-squares formulation

Now, suppose $f \in [L^2(\Omega)]^m$, $g \in [H^{1/2}(\Omega)]^n$, let $\mathcal{V} = [H^1(\Omega)]^m$, and define the subspaces $\mathcal{V}_g = \{v \in \mathcal{V} : \mathcal{B}v = g \text{ on } \Gamma\}$, and $\mathcal{V}_0 = \{v \in \mathcal{V} : \mathcal{B}v = 0 \text{ on } \Gamma\}$.

Form the functional

$$I(v) = \|\mathcal{L}v - f\|^2 \quad \text{for } v \in \mathcal{V}_g, \tag{5.4}$$

and note that

$$0 = I(u) \leq I(v), \tag{5.5}$$

$\forall v \in \mathcal{V}_g$.

Thus a solution u to problem (5.1) minimizes the functional I, and the least-squares method amounts to finding this minimizer, i.e., find $u \in \mathcal{V}_g$ such that

$$I(u) = \inf_{v \in \mathcal{V}_g} I(v). \tag{5.6}$$

A necessary condition for a function $u \in \mathcal{V}_g$ to satisfy equation (5.6), is

$$\lim_{\tau \to 0} \frac{\partial}{\partial \tau} I(u + \tau v) \equiv 2(\mathcal{L}u - f, \mathcal{L}v) = 0, \tag{5.7}$$

$\forall v \in \mathcal{V}_0$.

So, the minimization of the least-squares functional I leads to the variational problem: find $u \in \mathcal{V}_g$ such that

$$a(u, v) = l(v), \tag{5.8}$$

$\forall v \in \mathcal{V}_0$, where

$$a(u, v) = (\mathcal{L}u, \mathcal{L}v), \tag{5.9a}$$

$$l(v) = (f, \mathcal{L}v). \tag{5.9b}$$

5.3 Weak enforcement of boundary conditions

Up to now, the boundary conditions $\mathcal{B}u = g$ have been imposed strongly by restricting the space in which we seek the solution. It is also possible to impose them weakly by including equation (5.1b) in the definition of the least-squares functional. We then redefine $I(v)$ to

$$I(v) = \|\mathcal{L}v - f\|^2 + \|\mathcal{B}v - g\|^2_{1/2,\Gamma} \quad \text{for } v \in \mathcal{V}, \tag{5.10}$$

Seeking a minimizer to I in $\mathcal{V}$ leads to the following variational problem: find $u \in \mathcal{V}$ such that

$$a(u, v) = l(v), \tag{5.11}$$

$\forall v \in \mathcal{V}$, where

$$a(u, v) = (\mathcal{L}u, \mathcal{L}v) + (\mathcal{B}u, \mathcal{B}v)_{1/2,\Gamma}, \tag{5.12a}$$

$$l(v) = (f, \mathcal{L}v) + (g, \mathcal{B}v)_{1/2,\Gamma}. \tag{5.12b}$$

5.4 Incorporating constitutive relations

Additional equations describing constraints on, or relations between, variables arise in many applications, e.g., non-newtonian flows or Stokes flow. Both the divergence constraint (2.1d) and the constitutive relations (2.2) in the Maxwell equations may be considered as being of this type.

These extra constraints on the system of PDE:s are in general difficult to handle in the analysis. However, in a least-squares method we treat these equations in the same manner as we treated boundary conditions in the previous section, i.e., by adding terms to the least-squares functional. We can then use the tools for the least-squares method to analyze the complete system.

In the general framework presented here, the matrices A_i in equation (5.2) are thus allowed to be rectangular matrices of type $M \times m$, where $M \geq m$.

5.5 The least-squares finite element method

We introduce a finite element space $\mathcal{V}_h$ as, e.g., the space of all continuous piecewise vector polynomial functions v_h of degree less than or equal to p, such that, in each element, $v_h \in \mathcal{P}_p$. Furthermore, h denotes the mesh size of the underlying triangulation.

Assuming that g can be exactly represented by continuous piecewise polynomials, and if not, replacing it by its L^2-projection Pg, we define the

finite element subspace $\mathcal{V}_{h,g}$ of $\mathcal{V}_g$ by $\mathcal{V}_{h,g} = \mathcal{V}_h \cap \mathcal{V}_g$, and similarly we define $\mathcal{V}_{h,0} = \mathcal{V}_h \cap \mathcal{V}_0$.

The least-squares finite element method corresponding to (5.6) can now be formulated by restricting the minimization problem: find $u_h \in \mathcal{V}_{h,g}$ such that

$$I(u_h) = \inf_{v \in \mathcal{V}_{h,g}} I(v). \tag{5.13}$$

Necessary conditions for a minimum in $\mathcal{V}_{h,g}$ lead to the variational problem: find $u_h \in \mathcal{V}_{h,g}$ such that

$$a(u_h, v) = l(v), \tag{5.14}$$

$\forall v \in \mathcal{V}_{h,0}$, where $a(\cdot,\cdot)$ and $l(\cdot)$ are defined as in equation (5.9).

5.6 A priori error estimates

Using standard techniques, it is possible to prove the following result for a general least-squares finite element method:

Theorem 5.1 *Let $u \in \mathcal{V} = [H^1(\Omega)]^m$ be a solution to problem 5.1. For an approximate solution $u_h \in \mathcal{V}_h$ obtained by LSFEM, as defined by equation (5.14), there is a constant C, independent of u and h, such that*

$$|||u - u_h||| \leq C h^p |u|_{p+1}, \tag{5.15}$$

where $|||v|||^2 = a(v, v)$.

Moreover, for elliptic problems, it is possible to derive an improved result. We say that the problem is elliptic if the bilinear form $a(\cdot,\cdot)$ is coercive with respect to the H^1-norm.

Theorem 5.2 *Let $u \in \mathcal{V} = [H^1(\Omega)]^m$ be a solution to problem (5.1), where $\mathcal{L}$ is a continuous linear first order* elliptic *differential operator. For an approximate solution $u_h \in \mathcal{V}_h$ obtained by LSFEM, as defined by equation (5.14), there are constants C_1 and C_2 independent of u and h such that*

$$\|u - u_h\|_1 \leq C_1 h^p |u|_{p+1}, \tag{5.16}$$

and

$$\|u - u_h\| \leq C_2 h^{p+1} |u|_{p+1}. \tag{5.17}$$

6 Least-squares formulations for the div-curl problem

As is clear from the previous section, LSFEM suffers from strong regularity requirements on the exact solution. Optimal convergence will be achieved only in very smooth domains with no corners or edges and the suboptimality will remain even in the presence of mesh refinement. This is due mainly to the use of L^2-norms in the minimizing functional, combined with continuous node based finite element spaces which are dense in H^1.

Several attempts to resolve this shortcoming have been made, most of them involve using a weaker norm such as a weighted L^2-norm [22][27] or a discrete version of the H^{-1}-norm [5][15][17]. In Paper II and Paper III, we present another approached based on enrichment of the finite element space by allowing some discontinuity close to the singularities.

Theoretically, a natural approach to apply LSFEM to problems with low regularity is to, when forming the least-squares functional, choose a norm such that convergence is achieved. For practical reasons, we must however be able to compute the functional and the inner products induced by the norm.

A way to perform these computations in a discrete H^{-1}-norm was presented by Bramble *et al.* [15]. The method involves the construction of a preconditioner that approximates the solution operator to a Laplace-type problem. The main drawback with this approach is that it leads to algebraic problems with dense matrices [10].

The idea when applying weighted L^2-norms, is to introduce a function, centered at the singularity, which exactly cancels the singularity and thus yields convergence of the norm. These norms, together with mesh refinement, were used by Cox and Fix [27] to restore optimal convergence of LSFEM when solving the first order Laplace system on an L-shaped domain in 2D. Manteuffel *et al.* [39] developed the idea and applied it to an interface problem. The main drawback with this approach is that one needs exact knowledge of the behaviour of the solution in the vicinity of the corner. This is possible to handle in 2D but is considerably more difficult in 3D. Further, the error at the singularity is still very large.

6.1 Minimization over the dual space

Cai *et al.* [22] recently constructed a method of least-squares type they named First-Order System $\mathcal{L}\mathcal{L}^*$, FOS$\mathcal{L}\mathcal{L}^*$, where $\mathcal{L}^*$ denotes the adjoint of the linear operator $\mathcal{L}$ of equation (5.2). Instead of using H^{-1}-norm,

they consider minimization in the dual norm $||v||_B = \sup_{w \in \mathcal{D}^*}(v, w)/||\mathcal{L}^* w||$, where $\mathcal{D}^*$ is the domain of $\mathcal{L}^*$. They show that this is the same as minimizing the L^2-error over the dual space.

An application of this approach to the magnetostatic problem is presented in Paper IV. We apply adaptive mesh refinement techniques based on an a posteriori error estimate for the magnetic energy which we derive in the paper. We note that, with suitable scaling, the weak form for this formulation becomes identical to a magnetic vector potential formulation with the Coulumb gauge applied with penalty weight one.

6.2 Discontinuous LSFEM

The idea with this approach is to construct a finite element space, enabling us to avoid the strong regularity requirements normally present for LSFEM. This is done by introducing discontinuous elements in the least-squares method, an idea first introduced by Bramble *et al.* [16]. We thus obtain a convergent scheme also for problems with singularities.

In Paper II we use discontinuous elements to approximate $H(\mathrm{div})$ by weakly imposing normal continuity, the penalty term for the discontinuity is naturally incorporated in the least-squares functional. We prove stability and optimal a priori error estimates for the proposed scheme. In Paper III we extend the analysis to problems posed in $H(\mathrm{div}) \cap H(\mathrm{curl})$. Numerical computations on three-dimensional nonconvex domains are presented to demonstrate the approach.

This method does not need any a priori knowledge about the solution since we only use the standard L^2-norm. The cost we have to pay is the extra degrees of freedom introduced by the discontinuous elements. This cost can be reduced by applying the conforming approximation spaces described in Sections 7.1 and 7.3.

7 Finite element spaces for div-curl problems

We will in general terms describe some approximation spaces for these types of problems. Let $\mathcal{K}$ be a decomposition of the domain Ω into, e.g., tetrahedral, finite elements K. The index h denotes the mesh function and is a measure of the local size of the elements in the mesh, $h_K = h|_K = \mathrm{diam}(K)$, and we assume a minimal angle condition on the triangulation, see Brenner and Scott [18]. By $\mathcal{P}_p(K)$ we denote the set of polynomial functions of degree less than or equal to p defined on the element K.

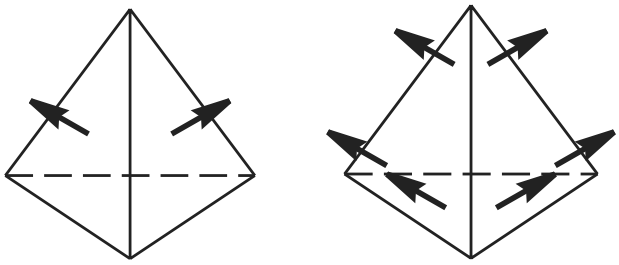

(a) RT_0 (b) BDM_1

Figure 2: The degrees of freedom for the lowest order RT or BDM elements are the normals on the faces.

7.1 $H(\mathbf{div})$-spaces

In order to construct a finite element space $\mathcal{V}_h$ to approximate $H(\mathrm{div}) = \{v \in [L^2]^n : \nabla \cdot v \in L^2\}$, we need continuity (up to the sign) of $v \cdot n$, where $v \in \mathcal{V}_h$, at the element interfaces. Two established ways to achieve this are the Raviart-Thomas (RT) elements [48] and the Brezzi-Douglas-Marini (BDM) elements [19][20]. The book by Brezzi and Fortin [21] gives a good overview of different element types for approximating $H(\mathrm{div})$.

For the lowest order BDM-elements, the degrees of freedom are associated with linear moments of the normal field on the element faces. The most important property is that the p:th-order interpolation operator π_K, based on these elements, commute with the divergence operator in the following sense,

$$\nabla \cdot \pi_K v = P_{p-1,K} \nabla \cdot v, \tag{7.1}$$

where $P_{p,K}$ denotes the L^2-projection onto $\mathcal{P}_p(K)$. This property makes it possible to obtain the following interpolation error estimate

$$\|\nabla \cdot (v - \pi_K v)\|_K \leq C h_K^\alpha |\nabla \cdot v|_{\alpha,K}, \tag{7.2}$$

where C does not depend h and $0 \leq \alpha \leq p$; see [21] for proofs. Similar results hold for the RT-elements.

The gain is that we may exploit the natural regularity of the problem and establish estimates involving only the divergence of the solution, while for continuous nodal elements we typically have to express our results in the stronger $|\cdot|_{\alpha+1,K}$-norm.

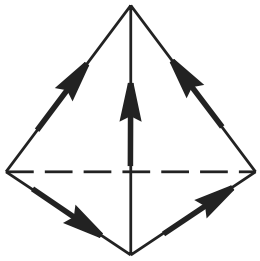

Figure 3: The degrees of freedom for the lowest order Nédédec elements are aligned with the edges.

7.2 $H(\mathbf{curl})$-spaces

Instead of ensuring normal continuity, we need for $H(\text{curl}) = \{v \in [L^2]^n : \nabla \times v \in [L^2]^n\}$ to impose tangential continuity on the finite element space. The most popular construction used in the electromagnetic community is due to Nédélec [45] and the elements are called Nédélec or edge elements, since the degrees of freedom for the lower order elements are located and aligned with the edges of the element.

Similarly to how interpolation on the BDM-elements commute with the divergence-operator, the interpolation on edge elements commute with the curl-operator. We thus have an analogous interpolation error estimate [25]:

$$\|\nabla \times (v - \pi_K v)\|_K \leq C h^\alpha |\nabla \times v|_{\alpha,K}, \quad 1/2 < \alpha \leq p. \tag{7.3}$$

The reasons why the edge elements are so well suited to approximate Maxwell's equations are still an area of research. The concept of discrete compactness [12][36][41] coupled to the property of commuting *de Rahm* diagrams [11][29] are steps towards a theoretical understanding. In [24], Caorsi *et al.* show convergence of the edge element by considering the fact that the operator of the underlying variational eigenproblem is non-compact. For the engineer, the more important property of the Nédélec spaces may be that the kernel of the curl-operator in the discrete space, is exactly the gradient of a standard node based finite element function.

7.3 $H(\mathbf{div}) \cap H(\mathbf{curl})$-spaces

We describe here in short the use of the Crouzeix-Raviart (CR) elements for a non-conforming approximation of $H(\text{div}) \cap H(\text{curl})$. The linear CR-

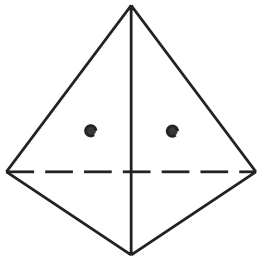

Figure 4: The degrees of freedom for the lowest order Crouzeix-Raviart are the field at the midpoint of the faces.

elements ensure continuity of the average over the element faces. The degrees of freedom are the constant moments on the faces. As for scalar polynomial elements, we use a tensor product element $[CR]^3$ in the approximation of vector functions. The generalization to higher order is not straightforward, and since we only need low order CR-elements we do not discuss that issue further.

An interpolation operator based on these elements commute with both the curl and the divergence operator, and both (7.2) and (7.3) are valid with $0 < \alpha \leq 1$.

8 Error control and adaptive mesh refinement

8.1 Computational errors

When modeling physical phenomena with finite element methods we only obtain an approximate solution. It is important to have an idea of which errors we get and how to control them to achieve better accuracy. We can split the error into three components: the modeling error that has to to do with how well the mathematical model we use describes the actual physics, the algebraic error which arises when using iterative (approximate) solvers for the discrete matrix problem, and the discretization error which comes from seeking the solution of the mathematical model in finite dimensional function spaces.

The algebraic error is in general easy to control and small in compari-

son to the other. Moreover, in electromagnetics, Maxwell's equations (2.1) are normally considered to be exact. Modeling error arises never the less when describing different materials; the constitutive equations (2.2) are a simplification for general materials.

A large portion of the research in the finite element area is concerned with handling the discretization error. The goal is to minimize the error in the finite element model, measured in some way, compared with the mathematical model and to do it at a low cost. This is done by deriving an error indicator and increase the accuracy of the discrete model only where it is most needed. The indicator is based on an a posteriori error estimate, i.e., a bound of the error based on information on the computed solution.

8.2 Residual based a posteriori estimates

The simplest error estimates are derived for the energy norm, i.e., the (semi) norm induced by the bilinear form. For least-squares methods this is an easy derivation, since the energy norm of the error is equal to the least-squares residual.

Let $|||v|||^2 = a(v,v)$, where $a(\cdot,\cdot)$ is defined as in equation (5.9), and $e = u - u_h$, where u denotes the exact solution and u_h the LSFEM solution. Then we have

$$|||e|||^2 = a(e,e) = (\mathcal{L}(u-u_h), \mathcal{L}(u-u_h)) = \|f - \mathcal{L}u_h\|^2 = \|R(u_h)\|^2. \quad (8.1)$$

This exact representation of the error is only of interest as an error estimate if the energy norm is a relevant quantity, but it is never the less a natural indicator for mesh refinement. However, if the bilinear form is coercive with respect to an appropriate norm, e.g. the H^1-norm, we also get a relevant error estimator. This is then no longer an exact representation.

This estimator has been used as mesh refinement indicator for most LSFEM computations in this thesis. In Papers V and VI, we apply a version of the energy error estimator by Beck *et al.* [7]. For the derivation of this estimator, we refer to their paper.

8.3 Estimates based on duality

For a better estimate, one can introduce a dual problem which, loosely speaking, describes error propagation and the stability of the problem. This dual problem can then be solved and used in the error estimate. By varying data it is possible to achieve estimates in different norm or for various functionals of the solution. In Paper I, we used a duality argument to prove a priori convergence results for LSFEM applied to the magnetostatic problem.

8.4 Mesh refinement algorithms

It is clear that adaptively refined meshes are crucial in order to achieve good convergence [28][31], but there are many ways to perform this refinement process. First of all, there is the choice of which mesh refinement indicator to use; a choice that depends on the finite element method, which quantity to minimize, and in which norm [43]. In LSFEM, as noted in Section 8.2, there is an indicator naturally imposed by the least-squares functional which also may act as an a posteriori error estimate, depending on the coercivity of the bilinear form.

There is also the choice of how to split an element marked for refinement. In most computations in this thesis, isotropic mesh refinement was used. By this, we mean that one or more of the element's edges were split in halves starting with the longest edge. This procedure yields shape regular meshes without stretched elements; see Paper IV for more details.

In some applications it is necessary to use anisotropic mesh refinement which allows elements which are very thin in one direction. For Paper VI, where the eddy currents only exist in thin layers on the conductor surfaces, we extended the work on a posteriori analysis for anisotropic meshes by Siebert [50] and the work on anisotropic interpolation estimates by Apel [2] to the eddy current problem formulated with edge elements on hexahedrals.

9 General environment for finite element computations

All computations in this thesis has been performed using a finite element software developed by Bergström in cooperation with Levenstam, Samuelsson and Liu. The code is written in C++ and implements a general framework for finite element computations, including several different element types and an easy realization of different equation formulations. For a more thorough description of implementation details, we refer to Paper IX.

10 Summary of papers

10.1 Paper I

Least-Squares Finite Element Methods with Applications in Electromagnetics: In this paper we apply the least-squares finite element method (LSFEM) to two magnetostatic test cases, supplied by ABB Corporate Research, and a common time-harmonic test problem. We prove basic error estimates for

the method formulated with weak enforcement of boundary and interface conditions. We find that, in general, it is uncertain when LSFEM yields a correct solution, since the least-squares functional may not converge to zero due to the low regularity of the exact solution. However, we prove by duality arguments that convergence can be achieved in certain quantities, such as the magnetic energy, even in many of these cases. We present numerical computations in three spatial dimensions, illustrating our theoretical results.

10.2 Paper II

Discontinuous/Continuous Least-Squares Finite Element Methods for Elliptic Problems: Here, we propose a hybrid least-squares formulation combining discontinuous/continuous approximation in the vicinity of geometric singularities, where standard LSFEM fails, with continuous approximation elsewhere. The larger discontinuous approximation space enables us to avoid the strong regularity requirements normally present for LSFEM and exploit the natural stability of the problem, thus obtaining a convergent scheme even for problems with singularities. We prove stability and optimal a priori error estimates for the proposed scheme. The method is demonstrated by numerical examples for the first order Poisson system posed on three dimensional domains with corners. The problems include line and point singularities and discontinuous coefficients.

10.3 Paper III

Discontinuous Least-Squares Finite Element Methods for the Div-Curl Problem: In this paper we extend the formulation in Paper II to include the div-curl system. An analysis, including stability and error estimates, is presented for a model problem. We successfully solve both the Poisson system of Paper II, now stabilized with a curl-term, as well as a problem from Paper I where standard LSFEM encountered difficulties.

10.4 Paper IV

The $\mathcal{LL}^*$ Finite Element Method and Multigrid for the Magnetostatic Problem: This paper was presented at the *GAMM Workshop on CEM* held in Kiel in January 2001. The $\mathcal{LL}^*$ finite element method [22] is applied to the magnetostatic system (2.11) and the resulting discrete system is solved using multigrid techniques. We derive an a posteriori error estimate for the error in magnetic energy, and implement this estimate in an adaptive mesh refinement algorithm. Introducing a suitable scaling, we note that this method is

identical to a vector potential formulation using Coulumb gauging with the penalty weight equal to one.

10.5 Paper V

Eddy Current Computations Using Adaptive Grids and Edge Elements, published in IEEE Trans. Mag., vol. 38, 2002: This paper was presented by Dr. Liu at the *CompuMag* conference in the summer of 2001. We employ tetrahedral edge elements in an ungauged potential formulation together with adaptive mesh refinement techniques to compute the eddy currents in a model of a hydrogenerator. In the absence of a gauge condition, a procedure to assure solvability of the resulting algebraic system of equations is presented. The use of the ungauged formulation with vector and scalar potentials significantly improves the rate of convergence for the iterative algebraic solver, and the reasons for this improvement are discussed.

10.6 Paper VI

Edge Element Computations of Eddy Currents in Laminated Materials, submitted to IEEE Trans. Mag.: This paper will be presented by Dr. Liu at the 10th International IGTE Symposium on Numerical Field Calculation in Electrical Engineering in Graz, Austria, in September 2002. Here, we apply the formulation presented in Paper V to three dimensional computations of the power dissipation in laminated conductors. Results for hexahedral and tetrahedral elements are compared and we conclude that hexahedral elements aligned with the laminations give best results. Anisotropic mesh refinements techniques as described in section 8.4 are also included in the paper.

10.7 Paper VII

FEM Algorithms for Maxwell's Equations: This paper was presented by Rylander at *EMB 98 - Electromagnetic Computations for Analysis and Design of Complex Systems* in Linköping 1998. The paper is a joint contribution by Chalmers Finite Element Center presenting the activity in computational electromagnetics, including field computations using edge element by Rylander and Bondesson, together with results of Bergström, Levenstam, and Johnson using node based schemes for the time dependent Maxwell equations.

10.8 Paper VIII

Dispersion Analysis of Galerkin Least Squares Approximations of Maxwell's Equations: The results of this paper were presented at *Mathematical and Numerical Aspects of Wave Propagation* in Santiago de Compostela, Spain, in 2000 and appears in the printed proceedings. A formulation for electromagnetic wave propagation based on a standard Galerkin approach together with a least-squares formulation is analyzed. We show that the dispersion properties for this mixed formulation is superior to both the standard Galerkin scheme and the least-squares method on their own.

10.9 Paper IX

Object Oriented Implementation of a General Finite Element Code: This technical report describes the structure of our code developed for general finite element computations. The code is written in C++ and utilizes the possibilities of this language to offer easy extension of the code to new problems, element types, quadrature rules, etc. This report is included in the thesis in order to complement Papers I-VIII by supplying more details on the software used to perform the numerical computations.

References

[1] H. Ammari, A. Buffa, and J.-C. Nédélec. A justification of eddy currents model for the maxwell equations. *SIAM J. Appl. Math.*, 60(5):1805–1823, 2000.

[2] T. Apel. Interpolation of non-smooth functions on anisotropic finite element meshes. *Math. Model. Numer. Anal.*, 33(6):1149–1185, 1999.

[3] D.N. Arnold, R.S. Falk, and R. Winther. Multigrid in $H(\mathrm{div})$ and $H(\mathrm{curl})$. *Numer. Math.*, 85:197–217, 2000.

[4] F. Assous, P. Ciarlet, and E. Sonnendrücker. Resolution of the Maxwell equations in a domain with reentrant corners. *Modél. Math. Anal. Numér.*, 32(3):359–389, 1998.

[5] G. Bao and H. Yang. A least-squares finite element analysis for diffraction problems. *SIAM J. Numer. Anal.*, 37(2):665–682, 2000.

[6] R. Beck and R. Hiptmair. Multilevel solution of the time-harmonic Maxwell's equations based on edge elements. *Int. J. Numer. Meth. Engng*, 45(7):901–20, 10 July 1999.

[7] R. Beck, R. Hiptmair, R.H.W. Hoppe, and B. Wohlmuth. Residual based a posteriori error estimates for eddy current computations. *ESAIM-Mathematical Modelling and Numerical Analysis*, 34:159–182, 2000.

[8] O. Bíró. Edge element formulations of eddy current problems. *Comput. Methods Appl. Mech. Engrg.*, 169(3-4):391–405, 1999.

[9] O. Bíró and K. Preis. On the use of the magnetic vector potential in the finite element analysis of three-dimensional eddy currents. *IEEE Trans. Mag.*, 35(4):3145–3159, 1989.

[10] P.B. Bochev and M.D. Gunzburger. Finite element methods of least-squares type. *SIAM Rev.*, 40(4):789–837, 1998.

[11] D. Boffi. Fortin operator and discrete compactness for edge elements. *Numer. Math.*, 87(2):229–246, 2000.

[12] D. Boffi. A note on the de Rham complex and a discrete compactness property. *Appl. Math. Lett.*, 14(1):33–38, 2001.

[13] A. Bossavit. Solving Maxwell equations in a closed cavity, and the question of 'spurious modes'. *IEEE Trans. Mag.*, 26(2):702–705, 1990.

[14] A. Bossavit. "Hybrid" electric-magnetic methods in eddy-current problems. *Comput. Methods Appl. Mech. Engrg*, 178(3-4):383–91, 3 Aug. 1999.

[15] J.H. Bramble, R.D. Lazarov, and J.E. Pasciak. A least-squares approach based on a discrete minus one inner product for first order systems. *Math. Comp.*, 66(219):935–955, 1997.

[16] J.H. Bramble, R.D. Lazarov, and J.E. Pasciak. Least-squares for second order elliptic problems. *Comput. Methods in Appl. Mech. Engrg.*, 152:195–210, 1998.

[17] J.H. Bramble, R.D. Lazarov, and J.E. Pasciak. Least-squares methods for linear elasticity based on a discrete minus one inner product. *Comput. Methods Appl. Mech. Engrg.*, 191(8-10):727–744, 2001.

[18] S.C. Brenner and L.R. Scott. *The Mathematical Theory of Finite Element Methods*. Springer-Verlag, 1994.

[19] F. Brezzi, J. Douglas, Jr., M. Fortin, and L.D. Marini. Efficient rectangular mixed finite elements in two and three space variables. *RAIRO Modél. Math. Anal. Numér.*, 21(4):581–604, 1987.

[20] F. Brezzi, J. Douglas, Jr., and L. D. Marini. Recent results on mixed finite element methods for second order elliptic problems. In *Vistas in applied mathematics*, pages 25–43. Optimization Software, New York, 1986.

[21] F. Brezzi and M. Fortin. *Mixed and Hybrid Finite Element Methods*. Springer-Verlag, 1991.

[22] Z. Cai, T.A. Mantueffel, S.F. McCormick, and J. Ruge. First-order system $\mathcal{LL}^*$ (FOSLL*):scalar elliptic partial differential equations. submitted, 2000.

[23] Y. Cao and M.D. Gunzberger. Least-squares finite element approximations to solutions of interface problems. *SIAM J. Numer. Anal.*, 35(1):393–405, 1998.

[24] S. Caorsi, P. Fernandes, and M. Raffetto. On the convergence of Galerkin finite element approximations of electromagnetic eigenproblems. *SIAM J. Numer. Anal.*, 38(2):580–607, 2000.

[25] Z.M. Chen, Q. Du, and J. Zou. Finite element methods with matching and nonmatching meshes for Maxwell equations with discontinuous coefficients. *SIAM J. Numer. Anal.*, 37:1542–1570, 2000.

[26] M. Costabel and M. Dauge. Singularities of Maxwell's equations on polyhedral domains. In *Analysis, numerics and applications of differential and integral equations*, number 379 in Pitman Res. Notes Math. Ser., pages 69–76. Longman, Harlow, 1998.

[27] C.L. Cox and G.J. Fix. On the accuaracy of least squares methods in the presence of corner singularities. *Comp. & Maths. with Appls.*, 10(6):463–475, 1984.

[28] E. Dari, R.G. Durán, and C. Padra. Maximum norm estimators for three-dimensional elliptic problems. *SIAM J. Numer. Anal.*, 37(2):683–700, 2000.

[29] L. Demkowicz, P. Monk, L. Vardapetyan, and W. Rachowicz. de Rham diagram for *hp* finite element spaces. *Comput. Math. Appl.*, 39(7-8):29–38, 2000.

[30] K. Fujiwara, T. Nakata, and H. Ohashi. Improvement of convergence characteristic of ICCG method for the A-phi method using edge elements. *IEEE Trans. Mag.*, 32(3):804–7, May 1996.

[31] P. Ingelström, T. Rylander, K. Samuelsson, and A. Bondeson. Adaptive mesh techniques for the FEM-FDTD hybrid solver. In *Conference Proceedings, EMB 01 - Electromagnetic Computations*, Uppsala, Sweden, 2001.

[32] B.-N. Jiang. *Least-squares finite element method : Theory and applications in computational fluid dynamics and electromagnetics.* Springer-Verlag, 1998.

[33] B.-N. Jiang, J. Wu, and L.A. Povinelli. The origin of spurious solutions in computational electromagnetics. *J. Comp. Phys.*, 125:104–123, 1996.

[34] J. Jin. *The Finite Element Method in Electromagnetics.* John Wiley & Sons, Inc., 1993.

[35] P. Joly and C. Poirer. A new second order 3D edge element on tetrahedra for time dependent Maxwell's equations. In A. Bermúdez, D. Gómez, C. Hazard, P. Joly, and J.E. Roberts, editors, *Mathematical*

and numerical aspects of wave propagation, SIAM Proceedings, pages 842–847, 2000.

[36] F. Kikuchi. Theoretical analysis of Nedelec's edge elements. *Japan J. Indust. Appl. Math.*, 18(2):321–333, 2001. Recent topics in mathematics moving toward science and engineering.

[37] J.F. Lee, R. Lee, and A. Cangellaris. Time-domain finite-element methods. *IEEE Trans. Antennas. Propagat.*, 45(3):430, 1997.

[38] R.L. Lee and N.K. Madsen. A mixed finite element formulation for Maxwell's equations in the time domain. *J. Comput. Phys.*, 88(2):284–304, 1990.

[39] T.A. Manteuffel, S.F. McCormick, and G. Starke. First-order system of least-squares for second order elliptic problems with discontinuous coefficients. To appear.

[40] P. Monk. A comparison of three mixed methods for the time-dependent Maxwell's equations. *SIAM J. Sci. Statist. Comput.*, 13(5):1097–1122, 1992.

[41] P. Monk and L. Demkowicz. Discrete compactness and the approximation of Maxwell's equations in $\mathbf{R}^3$. *Math. Comp.*, 70(234):507–523, April 2001.

[42] P. Monk and A.K. Parrot. A dispersion analysis of finite element methods for Maxwell's equations. *SIAM J. Sci. Comp.*, 15(4):916–937, 1994.

[43] P. Monk and E. Süli. The adaptive computation of far-field patterns by a posteriori error estimation of linear functionals. *SIAM J. Numer. Anal.*, 36(1):251–274, 1998.

[44] P. Monk and D.-Q. Wang. A least-squares method for the Helmholtz equation. *Comput. Metods Appl. Mech. Engrg.*, 175:121–136, 1999.

[45] J.-C. Nédélec. Mixed finite elements in $\mathbf{R}^3$. *Numer. Math.*, 35(3):315–341, 1980.

[46] K.D. Paulsen and D.R. Lynch. Elimination of vector parasites in finite element Maxwell solutions. *IEEE Trans. Microwave Theory Tech.*, 39(3):395–404, 1991.

[47] K.D. Paulsen, D.R. Lynch, and J.W. Strohbehn. Three-dimensional finite, boundary, and hybrid element solutions of the Maxwell equations for lossy dielectric media. *IEEE Trans. Microwave Theory Tech.*, 36(4):682–693, 1988.

[48] P.-A. Raviart and J. M. Thomas. A mixed finite element method for 2nd order elliptic problems. In *Mathematical aspects of finite element methods (Proc. Conf., Consiglio Naz. delle Ricerche (C.N.R.), Rome, 1975)*, pages 292–315. Lecture Notes in Math., Vol. 606. Springer, Berlin, 1977.

[49] T. Rylander and A. Bondeson. Stable FEM-FDTD hybrid method for Maxwell's equations. *Comput. Phys. Comm.*, 125:75–82, March 2000.

[50] K.G. Siebert. An a posteriori error estimator for anisotropic refinement. *Numer. Math.*, 73(3):373–398, 1996.

[51] M. Touma Holmberg. *Three-dimensional Finite Element Computation of Eddy Currents in Synchronous Machines.* PhD thesis, Dept. of Electric Power Engineering, Chalmers University of Technology, 1998.

[52] J.Y. Wu and R. Lee. The advantages of triangular and tetrahedral edge elements for electromagnetic modeling with the finite-element method. *IEEE Trans. Antennas Propagat.*, 45(9), 1997.

[53] K.S. Yee. Numerical solution of initial boundary value problems involving Maxwell's equations in isotropic media. *IEEE Trans. Antennas Propagat.*, AP-14:302–307, May 1966.

[54] J.M. Yin. *The Finite Element Method in Electromagnetics.* John Wiley & Sons, 1993.

Paper I

Least-Squares Finite Element Methods with Applications in Electromagnetics *

Rickard Bergström†

Abstract

We investigate the application of the least-squares finite element method (LSFEM) to static and time harmonic Maxwell's equations in three spatial dimensions in cases of industrial significance. We find analytically and numerically that, with suitable residual weighting and mesh adaptivity, LSFEM gives satisfactory results for problems with discontinuous magnetic permeabilities of largely different orders of magnitude, but without strong corner singularities.

1 Introduction

In a least-squares finite element method (LSFEM) a sum of suitable residual norms is minimized over a piecewise polynomial space. The residuals may contain differential equations, constitutive equations, interface and boundary conditions.

LSFEM is a general method with the following features, see, e.g., Bochev and Gunzberger [5], Jiang [12], and [1]:

- applicability to general, possibly overspecified, first order systems,
- stability follows directly from well posedness of the continuous problem,
- essential boundary conditions may be imposed weakly, and
- the resulting discrete system of equations is symmetric positive definite.

*This research is supported by ABB Corporate Research

†Supported by the Swedish Foundation for Strategic Research through the National Graduate School in Scientific Computing and the National Network in Applied Mathematics

In particular, LSFEM is applicable to Maxwell's equations in first order form. With the divergence equations included, LSFEM does not suffer from the spurious solutions which may occur in certain Galerkin methods, see, e.g., Jiang, Wu, and Povinelli [13] and the book by Jiang [12].

The strong norm residual minimization of LSFEM in its standard form, makes computation of singular solutions difficult. Another difficulty concerns the weighting of the different residuals. In this paper, we address these problems, with focus on static and time harmonic problems.

The paper is organized as follows. In Section 2 we present the magnetostatic problem and formulate the least-squares method, in Section 3 we prove a priori and a posteriori estimates, in Section 4 we apply the method to magnetostatic problems, and in Section 5 we extend the method to time-harmonic problems.

2 The least-squares finite element method

2.1 A magnetostatic model problem

Assume that $\Omega = \bigcup_{i=1}^{n} \Omega^i$ is a domain in $\mathbf{R}^3$, where Ω and each Ω^i are bounded and either of class $\mathcal{C}^{1,1}$, but may be non-convex, or convex, and denote the interface between regions Ω^i and Ω^j by Γ^{ij}, with $i < j$, see Figure 1.

Let

$$\mathcal{V} = \bigoplus_{i=1}^{n} \mathcal{V}^i, \tag{2.1}$$

with $\mathcal{V}^i = [H^1(\Omega^i)]^3$. Assume that each subdomain have the magnetic permeability $\mu|_{\Omega^i} = \mu_r^i \, \mu_0$ where $\mu_r^i > 0$ is constant and μ_0 is the magnetic permeability in free space, $\mu_0 = 4\pi \times 10^{-7}$ H/m. The magnetostatic system then takes the form: find $B \in \mathcal{V}$ such that

$$\nabla \times \mu^{-1} B = J \quad \text{in } \Omega^i, \tag{2.2a}$$

$$\nabla \cdot B = 0 \quad \text{in } \Omega^i, \tag{2.2b}$$

$$B \cdot n = 0 \quad \text{on } \Gamma, \tag{2.2c}$$

and the interface conditions

$$[\mu^{-1} B \times n] = 0 \quad \text{on } \Gamma^{ij}, \tag{2.3a}$$

$$[B \cdot n] = 0 \quad \text{on } \Gamma^{ij}, \tag{2.3b}$$

hold. Here n is the exterior unit normal on the boundary Γ and a fixed unit normal on each interior interface Γ^{ij}, and $[u(x)] = \lim_{s\to 0^+} u(x+sn) - u(x-sn)$ with $x \in \Gamma^{ij}$, denotes the jump in u across the interface Γ^{ij}.

Remark 2.1 The assumption that the domains are convex or of class $\mathcal{C}^{1,1}$ is not realistic for engineering applications where we typically only have Lipschitz domains. We will discuss and relax this regularity constraint when we have proved error estimates in Section 3.

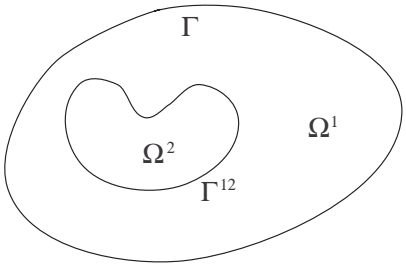

Figure 1: The notation used when a region is split into subregions.

2.2 Finite element spaces

Let $\mathcal{K}^i, i = 1, \ldots, n$, be decompositions of the subdomains Ω^i into, e.g., tetrahedral, elements K, and let $\mathcal{K} = \cup_{i=1}^n \mathcal{K}^i$ denote the resulting decomposition of Ω. Let h denote the mesh function defined by $h|_K = h_K = \mathrm{diam}(K)$, i.e., a measure of the local size of the elements in the mesh, and let $\hat{h} = \max_{K\in\mathcal{K}} h(K)$ denote the global mesh size. Non-matching meshes are allowed, but we assume local quasi-uniformity and a minimal angle condition on the triangulation, see Brenner and Scott [8]. Let

$$\mathcal{V}_h = \bigoplus_{i=1}^{n} \mathcal{V}_h^i, \tag{2.4}$$

with $\mathcal{V}_h^i$ defined by

$$\mathcal{V}_h^i = \{v \in [C^0(\overline{\Omega}^i)]^3 : v|_K \in \mathcal{P}_r(K), \text{for all } K \in \mathcal{K}^i\},$$

where $\mathcal{P}_r$ is the set of all vector polynomials of degree less than or equal to r. Thus $\mathcal{V}_h$ is the set of all piecewise vector polynomial functions of degree

r which are continuous in the subdomains Ω^i such that, in each element, $v|_K \in \mathcal{P}_r(K)$.

For the error analysis following below, we need the following approximation property of $\mathcal{V}_h$, see, e.g., [14] for a proof. There is an interpolation operator $\pi = \bigoplus_{i=1}^n \pi^i$ with $\pi^i : [H^1(\Omega^i)]^3 \mapsto \mathcal{V}_h$ such that for $v \in \bigoplus_{i=1}^n [H^s(\Omega^i)]^3$, it holds

$$\|v - \pi v\|_{m,K} \leq C h_K^{\alpha-m} |v|_{\alpha,S(K)}, \quad m = 0, 1, \tag{2.5}$$

where $\alpha = \min(r+1, s)$, $S(K)$ is the patch of elements neighboring K, and the constant C is independent of the mesh parameter h.

2.3 The least-squares finite element method with weak boundary and interface conditions

The solution B to problem (2.2)–(2.3) minimizes the least-squares functional

$$\begin{aligned} I(B) = \sum_{i=1}^{n} \Big(\|\mu(\nabla \times (\mu^{-1} B) - J)\|_{\Omega^i}^2 + \|\nabla \cdot B\|_{\Omega^i}^2 \Big) \\ + \sum_{1 \leq i < j \leq n} \Big(\|h^{-1/2} \tilde{\mu} [\mu^{-1} B \times n]\|_{\Gamma^{ij}}^2 + \|h^{-1/2} [B \cdot n]\|_{\Gamma^{ij}}^2 \Big) \\ + \|h^{-1/2} [B \cdot n]\|_{\Gamma}^2. \end{aligned} \tag{2.6}$$

Here we have introduced a weight μ in the volume integral terms containing the curl equation. This is a natural scaling of the equations and the least-squares functional is thus better balanced between the curl and the divergence conditions. The parameter $\tilde{\mu}$ corresponds to the multiplication with μ in the volume integrals, but is an average value since μ is not defined on the interface. We will return to the exact definition of this average. Moreover, on the boundary and interfaces, the $L^2(\Gamma)$-norm scaled by $h^{-1/2}$ has been used instead of the computationally cumbersome $H^{1/2}(\Gamma)$-norm, see Bochev and Gunzberger [5] and the references therein. For non-matching meshes it may be necessary to use an average also for h. The least-squares method amounts to finding this minimizer: find $B \in \mathcal{V}$ such that

$$I(B) = \inf_{v \in \mathcal{V}} I(v). \tag{2.7}$$

Remark 2.2 Note that the boundary condition (2.2c) and the interface conditions (2.3) are imposed weakly. Strongly imposed boundary and interface conditions have been suggested in e.g. Jiang, Wu, and Povinelli [13],

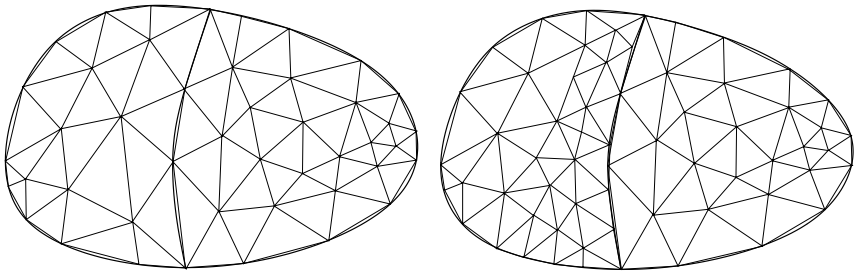

(a) *Conforming triangulation* (b) *Non-conforming triangulation*

Figure 2: Examples of matching and non-matching triangulations of two subdomains. In the first case, we have the choice of both strong and weak enforcement of interface conditions. For the non-matching grid, however, we must use weak enforcement.

but are non-trivial to implement in polyhedral domains since the normal is not defined everywhere. Further, enforcement through the least-squares functional makes it possible to use different finite element spaces on either side of the surfaces, and the convergence properties of the method is better when using weakly imposed conditions, see Costabel and Dauge [11] and Bao and Yang [3].

A necessary condition for a function $B \in \mathcal{V}$ to satisfy equation (2.7), is

$$\lim_{\tau \to 0} \frac{\partial}{\partial \tau} I(B + \tau \tilde{B}) \equiv 2(a(B, \tilde{B}) - l(\tilde{B})) = 0, \tag{2.8}$$

for all $\tilde{B} \in \mathcal{V}$, where

$$\begin{aligned} a(B, \tilde{B}) = \sum_{i=1}^{n} & (\nabla \times B, \nabla \times \tilde{B})_{\Omega^i} + (\nabla \cdot B, \nabla \cdot \tilde{B})_{\Omega^i} \\ & + \sum_{1 \le i < j \le n} \Big((h^{-1} \tilde{\mu} [\mu^{-1} B \times n], \tilde{\mu} [\mu^{-1} \tilde{B} \times n])_{\Gamma^{ij}} \\ & \quad + (h^{-1} [B \cdot n], [\tilde{B} \cdot n])_{\Gamma^{ij}} \Big) \\ & + (h^{-1} B \cdot n, \tilde{B} \cdot n)_{\Gamma}, \end{aligned} \tag{2.9}$$

and

$$l(\tilde{B}) = \sum_{i=1}^{n} (\mu J, \mu \nabla \times (\mu^{-1} \tilde{B}))_{\Omega^i}. \tag{2.10}$$

Thus seeking a minimizer to I in $\mathcal{V}$ leads to the variational problem: find $B \in \mathcal{V}$ such that

$$a(B, \tilde{B}) = l(\tilde{B}), \tag{2.11}$$

for all $\tilde{B} \in \mathcal{V}$.

The least-squares finite element method is defined by seeking an approximation B_h in $\mathcal{V}_h$ such that

$$I(B_h) = \inf_{v \in \mathcal{V}_h} I(v), \tag{2.12}$$

with corresponding variational form: find $B_h \in \mathcal{V}_h$ such that

$$a(B_h, \tilde{B}) = l(\tilde{B}), \tag{2.13}$$

for all $\tilde{B} \in \mathcal{V}_h$.

3 Error estimates

3.1 A priori error estimates

We begin by introducing the energy norm

$$|||v|||^2 = a(v, v) \quad \text{for } v \in \mathcal{V}, \tag{3.1}$$

Under our assumptions, $|||\cdot|||$ is a norm in $\mathcal{V}$ when there exists a unique solution to problem (2.2)–(2.3).

Further, we have the following interpolation error estimate.

Lemma 3.1 *If $v \in \bigoplus_{i=1}^{n}[H^s(\Omega)]^3, s \geq 1$, then there is an interpolation operator $\pi : \bigoplus_{i=1}^{n}[H^s(\Omega)]^3 \mapsto \mathcal{V}_h$ such that*

$$|||v - \pi v||| \leq C\hat{h}^{\alpha-1}|v|_\alpha, \tag{3.2}$$

with $\alpha = \min(r+1, s)$ and where C only depends on μ and Ω.

Proof. Let $\eta = v - \pi v$. We show that

$$|||\eta|||^2 \leq C \sum_{K \in \mathcal{K}} h_K^{-2}\|\eta\|_K^2 + |\eta|_{1,K}^2. \tag{3.3}$$

The desired result (3.2) then follows from (2.5). For the interior terms, we directly have

$$\|\nabla \times \eta\|_K^2 \leq C|\eta|_{1,K}^2, \tag{3.4}$$

and

$$\|\nabla \cdot \eta\|_K^2 \leq C|\eta|_{1,K}^2. \tag{3.5}$$

For the boundary term we get

$$\begin{aligned} \|h^{-1/2}\eta \cdot n\|_\Gamma^2 &= \sum_{\{K\in\mathcal{K}:\partial K\cap\Gamma\neq\emptyset\}} \|h^{-1/2}\eta\cdot n\|_{\partial K\cap\Gamma}^2 \\ &\leq \sum_{\{K\in\mathcal{K}:\partial K\cap\Gamma\neq\emptyset\}} Ch_K^{-1}\|\eta\|_K(h_K^{-1}\|\eta\|_K + |\eta|_{1,K}) \\ &\leq C \sum_{\{K\in\mathcal{K}:\partial K\cap\Gamma\neq\emptyset\}} h_K^{-2}\|\eta\|_K^2 + |\eta|_{1,K}^2, \end{aligned} \tag{3.6}$$

where we used the trace inequality $\|v\|_{\partial K}^2 \leq C\|v\|_K(h_K^{-1}\|v\|_K + |v|_{1,K})$. Finally, for the interface jump terms we use the triangle inequality

$$\|h^{-1/2}\,[\eta\cdot n]\|_{\Gamma^{ij}}^2 \leq \|h^{-1/2}\,\eta^i\cdot n\|_{\Gamma^i}^2 + \|h^{-1/2}\,\eta^j\cdot n\|_{\Gamma^j}^2, \tag{3.7}$$

and

$$\begin{aligned} \|h^{-1/2}\,\tilde{\mu}\,[\mu^{-1}\eta\times n]\|_{\Gamma^{ij}}^2 \leq \|h^{-1/2}\,\tilde{\mu}\,(\mu^i)^{-1}\,\eta^i\times n\|_{\Gamma^i}^2 \\ + \|h^{-1/2}\,\tilde{\mu}\,(\mu^j)^{-1}\,\eta^j\times n\|_{\Gamma^j}^2, \end{aligned} \tag{3.8}$$

and then treat them with the same technique as for the boundary term. □

Remark 3.1 If the meshes $\mathcal{K}^i$ match on the interfaces and πv satisfies the interface conditions (2.3), then the constant C is also independent of μ since the interface terms vanish.

Now we are ready to state the following result:

Theorem 3.2 *Let $B \in \bigoplus_{i=1}^n [H^s(\Omega)]^3$ be a solution to (2.11) and $B_h \in \mathcal{V}_h$ the approximate solution defined by (2.13). Then there is a constant C, independent of h, such that*

$$|||B - B_h||| \leq C\hat{h}^{\alpha-1}|B|_\alpha, \tag{3.9}$$

with $\alpha = \min(r+1, s)$.

Proof. Let $e = B - B_h$ denote the error. Then

$$\begin{aligned} |||e|||^2 &= a(e, B - B_h) \\ &= a(e, B - \pi B + \pi B - B_h) \\ &= a(e, B - \pi B), \end{aligned} \tag{3.10}$$

where we use the Galerkin orthogonality $a(e, \tilde{B}) = 0$, for $\tilde{B} \in \mathcal{V}_h$, in the last equality. Using the Cauchy-Schwarz inequality and dividing by $|||e|||$ we arrive at

$$\begin{aligned} |||e||| &\leq |||B - \pi B||| \\ &\leq C\hat{h}^{\alpha-1}|B|_\alpha, \end{aligned} \tag{3.11}$$

where we used Lemma 3.1 in the last inequality. □

3.2 A posteriori error estimates

A simple calculation gives that the energy norm of the error when using a bilinear form derived from least-squares principles simply equals the residual. Thus we can state the following a posteriori error estimate in the energy norm.

Theorem 3.3 *Let $B \in \mathcal{V}$ be a solution to (2.11) and $B_h \in \mathcal{V}_h$ the approximate solution defined by (2.13). Then*

$$|||B - B_h|||^2 = \sum_{K \in \mathcal{K}} \mathcal{R}_K(B_h) \cdot \mathcal{R}_K(B_h) \tag{3.12}$$

where the element residual $\mathcal{R}_K(B_h) \in \mathbf{R}^4$ is defined by

$$\mathcal{R}_K(B_h) = \begin{bmatrix} \|\mu(\nabla \times \mu^{-1} B_h - J)\|_K \\ \|\nabla \cdot B_h\|_K \\ \frac{1}{\sqrt{2}} \|h^{-1/2} \tilde{\mu}[\mu^{-1} B_h \times n]\|_{\partial K \setminus \Gamma} \\ \|\frac{1}{\sqrt{\alpha}} h^{-1/2} [B_h \cdot n]\|_{\partial K} \end{bmatrix}, \tag{3.13}$$

where α is a function, such that $\alpha = 1$ on faces F with $F \cap \Gamma \neq \emptyset$ and $\alpha = 2$ otherwise.

Remark 3.2 Under our assumptions, these results are meaningful since we have enough regularity on the solution B. In more realistic situations where Ω is only Lipschitz, we have $B \in \bigoplus_{i=1}^{n}[H^s(\Omega)]^3$ for $s \in (1/2, 1]$, see Amrouche, Bernardi, Dauge and Raviart [2], and the least-squares finite element method generally fails to converge to the correct solution, see e.g. Bramble, Lazarov and Pasciak [7] or the regularity results of Costabel [10]. However, the use of weak boundary and interface conditions still gives a theoretical convergence, see Costabel and Dauge [11].

For many applications, one wants to measure the error in other quantities than the energy norm. In the remainder of this section, we use duality arguments to derive an a posteriori estimate for the the error in energy,

$$W_{error} = \frac{1}{2}\int_{\Omega} \mu^{-1}|B|^2 - \frac{1}{2}\int_{\Omega} \mu^{-1}|B_h|^2. \tag{3.14}$$

Moreover, this estimate shows that we can have convergence even when $B \notin \mathcal{V}$, as is the case for a general Lipschitz domain with corners.

3.2.1 Definition of the dual problem

To prove estimates of the error in the energy, we start by studying the following problem: find $(\phi, p) \in H^s(\nabla\times, \Omega) \times H_0^1(\Omega)$ satisfying

$$\nabla \times \mu\nabla \times \phi - \nabla p = \Psi \quad \text{in } \Omega^i, \tag{3.15a}$$
$$\nabla \cdot \phi = \psi \quad \text{in } \Omega^i, \tag{3.15b}$$
$$p = 0, \quad \phi \times n = 0 \quad \text{on } \Gamma, \tag{3.15c}$$

with interface condition

$$[\mu^{-1}\phi \times n] = 0 \quad \text{on } \Gamma^{ij}, \tag{3.16a}$$
$$[\phi \cdot n] = 0 \quad \text{on } \Gamma^{ij}, \tag{3.16b}$$
$$[\mu\nabla \times \phi \times n] = 0 \quad \text{on } \Gamma^{ij}, \tag{3.16c}$$
$$[p] = 0 \quad \text{on } \Gamma^{ij}. \tag{3.16d}$$

Here we introduced the space $H^s(\nabla\times, \Omega) = \{v \in [H^s(\Omega)]^3 : \nabla \times v \in [H^s(\Omega)]^3\}$. This problem is analysed in Chen, Du, and Zou [9], where it is shown that there exists a unique solution. Furthermore, $p \equiv 0$ for all Ψ with $\nabla \cdot \Psi = 0$.

3.2.2 Estimate of the error in energy

Using the Helmholtz decomposition, see e.g. Bossavit [6], we can write the error $e = B - B_h = B^0 - (B_h^0 + B_h^\perp)$, where we have $\nabla \cdot F^0 = 0$, and $F^\perp = \nabla f$ for some scalar function f. We choose

$$\Psi = B^0 + B_h^0, \tag{3.17}$$

making $\nabla \cdot \Psi = 0$ and thus $p = 0$, and ψ such that it satisfies the auxiliary weak problem: find $\psi \in H^1(\Omega)$ such that

$$(\nabla\psi, \nabla v) = \sum_{i=1}^{n} (\nabla \cdot (\mu^{-1} B_h^\perp), v)_{\Omega^i} - \sum_{1 \le i < j \le n} ([\mu^{-1} B_h^\perp \cdot n], v)_{\Gamma^{ij}}, \tag{3.18}$$

for all $v \in H^1(\Omega)$. This problem is well posed and we have the equality $-(\nabla\psi, B_h^\perp) = (\mu^{-1} B_h^\perp, B_h^\perp)$ since $B_h^\perp$ is a gradient of a scalar function.

Taking the inner product of (3.15a) with $\mu^{-1} e^0 = \mu^{-1}(B^0 - B_h^0)$ and of (3.15b) with $\nabla \cdot e^\perp = -\nabla \cdot B^\perp$, yields for the right hand side

$$\begin{aligned} &(\mu^{-1} B^0, B^0) - (\mu^{-1} B_h^0, B_h^0) - (\psi, \nabla \cdot B_h^\perp) \\ &\quad = (\mu^{-1} B^0, B^0) - (\mu^{-1} B_h^0, B_h^0) + (\nabla\psi, B_h^\perp) \\ &\qquad - (\psi, [B_h^\perp \cdot n])_\Gamma - \sum_{1 \le i < j \le n} (\psi, [B_h^\perp \cdot n])_{\Gamma^{ij}} \\ &\quad = W_{error} - (\nabla \cdot \phi, [B_h^\perp \cdot n])_\Gamma - \sum_{1 \le i < j \le n} (\nabla \cdot \phi, [B_h^\perp \cdot n])_{\Gamma^{ij}}. \end{aligned} \tag{3.19}$$

We thus get

$$\begin{aligned} W_{error} &= \sum_{i=1}^{n} \Big((\mu^{-1} B^0, B^0)_{\Omega^i} - (\mu^{-1} B_h^0, B_h^0)_{\Omega^i} - (\mu^{-1} B_h^\perp, B_h^\perp)_{\Omega^i} \Big) \\ &\quad + \sum_{1 \le i < j \le n} (\nabla \cdot \phi, [B_h^\perp \cdot n])_{\Gamma^{ij}} + (\nabla \cdot \phi, [B_h^\perp \cdot n])_\Gamma \\ &= \sum_{i=1}^{n} \Big((\nabla \times \mu \nabla \times \phi, \mu^{-1} e^0)_{\Omega^i} - (\nabla p, \mu^{-1} e^0)_{\Omega^i} + (\nabla \cdot \phi, \nabla \cdot e^\perp)_{\Omega^i} \Big) \\ &\quad + \sum_{1 \le i < j \le n} (\nabla \cdot \phi, [e^\perp \cdot n])_{\Gamma^{ij}} + (\nabla \cdot \phi, [e^\perp \cdot n])_\Gamma \end{aligned} \tag{3.20}$$

$$
\begin{aligned}
&= \sum_{i=1}^{n} \Big((\nabla \times \phi, \nabla \times e^0)_{\Omega^i} + (\nabla \cdot \phi, \nabla \cdot e^{\perp})_{\Omega^i} + (\mu^{-1} p, \nabla \cdot e^0)_{\Omega^i} \Big) \\
&\quad + \sum_{1 \le i < j \le n} \Big((\mu \nabla \times \phi, [\mu^{-1} e^0 \times n])_{\Gamma^{ij}} + (\mu^{-1} p, [e^{\perp} \cdot n])_{\Gamma^{ij}} + (\nabla \cdot \phi, [e^{\perp} \cdot n])_{\Gamma^{ij}} \Big) \\
&\quad + (\nabla \cdot \phi, [n \cdot e^{\perp}])_{\Gamma} \\
&= \sum_{i=1}^{n} \Big((\nabla \times \phi, \nabla \times e)_{\Omega^i} + (\nabla \cdot \phi, \nabla \cdot e)_{\Omega^i} \Big) \\
&\quad + \sum_{1 \le i < j \le n} \Big((\mu \nabla \times \phi, [\mu^{-1} e \times n])_{\Gamma^{ij}} + (\nabla \times \phi, [e \cdot n])_{\Gamma^{ij}} \Big) + (\nabla \times \phi, [e^{\perp} \cdot n])_{\Gamma} \\
&= \sum_{i=1}^{n} \Big((\nabla \times (\phi - \pi\phi), \nabla \times e)_{\Omega^i} + (\nabla \cdot (\phi - \pi\phi), \nabla \cdot e)_{\Omega^i} \Big) \\
&\quad + \sum_{1 \le i < j \le n} \Big((h^{1/2} \tilde{\mu}^{-1} \mu \nabla \times \phi + h^{-1/2} [\mu^{-1} (\phi - \pi\phi) \times n], \tilde{\mu} h^{-1/2} [\mu^{-1} e \times n])_{\Gamma^{ij}} \\
&\qquad\qquad + (h^{1/2} \nabla \cdot \phi + h^{-1/2} [(\phi - \pi\phi) \cdot n], h^{-1/2} [e \cdot n])_{\Gamma^{ij}} \Big) \\
&\quad + (h^{1/2} \nabla \cdot \phi + h^{-1/2} [(\phi - \pi\phi) \cdot n], h^{-1/2} [e \cdot n])_{\Gamma}.
\end{aligned}
$$

The following estimate for the error in the energy is thereby proved.

Theorem 3.4 *Let ϕ be the solution to (3.15) with data according to (3.17) and (3.18), B the solution of (2.11), and B_h the LSFEM approximation (2.13), then the error in energy is bounded as*

$$
W(B) - W(B_h) \le \sum_{K \in \mathcal{K}} \mathcal{R}_K(B_h) \cdot \mathcal{W}_K(\phi), \tag{3.21}
$$

where the elementwise residual $\mathcal{R}_K(B_h)$ is defined in (3.13) and the element weight $\mathcal{W}_K(\phi)$ is

$$
\mathcal{W}_K(\phi) = \begin{bmatrix} \|\nabla \times (\phi - \pi\phi)\|_K \\ \|\nabla \cdot (\phi - \pi\phi)\|_K \\ \frac{1}{\sqrt{2}} \|h^{1/2} \tilde{\mu}^{-1} \mu \nabla \times \phi + h^{-1/2} [\mu^{-1} (\phi - \pi\phi) \times n]\|_{\partial K \setminus \Gamma} \\ \|\frac{1}{\sqrt{\alpha}} h^{1/2} \nabla \cdot \phi + h^{-1/2} [(\phi - \pi\phi) \cdot n]\|_{\partial K} \end{bmatrix}, \tag{3.22}
$$

with α as in (3.13).

Remark 3.3 Assuming $\phi \in \bigoplus_{i=1}^{n} [H^{s_\phi}(\Omega)]^3$ and $B \in \bigoplus_{i=1}^{n} [H^{s_B}(\Omega)]^3$, the

most important consequence of Theorem 3.4 is that for a geometry such that $s_\phi + s_B > 2$, we have convergence in the energy even if convergence in the solution itself can not be proved. The analysis in [9] and [2] makes it reasonable to believe that $s_\phi \geq 2s_B$, with $s_B \in (1/2, 1]$, making this true in many cases. A fact further indicated by our numerical experiments.

4 Two magnetostatic problems

4.1 Computational set up

Although not explicitly mentioned in the previous sections, one may also weight the different terms in the least-squares functional by constants without changing the analysis. We have used this possibility to make the enforcement of the interface terms stronger. For the first problem we weighted the terms containing the normal components by a factor 10^3, while the tangential condition was left unweighted. For the second problem considered, we weighted the tangential condition by a factor 10^3 and left the normal condition unweighted. This choice of coefficients has been based on numerical experiments.

Adaptivity was based on the a posteriori result in Theorem 3.4, and an assumed regularity $s_\phi = 4/3$ of ϕ, the solution to the dual problem. We have thus not solved the dual problem numerically. The element indicator used was then

$$I_K = h_K^{1/3} \mathcal{R}_K(B_h), \tag{4.1}$$

with $\mathcal{R}_K(B_h)$ as in equation (3.13).

4.2 Problem 1

4.2.1 Description of the problem

The geometry of this problem is described in Figure 4(a). The problem is axisymmetric in order to make two dimensional computations possible as reference. A three dimensional view can be seen in Figure 5. The model consists of an iron cylinder core encircled by a copper winding. The configuration is enclosed in air and surrounded by a box with perfectly conducting surfaces. The winding is modelled as a homogeneous copper coil.

Data for this problem are relative magnetic permeabilities $\mu_{r,Fe} = 10^4$ and $\mu_{r,Cu} = \mu_{r,air} = 1$ and $\mu_0 = 4\pi \times 10^{-7}$ H/m and the current density J is constant over the cross section of the coil and the total current is 1 A.

	Linear	Quadratic	Reference
No of elements	505 710	247 800	-
No of nodes	91 510	339 936	-
W_{air} (J)	$8.967 \times 10^{-7}(0.013)$	$9.081 \times 10^{-7}(0.001)$	9.089×10^{-7}
W_{cu} (J)	$3.333 \times 10^{-8}(0.078)$	$3.581 \times 10^{-8}(0.009)$	3.614×10^{-8}
W_{fe} (J)	$4.885 \times 10^{-10}(0.033)$	$4.802 \times 10^{-10}(0.015)$	4.731×10^{-10}

Table 1: The computed magnetic energies for Problem 1, using LSFEM and piecewise linear and quadratic polynomial elements, compared with reference values; the relative error is given in parenthesis. The reference values are from two dimensional computations done at ABB [4].

Reference computations in two dimensions done by ABB and reported in [4], gave the values of the magnetic energies in the different materials as listed in Table 1, where the magnetic energy is defined by

$$W_{\Omega^i} = \frac{1}{2} \int_{\Omega^i} B \cdot H \, dx. \tag{4.2}$$

4.2.2 Computational results

This problem was solved successfully to good accuracy, see Table 1. A field line plot is shown in Figure 5. In Figure 3(a) we plot the relative error in the magnetic energy as a function of the degrees of freedom, N, for quadratic and linear polynomial basis functions, and in Figure 3(b) the error indicator (4.1) and the least-squares functional are plotted.

We can note that the rate of convergence is the same for both linear and quadratic polynomials due to the low regularity of the problem, only the accuracy is different. Another indicator of the low regularity is that the least-squares functional does not decrease with refinement, in fact it increases. However, the increase is smaller with quadratic polynomials.

4.3 Problem 2

4.3.1 Description of the problem

The second problem is also an axisymmetric magnetostatic problem, but the geometry is more complicated than in Problem 1. It is given in Figure 4(b). The copper winding is the same, but the iron part has been extended and

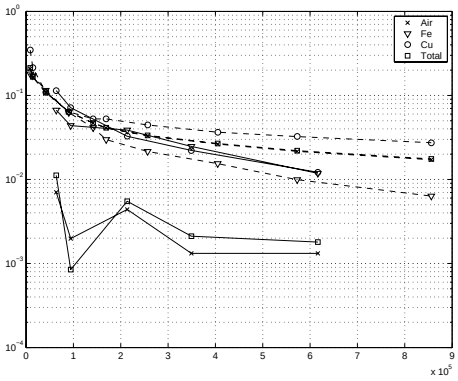

(a) *Relative error in energy in the different parts*

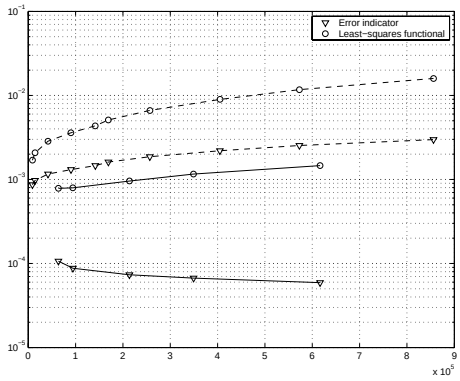

(b) *Error indicator and least-squares functional*

Figure 3: Computations for Problem 1 with quadratic (solid lines) and linear (dashed lines) basis functions.

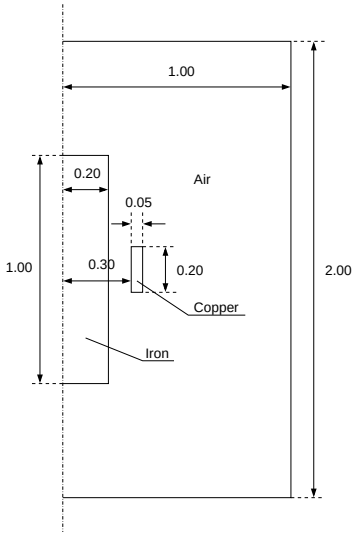

(a) *Problem 1*

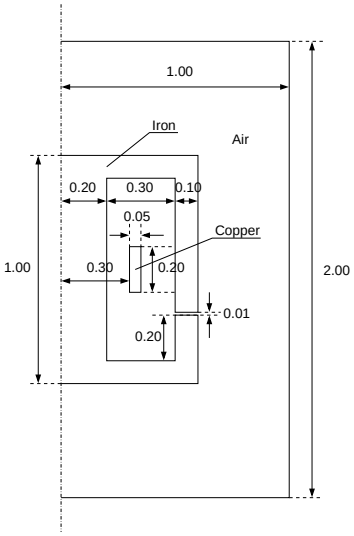

(b) *Problem 2*

Figure 4: Geometry of the two axisymmetric problems. The dimensions are given in meters.

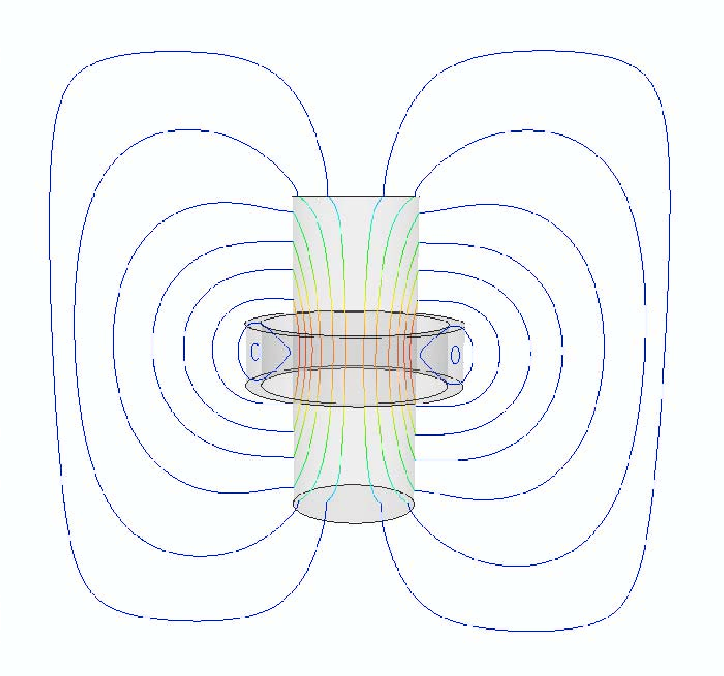

Figure 5: The magnetic field lines in a slice through the three dimensional solution of the axisymmetric Problem 1.

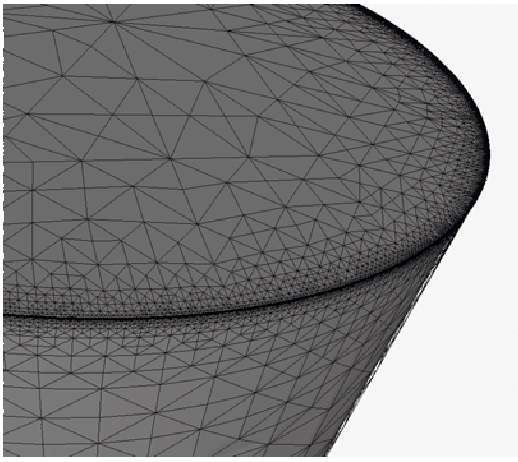

Figure 6: Detail of the mesh after adaptive refinement. The part shown is the top of the iron core of Problem 1.

	Linear	Quadratic	Reference
No of elements	1267028	198863	-
No of nodes	258537	261362	-
W_{air} (J)	$8.199 \times 10^{-7}(0.200)$	$7.573 \times 10^{-7}(0.261)$	1.025×10^{-6}
W_{cu} (J)	$3.274 \times 10^{-8}(0.086)$	$3.345 \times 10^{-8}(0.066)$	3.596×10^{-8}
W_{fe} (J)	$2.113 \times 10^{-6}(0.407)$	$1.516 \times 10^{-6}(0.575)$	3.564×10^{-6}

Table 2: The computed magnetic energies for Problem 2, using LSFEM and piecewise linear and quadratic polynomial elements, compared with reference values. The reference values are from two dimensional computations done at ABB [4].

almost encloses the coil. The problem has been tested with $\mu_{r,Fe} = 10^4$ as well as with $\mu_{r,Fe} = 10^2$, the other data are the same as in Problem 1.

4.3.2 Results

This problem has not been satisfactorily solved with LSFEM. For the case with $\mu_{r,Fe} = 10^2$ we still have convergence, but with poor accuracy, see Figure 7 and Table 2. The computations with $\mu_{r,Fe} = 10^4$ is not successful and not reported further.

We can also see that the use of quadratic polynomials does not give better results, the singularities are too dominant in this geometry.

5 Extension to the time-harmonic case

5.1 Description of the problem

As a third problem the "asymmetrical conductor with a hole problem" [15], as illustrated in Figure 10, has been used. It consists of an aluminium plate with a hole, placed under a copper winding, modeled as a homogeneous coil. There are no symmetries in this problem. The aluminium plate has a conductivity of $\sigma = 3.526 \times 10^7$ S/m and the magnetic permeability is $\mu_{r,Al} = 1$, as in the air and the copper. Since no magnetic material is present there are no singularities as in the previous two problems. Instead, we will get induced eddy currents in the conducting aluminium plate.

The coil is carrying a sinusoidal total current of 2742 A. The frequency is 50 Hz and the current density is constant over the cross section.

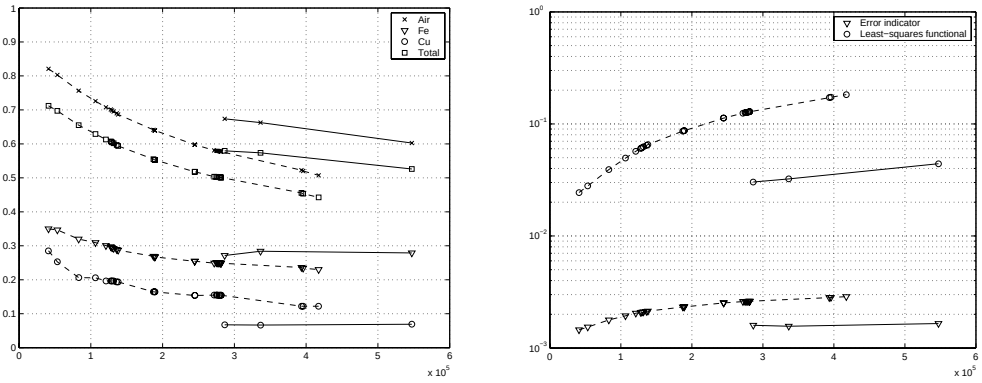

(a) *Relative error in energy in the different parts*

(b) *Error indicator and least-squares functional*

Figure 7: Computations for Problem 2 with quadratic (solid lines) and linear (dashed lines) basis functions.

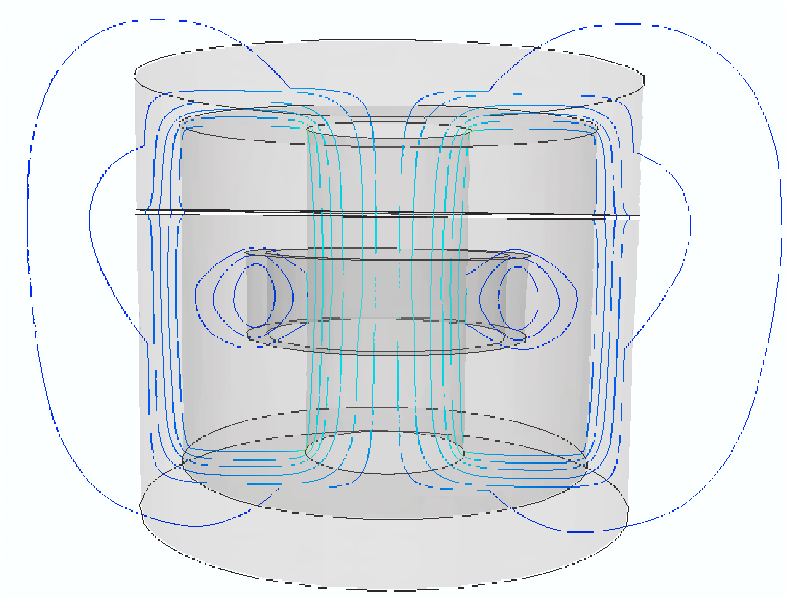

Figure 8: The magnetic field lines in a slice through the three dimensional solution of the axisymmetric Problem 2.

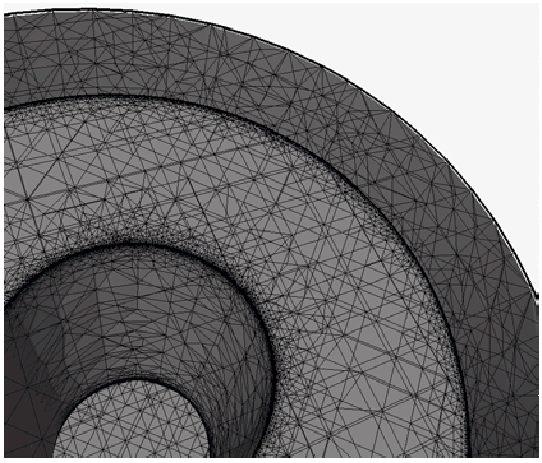

Figure 9: Detail of the mesh after adaptive refinement. The part shown is a top view of the interior of the iron core of Problem 2.

5.2 The equations

Since the current is sinusoidal and the frequency is low, we use the quasistatic time-harmonic equations

$$\nabla \times E = -j\omega B \quad \text{in } \Omega^i, \tag{5.1a}$$
$$\nabla \times H = J \quad \text{in } \Omega^i, \tag{5.1b}$$
$$\nabla \cdot B = 0 \quad \text{in } \Omega^i, \tag{5.1c}$$

where

$$B = \mu H, \tag{5.2a}$$
$$J = J_{sc} + \sigma E. \tag{5.2b}$$

Note that equation (5.1b) implies that $\nabla \cdot J = 0$. The interface conditions for this problem then becomes

$$[E \times n] = 0 \quad \text{on } \Gamma^{ij}, \tag{5.3a}$$
$$[H \times n] = 0 \quad \text{on } \Gamma^{ij}, \tag{5.3b}$$
$$[J \cdot n] = 0 \quad \text{on } \Gamma^{ij}, \tag{5.3c}$$
$$[B \cdot n] = 0 \quad \text{on } \Gamma^{ij}, \tag{5.3d}$$

where n is a unit normal to the interface and $[\cdot]$ denotes the jump across the surface as before. Since $\mu_r = 1$ in the whole region, the magnetic field is continuous over surfaces. The same is true for the tangential component of the electric field, E_t, while (5.3c) implies that $E_{Al}^+ \cdot n = 0$, where E_{Al}^+ denotes the field inside the aluminium plate, since $J = 0$ in the air. No further restrictions apply on the electric field.

The boundary conditions applied are

$$E \times n = 0 \quad \text{on } \Gamma, \tag{5.4a}$$

$$B \cdot n = 0 \quad \text{on } \Gamma. \tag{5.4b}$$

The placement of the outer boundary is not specified in description of the test case. We have enclosed the coil and the aluminium plate in a cube of approximately three times the size of a side in the plate.

5.3 The least-squares formulation

Even though the magnetic field is continuous in the whole region, we still have to introduce the discontinuous elements along the surfaces, due to the jump in the normal component of E. Setting up the least-squares functional for this system of equations then leads to the following expression,

$$\begin{aligned} I(E,H) = \sum_{i=1}^{3} \Big(& \|\nabla \times E + j\omega\mu H\|_{\Omega^i}^2 \\ & + \|\nabla \times H - \sigma E - J_{sc}\|_{\Omega^i}^2 + \|\nabla \cdot (\mu H)\|_{\Omega^i}^2 \Big) \\ + \sum_{1 \le i < j \le 3} & \Big(\|h^{-1/2}\ [E \times n]\|_{\Gamma^{ij}}^2 + \|h^{-1/2}\ E^+ \cdot n\|_{\Gamma_{Al}}^2 \Big) \\ + \sum_{1 \le i < j \le 3} & \Big(\|h^{-1/2}\ [H \times n]\|_{\Gamma^{ij}}^2 + \|h^{-1/2}\ [\mu H \cdot n]\|_{\Gamma^{ij}}^2 \Big) \\ & + \|h^{-1/2}\ [E \times n]\|_{\Gamma}^2 + \|h^{-1/2}\ [\mu H \cdot n]\|_{\Gamma}^2, \end{aligned} \tag{5.5}$$

where the second of the interface terms signify that the normal component of the E field inside the aluminium should be zero on the interface.

The conditions for a minimum of $I(E,H)$ give the following variational formulation for $U = (E,H)$: find U such that

$$a_\Omega(U,\tilde{U}) + a_1(U,\tilde{U}) + a_2(U,\tilde{U}) + a_3(U,\tilde{U}) = l(\tilde{U}), \tag{5.6}$$

for all $\tilde{U}$, where

$$a_\Omega(U,\tilde{U}) = \sum_{i=1}^{3}(\nabla\times E + j\mu\omega H, \nabla\times\tilde{E} + j\omega\mu\tilde{H})_{\Omega^i} \tag{5.7a}$$
$$+ (\nabla\times H - \sigma E, \nabla\times\tilde{H} - \sigma\tilde{E})_{\Omega^i}$$
$$+ (\nabla\cdot(\mu H), \nabla\cdot(\mu\tilde{H}))_{\Omega^i},$$
$$l(\tilde{U}) = \sum_{i=1}^{3}(J_{sc}, \nabla\times\tilde{H} - \sigma\tilde{E})_{\Omega^i}. \tag{5.7b}$$

and for the interface terms,

$$a_1(U,\tilde{U}) = \sum_{1\le i<j\le 3}(h^{-1}[E\times n], [\tilde{E}\times n])_{\Gamma^{ij}} \tag{5.8a}$$
$$+ (h^{-1}E^+\cdot n, \tilde{E}^+\cdot n)_{\Gamma_{Al}},$$
$$a_2(U,\tilde{U}) = \sum_{1\le i<j\le 3}\Big((h^{-1}[H\times n], [\tilde{H}\times n])_{\Gamma^{ij}} \tag{5.8b}$$
$$+ (h^{-1}[\mu H\cdot n], [\mu\tilde{H}\cdot n])_{\Gamma^{ij}}\Big),$$
$$a_3(U,\tilde{U}) = (h^{-1}[E\times n], [\tilde{E}\times n])_{\Gamma} \tag{5.8c}$$
$$+ (h^{-1}[\mu H\cdot n], [\mu\tilde{H}\cdot n])_{\Gamma}.$$

Note that in these expressions we are dealing with complex vector fields. In practise, one separates the real and imaginary parts and thus has to work with 12 unknown variables.

5.4 Computational results

As expected, in the absence of singularities, this problem could be solved successfully with LSFEM. Comparison with experimental data is shown in Figure 11(a). The currents induced in the aluminium plate are shown in Figure 12. However, due to the size of the problem, we have only been able to compute using linear polynomial basis functions and not reaching the desired accuracy. The convergence though is good as shown in Figure 11(b), since the L^2 norm of the residual is equivalent to the error in energy norm.

In this example we do not have an increasing residual, see Figure 11(b), which caused problems in the previous examples. Hence, it has been possible

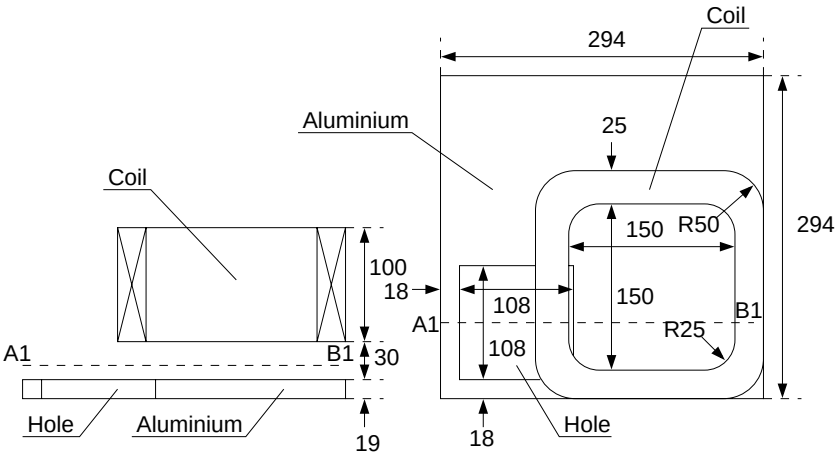

Figure 10: The geometry of Problem 3, a) front view, b) top view. The dimensions are given in millimeters.

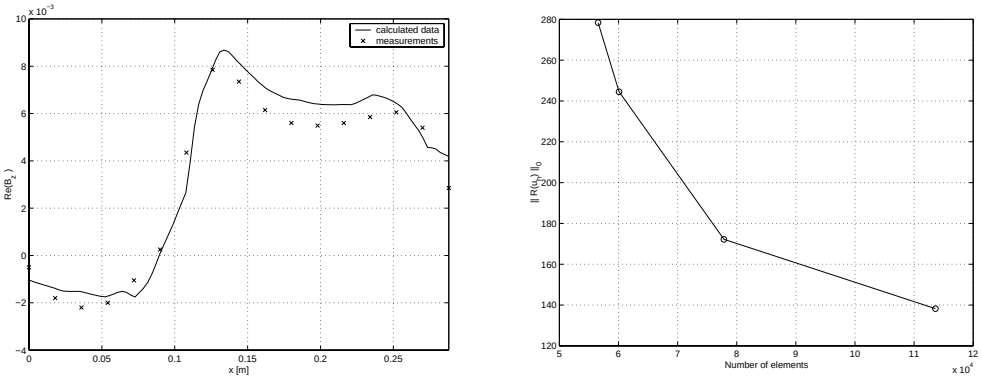

(a) *Comparison with experimental data taken along line A1-B1 in Figure 10.*

(b) *The least-squares functional during refinement*

Figure 11: Computations for Problem 3 with linear basis functions.

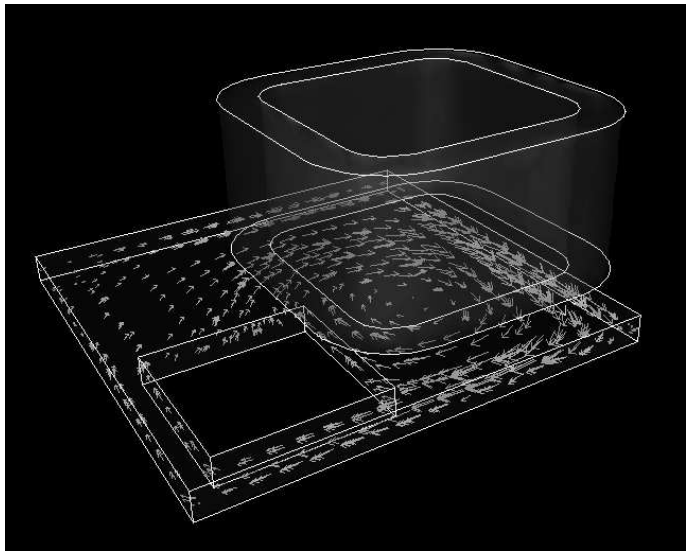

Figure 12: Vector plot of the induced current in the aluminium plate of Problem 3.

to use the least-squares residual as refinement criterion:

$$\begin{aligned} I_K = &\|\nabla \times E + j\omega\mu H\|_K^2 \\ &+ \|\nabla \times H - \sigma E - J_{sc}\|_K^2 \\ &+ \|\nabla \cdot (\mu H)\|_K^2, \end{aligned} \tag{5.9}$$

References

[1] First-order system least squares philosophy. `ftp://amath.colorado.edu/pub/fosls/FOSLoSophy.ps`.

[2] C. Amrouche, C. Bernardi, M. Dauge, and V. Girault. Vector potentials in three-dimensional nonsmooth domains. *Math. Methods Appl. Sci.*, 21:823–864, 1998.

[3] G. Bao and H. Yang. A least-squares finite element analysis for diffraction problems. *SIAM J. Numer. Anal.*, 37(2):665–682, 2000.

[4] R. Bergström, A. Bondeson, C. Johnson, M.G. Larson, Y. Liu, and K. Samuelsson. Adaptive finite element methods in electromagnetics. Technical Report 2, Swedish Institute of Applied Mathematics (ITM), 1999.

[5] P.B. Bochev and M.D. Gunzburger. Finite element methods of least-squares type. *SIAM Rev.*, 40(4):789–837, 1998.

[6] A. Bossavit. *Computational Electromagnetism.* Academic Press, 1998.

[7] J.H. Bramble, R.D. Lazarov, and J.E. Pasciak. A least-squares approach based on a discrete minus one inner product for first order systems. *Math. Comp.*, 66(219):935–955, 1997.

[8] S.C. Brenner and L.R. Scott. *The Mathematical Theory of Finite Element Methods.* Springer-Verlag, 1994.

[9] Z.M. Chen, Q. Du, and J. Zou. Finite element methods with matching and nonmatching meshes for Maxwell equations with discontinuous coefficients. *SIAM J. Numer. Anal.*, 37:1542–1570, 2000.

[10] M. Costabel. A coercive bilinear form for Maxwell's equations. *J. Math. Anal. Appl.*, 157(2):527–541, 1991.

[11] M. Costabel and M. Dauge. Un résultat de densité pour les équations de Maxwell régularisées dans un domaine lipschitzien. *C. R. Acad. Sci. Paris Sér. I Math.*, 327(9):849–854, 1998.

[12] B.-N. Jiang. *Least-squares finite element method : Theory and applications in computational fluid dynamics and electromagnetics.* Springer-Verlag, 1998.

[13] B.-N. Jiang, J. Wu, and L.A. Povinelli. The origin of spurious solutions in computational electromagnetics. *J. Comp. Phys.*, 125:104–123, 1996.

[14] L.R. Scott and S. Zhang. Finite element interpolation of nonsmooth functions satisfying bundary conditions. *Math. Comp.*, 54:483–493, 1990.

[15] L. Turner. Benchmark problems for the validation of eddy current computer codes. *COMPEL*, 9:123–216, 1990.

Paper II

Discontinuous/Continuous Least-Squares Finite Element Methods for Elliptic Problems *

Rickard Bergström† and Mats G. Larson‡

Abstract

Least-squares finite element methods typically suffer from requirements on the solution to be very regular. This rules out, e.g., applications posed on nonconvex domains. In this paper we study a least-squares formulation where the discrete space is enriched by discontinuous elements in the vicinity of singularities, making computation of less regular problems possible. We apply this technique to the first order Poisson problem, show coercivity and a priori estimates, and present numerical results in 3D.

1 Introduction

Despite the fact that the least-squares finite element method (LSFEM) suffers from several short comings, mainly concerning the regularity of the exact solution, the advantages it offers, such as yielding symmetric positive definite matrix problems, have made the method attractive in several areas. Applications include among others the convection-diffusion equation [22], the Stokes [5] and the Navier-Stokes equations [4], Helmholtz' equation [21], Navier's equation [11], and Maxwell's equations [19]. For a review of the least-squares finite element method and more references to the mentioned applications, we refer to the paper by Bochev and Gunzberger [6].

This paper is concerned with the complication involving nonconvex polyhedral domains, possibly in the context of an interface problem. The difficulty that arises with the least-squares finite element method is due to the

*Research supported by ABB Corporate Research, Sweden

†Supported by the Swedish Foundation for Strategic Research through the National Graduate School in Scientific Computing and the National Network in Applied Mathematics

‡Supported by Swedish Research Council for Engineering Sciences

strong regularity requirement for the method, a requirement only fulfilled in smooth domains. In [14], weighted L^2-norms were used in two space dimensions to achieve optimal convergence. A similar formulation is studied in [20] for an interface problem. Also in [13], a weighted norm is used when stabilizing Maxwell's equations with a quadratic divergence term. This approach, however, requires a precise knowledge of the behaviour of the solution at the geometric singularity, a knowledge which one may not have.

Another approach is based on a discrete minus one inner product by Bramble *et al.* [7]. Combined with the Raviart-Thomas elements a formulation which is optimal with respect to regularity and approximation on general polygonal domains is derived. The construction of the inner product leads however to dense matrices.

Here we study a least-squares formulation, based on the use of discontinuous elements to approximate $H(\mathrm{div})$, which allows us to get optimal estimates in the $H(\mathrm{div})$-norm. The interface problem has been handled in [12] and we use a similar approach. The introduction of discontinuous elements in this setting was made by Bramble *et al.*[8].

We prove optimal convergence results for the method applied to the first order system formulation of the Poisson problem. Moreover, we present numerical results for model problems in three spatial dimensions. In order to reduce computational cost, we introduce an adaptive hybrid scheme based on discontinuous approximation only in the vicinity of singularities and continuous approximation elsewhere, combined with adaptive mesh refinement.

The model problems include a line singularity, a point singularity, and an interface problem including both types of singularities. The proposed hybrid scheme performs well for all these problems. In some cases, depending on the formulation of the boundary conditions, we find that also the standard least-squares method performs surprisingly well, but does not capture the singularity correctly.

The rest of this paper is organized as follows. In Section 2, we present the problem and formulate the discontinuous/continuous least-squares method; in Section 3, we state and prove coercivity of the bilinear form and a priori error estimates based on interpolation on the BDM spaces and introduce variations on the scheme; in Section 4, we introduce the adaptive hybrid formulation for efficient computations and discuss adaptivity issues; in Section 5, we present the numerical results.

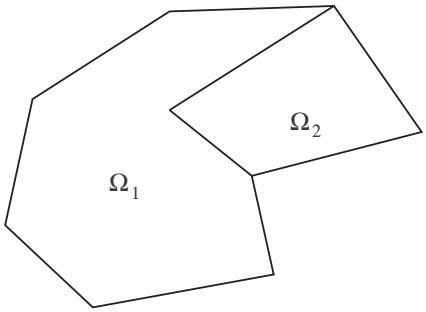

Figure 1: A polygonal domain with two subdomains.

2 The least-squares finite element method

2.1 Model problem

We consider the problem: find u such that

$$-\nabla \cdot A\nabla u = f \quad \text{in } \Omega, \tag{2.1a}$$
$$n \cdot A\nabla u = g_N \quad \text{on } \Gamma_N, \tag{2.1b}$$
$$u = g_D \quad \text{on } \Gamma_D, \tag{2.1c}$$

where $\Omega \subset \mathbf{R}^3$ is a polyhedral domain with boundary $\Gamma = \Gamma_D \cup \Gamma_N$, see Grisvard [17] for a definition, $f \in L^2(\Omega)$, n is the exterior unit normal, $g_N \in H^{1/2}(\Gamma_N)$ and $g_D \in H^{3/2}(\Gamma_D)$. A is a symmetric piecewise constant matrix $A = A^i$ for $x \in \Omega^i$, with $\{\Omega^i\}$ a partition of Ω into polyhedral subdomains Ω^i. Further we assume that there are constants c_A and C_A such that $c_A|x|^2 \leq x \cdot Ax \leq C_A|x|^2$.

Introducing the flux

$$\sigma = A\nabla u, \tag{2.2}$$

we may write problem (2.1) as the first order system: find (u, σ) such that

$$-\nabla \cdot \sigma = f \quad \text{in } \Omega, \tag{2.3a}$$
$$\sigma - A\nabla u = 0 \quad \text{in } \Omega, \tag{2.3b}$$
$$n \cdot \sigma = g_N \quad \text{on } \Gamma_N, \tag{2.3c}$$
$$u = g_D \quad \text{on } \Gamma_D. \tag{2.3d}$$

Under our assumptions on data, the solution (u, σ) to (2.3) resides in at least $H^1(\Omega) \times H(\mathrm{div}; \Omega)$, with u uniquely determined if $\Gamma_D \neq \emptyset$. To be more

precise, we have for a nonconvex Ω, that the minimal regularity for u is $H^{3/2+\delta}(\Omega)$, with $0 < \delta < 1/2$ depending on the geometry, and consequently, for σ we have $[H^{1/2+\delta}(\Omega)]^3$, see e.g. [1], [15], and [17]. By minimal regularity, we mean that for some f, there are solutions u such that $u \notin H^{3/2+\delta}(\Omega)$, but $u \in H^{3/2+\delta-\epsilon}(\Omega)$, for all $\epsilon > 0$ [2]. We denote the space in which the solution resides by $\mathcal{V} \times \mathcal{W}$. The space $H(\mathrm{div}; \Omega)$ mentioned above is defined as

$$H(\mathrm{div}; \Omega) = \{v \in [L^2(\Omega)]^3 : \nabla \cdot v \in L^2(\Omega)\}, \tag{2.4}$$

and is a Sobolev space with the product norm

$$\|v\|^2_{H(\mathrm{div})} = \|\nabla \cdot v\|^2 + \|v\|^2. \tag{2.5}$$

2.2 Finite element spaces

Let $\mathcal{K}$ be a triangulation of Ω into shape regular tetrahedra K which respects the subdomains, i.e., all $K \subset \Omega^i$ for some i. Denote the set of all faces F by $\mathcal{F}$ and divide it into three disjoint sets

$$\mathcal{F} = \mathcal{F}_I \cup \mathcal{F}_D \cup \mathcal{F}_N, \tag{2.6}$$

where $\mathcal{F}_I$ is the set of all faces in the interior of Ω, $\mathcal{F}_D$ the faces on the Dirichlet part of the boundary Γ_D, and $\mathcal{F}_N$ the faces on the Neumann part Γ_N. We let $h : \Omega \to \mathbf{R}$ denote the mesh function such that $h|_K = h_K = \mathrm{diam}(K)$ and $h|_F = h_F = \mathrm{diam}(F)$, i.e., a measure of the size of the element K or the face F. Finally, we define the piecewise polynomial space

$$\mathcal{V}_h \times \mathcal{W}_h = \mathcal{CP}_p \times [\mathcal{DP}_p]^3, \tag{2.7}$$

where

$$\mathcal{CP}_p = \mathcal{DP}_p \cap C(\Omega), \tag{2.8}$$

$$\mathcal{DP}_p = \bigoplus_{K \in \mathcal{K}} \mathcal{P}_p(K), \tag{2.9}$$

and $\mathcal{P}_p(K)$ is the space of all polynomials of degree less than or equal to p defined on K. The degree of the polynomials, as well as the meshsize, may vary from element to element so that $p|_K = p_K$, and thus we allow h-p adaptivity.

2.3 The discontinuous/continuous least-squares finite element method

The discontinuous/continuous least-squares finite element method (D/C LS-FEM) reads: find $(u_h, \sigma_h) \in \mathcal{V}_h \times \mathcal{W}_h$ such that

$$I(u_h, \sigma_h) = \inf_{(v,\chi)\in\mathcal{V}_h\times\mathcal{W}_h} I(v, \chi), \tag{2.10}$$

where the least-squares functional $I(\cdot,\cdot)$ is defined by

$$\begin{aligned} I(v,\chi) = &\sum_{K\in\mathcal{K}} \left(\|\nabla\cdot\chi + f\|_K^2 + \|A^{-1/2}(\chi - A\nabla v)\|_K^2\right) \\ &+\sum_{F\in\mathcal{F}_I}\|h^{-1/2}[n\cdot\chi]\|_F^2 + \sum_{F\in\mathcal{F}_N}\|n\cdot(\chi - g_N)\|_F^2 + \sum_{F\in\mathcal{F}_D}\|h^{-1/2}(v - g_D)\|_F^2. \end{aligned} \tag{2.11}$$

Note that the both Dirichlet (2.3c) and Neumann (2.3d) boundary conditions as well as normal continuity of the flux on interior faces, are imposed weakly through the least-squares functional. Furthermore, we assume that boundary data can be represented by functions in the finite element space.

Remark 2.1 We have the option of applying a weighting of the different terms in the least-squares functional by inserting a constant in front of each term, and still get equivalent schemes [12][25]. For a clearer presentation we have not included these weights in the notation.

The corresponding variational equation takes the form: find $(u_h, \sigma_h) \in \mathcal{V}_h \times \mathcal{W}_h$ such that

$$a(u_h, \sigma_h; v, \chi) = l(v, \chi), \tag{2.12}$$

for all $(v, \chi) \in \mathcal{V}_h \times \mathcal{W}_h$. Here $a(\cdot\,;\cdot)$ is a bilinear form and $l(\cdot)$ a linear functional, defined by

$$\begin{aligned} a(u,\sigma;v,\chi) = &\sum_{K\in\mathcal{K}} (\nabla\cdot\sigma, \nabla\cdot\chi)_K + (A^{-1}(\sigma - A\nabla u), (\chi - A\nabla v))_K \\ &+ \sum_{F\in\mathcal{F}_I} (h^{-1}[n\cdot\sigma], [n\cdot\chi])_F \\ &+ \sum_{F\in\mathcal{F}_N} (n\cdot\sigma, n\cdot\chi)_F \\ &+ \sum_{F\in\mathcal{F}_D} (h^{-1}u, v)_F \end{aligned} \tag{2.13a}$$

$$l(v,\chi) = \sum_{K\in\mathcal{K}} (f, \nabla\cdot\chi)_K + \sum_{F\in\mathcal{F}_N} (g_N, n\cdot\chi)_F + \sum_{F\in\mathcal{F}_D} (h^{-1}g_D, v)_F. \tag{2.13b}$$

3 Error estimates

3.1 Coercivity and continuity

We begin our analysis by introducing the (semi) norm

$$|||(u,\sigma)|||^2 = \sum_{K\in\mathcal{K}} \left(\|\nabla\cdot\sigma\|_K^2 + \|A^{-1/2}\sigma\|_K^2 + \|A^{1/2}\nabla u\|_K^2\right) + \sum_{F\in\mathcal{F}_I} \|h^{-1/2}[n\cdot\sigma]\|_F^2 + \sum_{F\in\mathcal{F}_N} \|n\cdot\sigma\|_F^2 + \sum_{F\in\mathcal{F}_D} \|h^{-1/2}u\|_F^2. \tag{3.1}$$

We then have the following basic estimates.

Proposition 3.1 *It holds*

$$m|||(u,\sigma)|||^2 \le a(u,\sigma;u,\sigma) \qquad \forall (u,\sigma)\in\mathcal{V}_h\times\mathcal{W}_h, \tag{3.2}$$

$$a(u,\sigma;v,\chi) \le M|||(u,\sigma)|||\,|||(v,\chi)||| \qquad \forall (u,\sigma) \text{ and } (v,\chi)\in\mathcal{V}\times\mathcal{W}, \tag{3.3}$$

with constants m and M independent of h.

Remark 3.1 In our analysis, we do not consider m and M's dependence on A. Following [20] it is reasonable to believe that these constant do not depend on the size of the discontinuities of A, only its variations in each subdomain.

In order to prove Proposition 3.1, we need the following version of Poincare's inequality.

Lemma 3.2 *For $v\in H^1(\Omega)$, we have*

$$\|v\|_\Omega^2 \le C\left(\|\nabla v\|_\Omega^2 + \|v\|_{\Gamma_D}^2\right). \tag{3.4}$$

Proof of Proposition 3.1. To prove (3.2) we start from the definition (2.13a) of the bilinear form

$$a(u,\sigma;u,\sigma) = \sum_{K\in\mathcal{K}} \left(\|\nabla\cdot\sigma\|_K^2 + \|A^{-1/2}(\sigma - A\nabla u)\|_K^2\right) + \sum_{F\in\mathcal{F}_I} \|h^{-1/2}[n\cdot\sigma]\|_F^2 + \sum_{F\in\mathcal{F}_N} \|n\cdot\sigma\|_F^2 + \sum_{F\in\mathcal{F}_D} \|h^{-1/2}u\|_F^2. \tag{3.5}$$

We have

$$\|A^{-1/2}\sigma - A^{1/2}\nabla u\|^2 = \|A^{-1/2}\sigma\|^2 - (\nabla u, \sigma) + \|A^{1/2}\nabla u\|^2 \tag{3.6}$$

$$\geq \|A^{-1/2}\sigma\|^2 - |(\nabla u, \sigma)| + \|A^{1/2}\nabla u\|^2. \tag{3.7}$$

We thus only need to estimate $|(\nabla u, \sigma)|$. Using Green's formula we get

$$(\nabla u, \sigma) = -\sum_{K\in\mathcal{K}} (u, \nabla\cdot\sigma)_K + \sum_{F\in\mathcal{F}_I} (u, [n\cdot\sigma])_F + \sum_{F\in\mathcal{F}_N\cup\mathcal{F}_D} (u, n\cdot\sigma)_F. \tag{3.8}$$

The first term on the right hand side in (3.8) may be estimated using the Cauchy-Schwarz and ϵ-inequalities followed by an application of Lemma 3.2,

$$\sum_{K\in\mathcal{K}} (u, \nabla\cdot\sigma)_K \leq C\epsilon\|u\|^2 + C\epsilon^{-1}\|\nabla\cdot\sigma\|^2 \tag{3.9}$$

$$\leq C\epsilon\left(\|A^{1/2}\nabla u\|^2 + \sum_{F\in\mathcal{F}_D}\|h^{-1/2}u\|_F^2\right) + C\epsilon^{-1}\|\nabla\cdot\sigma\|^2,$$

for any $\epsilon > 0$ and $h \leq 1$. Next, for the second term, we again invoke the Cauchy-Schwarz and ϵ-inequalities to get

$$\sum_{F\in\mathcal{F}_I} (u, [n\cdot\sigma])_F \leq C\sum_{F\in\mathcal{F}_I} \epsilon\|h^{1/2}u\|_F^2 + \epsilon^{-1}\|h^{-1/2}[n\cdot\sigma]\|_F^2 \tag{3.10}$$

$$\leq C\epsilon\left(\sum_{K\in\mathcal{K}}\|A^{1/2}\nabla u\|_K^2 + \sum_{F\in\mathcal{F}_D}\|h^{-1/2}u\|_F^2\right) \tag{3.11}$$

$$+ C\epsilon^{-1}\sum_{F\in\mathcal{F}_I}\|h^{-1/2}[n\cdot\sigma]\|_F^2. \tag{3.12}$$

Here we estimated the first term on the right hand side in (3.10) using elementwise trace inequalities followed by Lemma 3.2,

$$\sum_{F\in\mathcal{F}_I}\|h^{1/2}u\|_F^2 \leq C\sum_{K\in\mathcal{K}}\|u\|_K^2 + h^2\|\nabla u\|_K^2 \tag{3.13}$$

$$\leq C\left(\sum_{K\in\mathcal{K}}\|A^{1/2}\nabla u\|_K^2 + \sum_{F\in\mathcal{F}_D}\|h^{-1/2}u\|_F^2\right). \tag{3.14}$$

Finally, the third term on the right hand side in (3.8) can with the same technique be estimated as follows:

$$\sum_{F\in\mathcal{F}_D\cup\mathcal{F}_N}(u,n\cdot\sigma)_F \le C\sum_{F\in\mathcal{F}_D}\left(\epsilon^{-1}\|h^{-1/2}u\|_F^2+\epsilon\|h^{1/2}n\cdot\sigma\|_F^2\right) \tag{3.15}$$

$$+C\sum_{F\in\mathcal{F}_N}\left(\epsilon\|u\|_F^2+\epsilon^{-1}\|n\cdot\sigma\|_F^2\right)$$

$$\le C\epsilon\sum_{K\in\mathcal{K}}\left(\|A^{1/2}\nabla u\|_K^2+\|A^{-1/2}\sigma\|_K^2\right) \tag{3.16}$$

$$+C\epsilon^{-1}\sum_{F\in\mathcal{F}_N}\|n\cdot\sigma\|_F^2+C(\epsilon+\epsilon^{-1})\sum_{F\in\mathcal{F}_D}\|h^{-1/2}u\|_F^2,$$

for all $\epsilon>0$. In (3.16) we used the inverse inequality

$$\|h^{1/2}n\cdot\sigma\|_{\partial K}\le C\|A^{-1/2}\sigma\|_K, \tag{3.17}$$

for $\sigma\in\mathcal{P}_p(K)$. Note that the constant C depends on the order of polynomials p. Collecting these estimates, we get

$$|(\nabla u,\sigma)|\le C_1\epsilon\sum_{K\in\mathcal{K}}\left(\|A^{1/2}\nabla u\|_K^2+\|A^{-1/2}\sigma\|_K^2\right)+C_2\epsilon^{-1}\sum_{K\in\mathcal{K}}\|\nabla\cdot\sigma\|_K^2$$

$$+C_2\epsilon^{-1}\left(\sum_{F\in\mathcal{F}_N}\|n\cdot\sigma\|_F^2+\sum_{F\in\mathcal{F}_I}\|h^{-1/2}[n\cdot\sigma]\|_F^2\right) \tag{3.18}$$

$$+(C_1\epsilon+C_2\epsilon^{-1})\sum_{F\in\mathcal{F}_D}\|h^{-1/2}u\|_F^2.$$

Inserting (3.18) into (3.5) and (3.6), we get

$$a(u,\sigma;u,\sigma)\ge(1-C_2\epsilon^{-1})\sum_{K\in\mathcal{K}}\|\nabla\cdot\sigma\|_K^2 \tag{3.19}$$

$$+(1-C_1\epsilon)\sum_{K\in\mathcal{K}}\left(\|A^{-1/2}\sigma\|_K^2+\|A^{1/2}\nabla u\|_K^2\right)$$

$$+(1-C_2\epsilon^{-1})\left(\sum_{F\in\mathcal{F}_N}\|n\cdot\sigma\|_F^2+\sum_{F\in\mathcal{F}_I}\|h^{-1/2}[n\cdot\sigma]\|_F^2\right)$$

$$+(1-C_1\epsilon-C_2\epsilon^{-1})\sum_{F\in\mathcal{F}_D}\|h^{-1/2}u\|_F^2.$$

Choosing ϵ such that $C_1\epsilon \leq 1/2$ and increasing the weights α_i on the remaining terms so that $\alpha_i - C_2\epsilon^{-1} > 0$, we have

$$\tilde{a}(u,\sigma;u,\sigma) \geq m|||(u,\sigma)|||^2, \tag{3.20}$$

where $\tilde{a}(\cdot,\cdot)$ denotes the weighted least-squares functional, see Remark 2.3. Finally, we note that all forms with positive weights are equivalent and thus the proof of (3.2) follows.

The continuity (3.3) is a direct consequence of the Cauchy-Schwarz and triangle inequalities. □

3.2 A priori error estimates

We begin by introducing the interpolation operator, $\Pi : (u,\sigma) \mapsto (\pi_u u, \pi_\sigma \sigma)$, with π_u the standard Scott-Zhang interpolation operator, see [23], and π_σ an interpolation operator onto the Brezzi-Douglas-Marini (BDM) spaces, see [10]. These elements have the degrees of freedom associated with the moments of the field in the interior of the element and the normal trace on the faces. The BDM-interpolant ensures normal continuity across element faces and can be defined for functions satisfying $\sigma \in [L^s]^3$ and $\nabla \cdot \sigma \in L^2$, with $s > 2$. This restriction is necessary to define the normal traces of the definition and we remark that solutions to (2.1) satisfy this condition. The most important property of π_σ is that on an affine element,

$$\nabla \cdot \pi_\sigma \sigma = P_{p-1,K} \nabla \cdot \sigma, \tag{3.21}$$

where $P_{p-1,K}$ denotes the $L^2(K)$-projection onto $\mathcal{P}_{p-1}(K)$. This identity can be seen by elementwise integration by parts and using the definition of the interpolant, see [9].

We then have the following interpolation error estimate.

Lemma 3.3 *Let K be an affine element and π_σ the BDM-interpolation operator. Then there is a constant C depending only on the polynomial order and the shape of K, such that*

$$\|(\sigma - \pi_\sigma \sigma)\|_K \leq C h_K^\alpha |\sigma|_{\alpha,K}, \qquad 1/2 < \alpha \leq p+1, \tag{3.22a}$$

$$\|\nabla \cdot (\sigma - \pi_\sigma \sigma)\|_K \leq C h_K^\alpha |\nabla \cdot \sigma|_{\alpha,K}, \qquad 0 < \alpha \leq p. \tag{3.22b}$$

An estimate in the energy norm can now be formulated.

Lemma 3.4 *For $(u,\sigma) \in H^{s+1}(\Omega) \times H^s(div;\Omega)$, with $s > 0$, it holds*

$$|||(u,\sigma) - (\pi_u u, \pi_\sigma \sigma)|||^2 \leq C \sum_{K\in\mathcal{K}} h_K^{2\alpha} \big(\|\nabla\cdot\sigma\|^2_{\alpha,K} + \|\sigma\|^2_{\alpha,K} + \|u\|^2_{\alpha+1,K} \big), \tag{3.23}$$

with $\alpha = \min(p,s)$.

Proof. Note that the BDM-interpolant of σ has continuous normal component, so all interior face terms cancel. The boundary conditions may be exactly represented in the approximating space and are thus also zero. The result then follows by applying Lemma 3.3 and the corresponding estimate for the Scott-Zhang interpolator [23]. □

Now, we are ready to state the following main result:

Theorem 3.5 *Let $(u,\sigma) \in H^{s+1}(\Omega) \times H^s(div;\Omega)$ with $s > 0$ be the exact solution to (2.3) and $(u_h,\sigma_h) \in \mathcal{V}_h \times \mathcal{W}_h$ the approximate solution defined by (2.12). Then it holds*

$$|||(u-u_h,\sigma-\sigma_h)|||^2 \leq C \sum_{K\in\mathcal{K}} h_K^{2\alpha} \big(\|\nabla\cdot\sigma\|^2_{\alpha,K} + \|\sigma\|^2_{\alpha,K} + \|u\|^2_{\alpha+1,K} \big), \tag{3.24}$$

with $\alpha = \min(p,s)$ and the constant C independent of the meshsize h.

Proof. We first add and subtract an interpolant and then use the triangle inequality to get

$$|||(u-u_h,\sigma-\sigma_h)||| \leq |||(u-\pi_u u,\sigma-\pi_\sigma\sigma)||| + |||(\pi_u u-u_h,\pi_\sigma\sigma-\sigma_h)|||. \tag{3.25}$$

For the second term, invoking coercivity (3.2), we obtain

$$\begin{aligned} m|||(\pi_u u - u_h,\pi_\sigma\sigma-\sigma_h)|||^2 & \qquad (3.26)\\ &\leq a((\pi_u u - u_h,\pi_\sigma\sigma-\sigma_h),(\pi_u u - u_h,\pi_\sigma\sigma-\sigma_h))\\ &= a((\pi_u u - u,\pi_\sigma\sigma-\sigma),(\pi_u u - u_h,\pi_\sigma\sigma-\sigma_h)) \qquad (3.27)\\ &\leq |||(\pi_u u - u,\pi_\sigma\sigma-\sigma)|||\,|||(\pi_u u - u_h,\pi_\sigma\sigma-\sigma_h)|||, \qquad (3.28) \end{aligned}$$

where we used the Galerkin orthogonality (2.12) in (3.27) and continuity of the bilinear form (3.3) in (3.28). Dividing by $|||(\pi_u u - u_h,\pi_\sigma\sigma-\sigma_h)|||$ and inserting this estimate in (3.25), we arrive at

$$\begin{aligned} |||(u-u_h,\sigma-\sigma_h)|||^2 &\leq (1+1/m)^2 |||(u-\pi_u u,\sigma-\pi_\sigma\sigma)|||^2 \qquad (3.29)\\ &\leq C \sum_{K\in\mathcal{K}} h_K^{2\alpha} \big(\|\nabla\cdot\sigma\|^2_{\alpha,K} + \|\sigma\|^2_{\alpha,K} + \|u\|^2_{\alpha+1,K} \big), \end{aligned}$$

where Lemma 3.4 was used in the last inequality. □

3.3 Variations on the same theme

Up to now, we have presented the method using nodal finite elements and only made the flux discontinuous. There are of course other ways to implement this formulation, which only leads to small variations in the analysis.

3.3.1 Discontinuous least-squares finite element method

For practical reasons, one may choose to have also u discontinuous. This will lead to easier implementation since we may group the unknowns into small blocks, one for each node. We would then add the term

$$\sum_{F \in \mathcal{F}_I} \|h^{-1/2}[u]\|^2 \tag{3.30}$$

to the least-squares functional (2.11) in order to impose continuity of u.

3.3.2 BDM/continuous least-squares finite element method

Instead of making the flux discontinuous and imposing the normal continuity weakly, one may instead use a conforming approximation of $H(\mathrm{div})$, such as the BDM or RT-elements [10]. As discussed in Section 3.2, this ensures continuity of $n \cdot \sigma$ at the interfaces and thus these terms will be zero in the least-squares functional.

4 An adaptive hybrid method

Since the solution to problem (2.3) is of low regularity only close to corners and edges and standard continuous finite elements work well to approximate the regular part of the solution, it is natural to combine completely continuous and discontinuous/continuous approximations. It is thus sufficient to use the discontinuous approximation in the vicinity of a geometric singularity, where the extra degrees of freedom inflicted by the discontinuous method pay off.

Denote by Ω_D a region, conforming with the triangulation $\mathcal{K}$, surrounding the geometric singularities, where we have to use D/C LSFEM, and let $\Omega_C = \Omega \backslash \Omega_D$. In Ω_C we have the solution $(u, \sigma) \in H^{s_C+1} \times [H^{s_C}]^3$, with $s_C \geq 1$, and may use continuous LSFEM with polynomials of degree p_C. If

the decomposition $\Omega = \Omega_C \cup \Omega_D$ is chosen such that s_C is considerably larger than s, we can also benefit from this by using high order polynomials in Ω_C. Further, let $\mathcal{K}_D = \{K \in \mathcal{K} : K \subset \Omega_D \text{ or } \overline{K} \cap \overline{\Omega}_D \neq \emptyset\}$ be the elements covering Ω_D and the neighboring elements, and define $\mathcal{K}_C$ analogously.

We then have the following extension of our earlier a priori error estimate:

Theorem 4.1 *Let $(u, \sigma) \in H^{s+1}(\Omega) \times H^s(div; \Omega)$ with $s > 0$ be the exact solution to (2.3) and $(u_h, \sigma_h) \in \mathcal{V}_h \times \mathcal{W}_h$ the approximate solution of the hybrid method proposed in this section. Using the notation introduced above, it holds*

$$\begin{aligned} |||(u - u_h, \sigma - \sigma_h)|||^2 \leq C \sum_{K \in \mathcal{K}_D} h_K^{2\alpha} \big(\|\nabla \cdot \sigma\|_{\alpha,K}^2 + \|\sigma\|_{\alpha,K}^2 + \|u\|_{\alpha+1,K}^2 \big) \\ + C \sum_{K \in \mathcal{K}_C} h_K^{2\alpha_C} \big(\|\sigma\|_{\alpha_C+1,K}^2 + \|u\|_{\alpha_C+1,K}^2 \big), \end{aligned} \tag{4.1}$$

with $\alpha = \min(p, s)$ and $\alpha_C = \min(p_C, s_C)$ and the constant C independent of the meshsize.

The natural mesh refinement indicator in a least-squares method is the the functional we try to minimize, i.e.,

$$\begin{aligned} \eta_K = \|\nabla \cdot \sigma + f\|_K^2 + \|A^{-1/2}(\sigma - A\nabla u)\|_K^2 \\ + \|h^{-1/2}[n \cdot \sigma]\|_{\partial K \cap \mathcal{F}_I}^2 + \|n \cdot (\sigma - g_N)\|_{\partial K \cap \mathcal{F}_N}^2 \\ + \|h^{-1/2}(u - g_D)\|_{\partial K \cap \mathcal{F}_D}^2, \end{aligned} \tag{4.2}$$

where η_K denotes the element indicator. We use isotropic mesh refinement, splitting each element marked for refinement into two to eight new elements by successively dividing the longest edge, see [3] for more details. However, for problems with singularities like we treat in this paper, it would be desirable to use anisotropic or graded mesh refinement [16][24]. This seem to be an unexploited area in the least-squares society.

5 Numerical examples

In order to illustrate the theoretical results, we present numerical results for three examples, all computed in three spatial dimensions and using the adaptive method described in section 4: an L-shaped domain representing a line singularity, a sphere where a cone has been removed representing a point singularity, and finally a cube, where one octant has a different material parameter. For the first two examples analytic solutions are known.

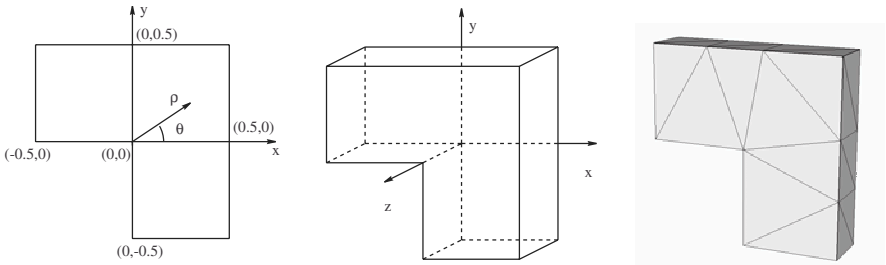

(a) *The x-y plane* (b) *The domain* (c) *Initial mesh*

Figure 2: The L-shaped domain with a line singularity.

5.1 Line singularity

We consider the problem

$$-\nabla \cdot \sigma = 0 \qquad \text{in } \Omega, \tag{5.1a}$$

$$\sigma - \nabla u = 0 \qquad \text{in } \Omega, \tag{5.1b}$$

$$u = g(\rho, \theta, z) \qquad \text{on } \Gamma_D, \tag{5.1c}$$

$$n \cdot \sigma = 0 \qquad \text{on } \Gamma_N, \tag{5.1d}$$

where Ω is the domain showed in Figure 2 with $z \in (0, 0.2)$, $\Gamma_N = \{x \in \Omega; z = 0.0 \text{ or } z = 0.2\}$ and $\Gamma_D = \partial\Omega \backslash \Gamma_N$. The function g is chosen so that the exact solution of u is

$$u(\rho, \theta, z) = \rho^{2/3} \sin(2\theta/3 + \pi/3). \tag{5.2}$$

We remark that the solution is independent of the z-coordinate and is thus two dimensional.

The error for the discontinuous/continuous least-squares finite element method compared with standard LSFEM is presented in Figure 3. We clearly see that D/C LSFEM shows better performance. The continuous method can not represent the solution correctly in the vicinity of the corner. It seems as if the geometry is rounded off and the singularity is absent. In Figure 4(a) we see that the computed flux is incorrect for standard LSFEM while, with discontinuous elements we can represent the solution correctly at the corner as in Figure 4(b). The error is however local and does not pollute the solution far from the singularity. We remark that the reason the standard LSFEM gives a solution that is only locally erroneous, is that on

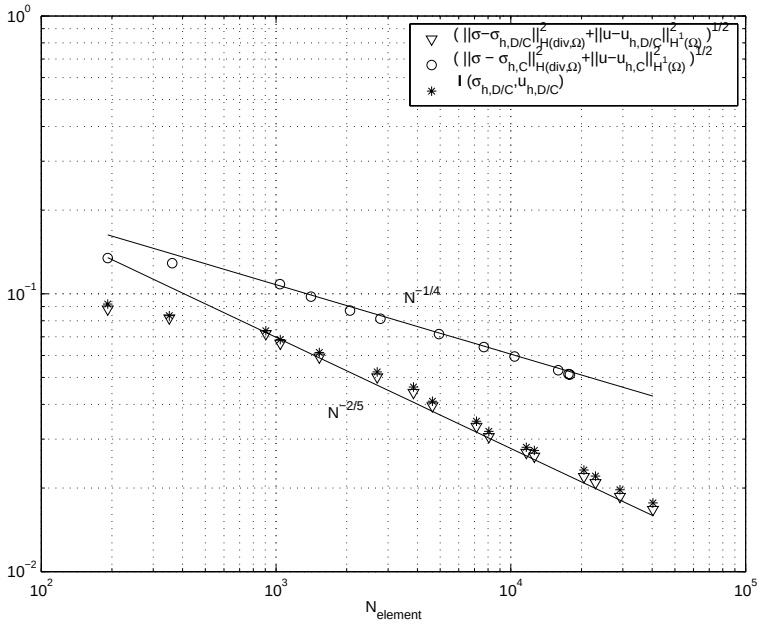

Figure 3: Error for standard LSFEM and D/C LSFEM in the line singularity example. Circles denote the error for standard LSFEM and triangles the error for D/C LSFEM measured in the $H^1(\Omega)\times H(\mathrm{div};\Omega)$-norm; stars denote the D/C LSFEM residual.

a Dirichlet boundary, and specifically in the corner, we have no condition on the flux σ . Thus the least-squares method is able to adapt in the way shown in Figure 4(a).

5.2 Point singularity

In this section we solve the following problem, described in spherical coordinates,

$$-\nabla\cdot\sigma = 0 \qquad \text{in } \Omega, \tag{5.3a}$$

$$\sigma - \nabla u = 0 \qquad \text{in } \Omega, \tag{5.3b}$$

$$u = P_\nu(\cos(\theta)) \qquad \text{on } \Gamma_D, \tag{5.3c}$$

where $\Omega = \{(r,\theta,\phi) : r\in[0,1), \theta\in(\beta,\pi], \phi\in[0,2\pi)\}$ with $\beta = \pi/16$, P_ν is the first class Legendre function of order ν, and $\Gamma_D = \partial\Omega$. The exact

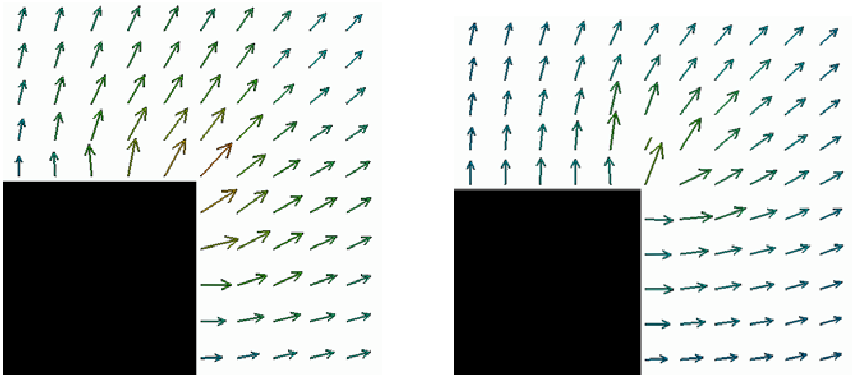

(a) *Standard LSFEM* (b) *D/C LSFEM*

Figure 4: The flux in the vicinity of the corner of the L-shaped domain. Note that for standard LSFEM, the flux is not correctly represented.

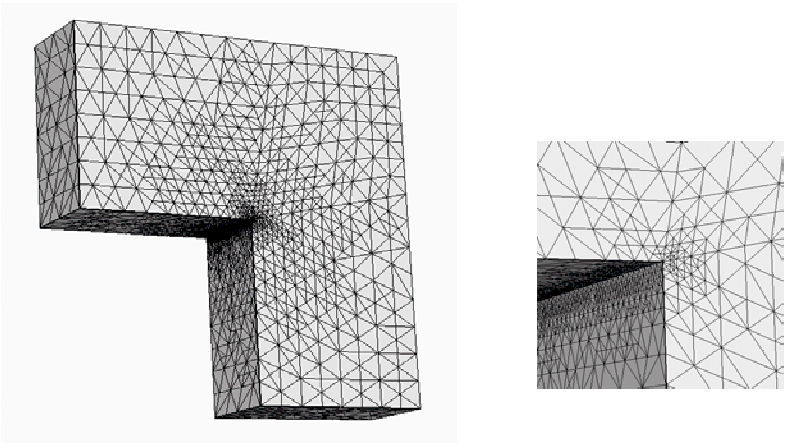

Figure 5: The mesh achieved after 20 refinement steps.

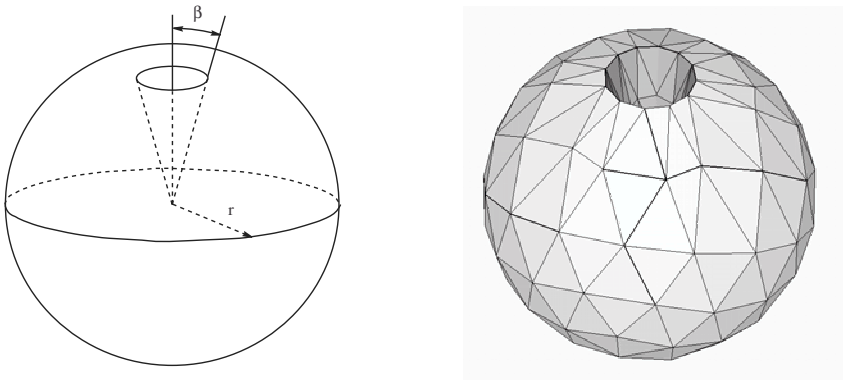

(a) *Geometry* (b) *Initial mesh*

Figure 6: The cone problem with a point singularity.

solution of u to this problem is

$$u(r,\theta) = r^{\nu} P_{\nu}(\cos(\theta)), \tag{5.4}$$

with ν depending on β; in our case $\nu \simeq 0.215$ for $\beta = \pi/16$, see [18].

Also in this problem, the Discontinuous/Continuous LSFEM is superior to the standard LSFEM, cf. Figure 7. The behaviour of the standard LSFEM is similar to the previous case and also here the singularity is absent.

5.3 Interface problem

In the previous examples, the material parameter is constant in the whole domain. We will now demonstrate an example where A has a jump across an interior interface. The domain is $\Omega = \Omega_1 \cup \Omega_2$ where $\Omega_1 = \{x \in (0, 0.5)^3\}$ and $\Omega_2 = \{x \in (0,1)^3\} \backslash \overline{\Omega}_1$.

The problem we solve is

$$-\nabla \cdot \sigma = 1 \quad \text{in } \Omega, \tag{5.5a}$$

$$\sigma - A\nabla u = 0 \quad \text{in } \Omega, \tag{5.5b}$$

$$u = 0 \quad \text{on } \Gamma_D. \tag{5.5c}$$

We choose $A_2 = 1.0$ and let $A_1 = \{10, 100, 1000\}$ for three different cases respectively. Figure 9(a) shows the domain and the initial mesh.

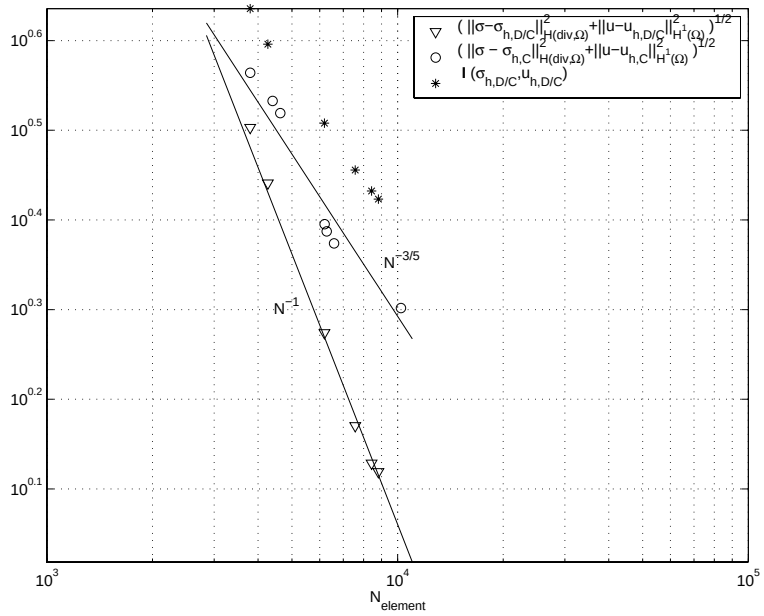

Figure 7: Error for standard LSFEM and D/C LSFEM in the cone singularity example. Circles denote the error for standard LSFEM and triangles the error for D/C LSFEM measured in the $H^1(\Omega) \times H(\mathrm{div})(\Omega)$-norm; stars denote the D/C LSFEM residual.

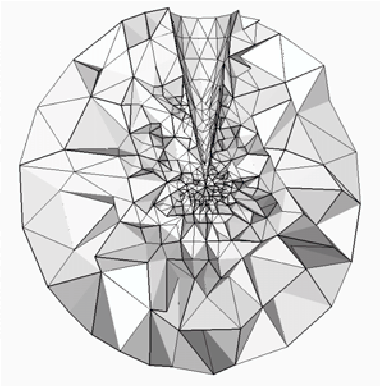

(a) *A slice through the mesh*

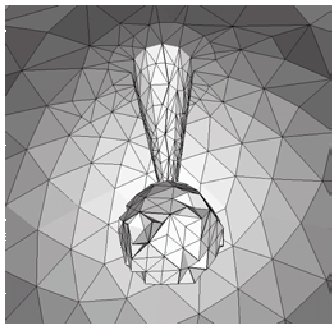

(b) *The ball with discontinuous elements at the cone tip*

Figure 8: The mesh achieved after 8 refinement steps.

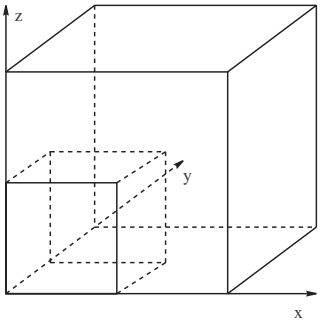

(a) *Geometry*

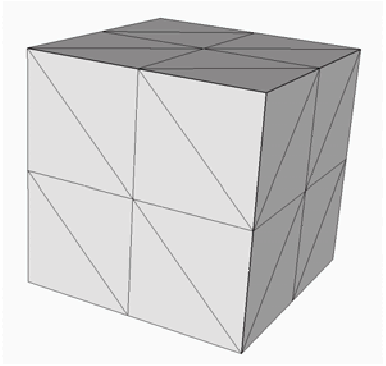

(b) *Initial mesh*

Figure 9: The cube domain in the interface problem.

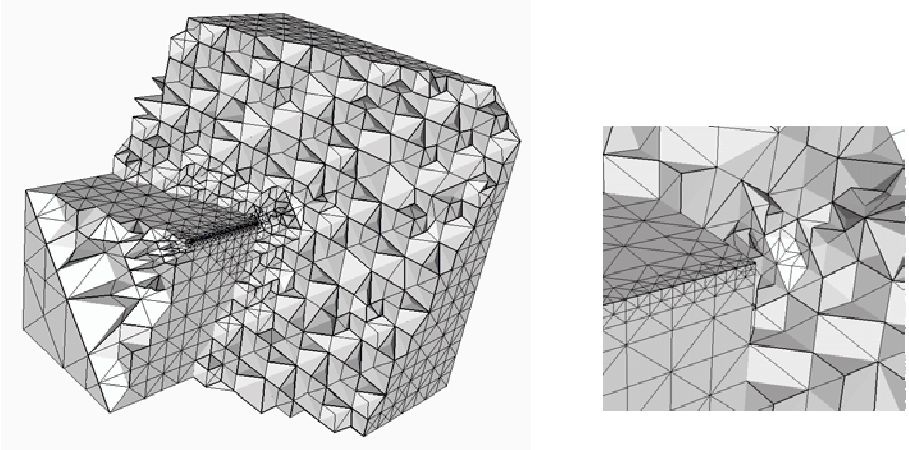

(a) *A slice through the mesh* (b) *Detail of the corner*

Figure 10: The mesh achieved after 14 refinement steps.

For this problem we do not have an exact solution to compare with. However, based on the experience of previous two examples, we rely on the least-squares functional as an error indicator.

Two methods were tested: first with continuous elements in each of the subdomains, but with weakly enforced interface conditions, and secondly with a layer of discontinuous elements around the interface.

The method with continuous elements in each subdomain shows a performance similar to the first example. Since the normal continuity is enforced only weakly, the standard method is able to adapt by rounding off the corner as discussed in Section 5.1. We have therefore chosen not the present the convergence results for this setting.

The least-squares residual for the discontinuous/continuous solution in the three cases with different material parameters is shown in Figure 11. As we clearly see from the plot, the convergence is not affected by the ratio of the size of the parameters. However, with increasing ratio, the algebraic system of equations becomes more difficult to solve.

6 Conclusions

We have formulated and analysed the discontinuous/continuous least-squares finite element method. To obtain an efficient scheme, we propose an adap-

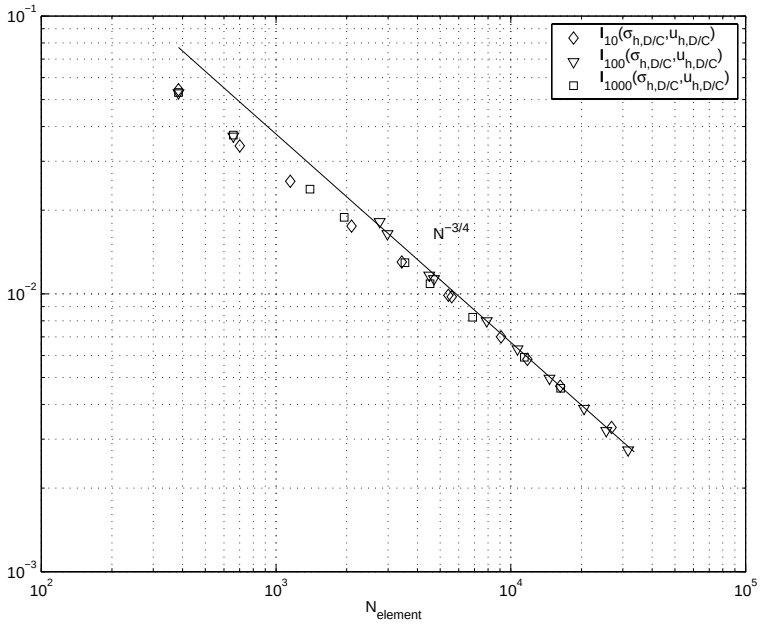

Figure 11: The least-squares functional for $A_1/A_2 = 10$ (diamonds), $A_1/A_2 = 100$ (triangles), and $A_1/A_2 = 1000$ (squares).

tive hybrid method based on discontinuous/continuous approximation only in the vicinity of singularities and fully continuous approximation elsewhere, combined with adaptive mesh refinement.

Furthermore, we present numerical results for the Poisson problem posed on nonconvex domains in three spatial dimensions, which lead to geometrical singularities in the solution, as well as an interface problem.

From the numerics, we see that the standard least-squares finite element method manages to produce a solution only as long as the conflicting conditions on the flux that causes the singularities, are not explicit in the problem. However, the computed solution does not capture the singularities and it appears the corners have been rounded off. This defect does not seem to pollute the solution.

In contrast, the proposed hybrid method performs well in all these cases, and the approximate solution displays a correct normal flux at the corner.

References

[1] C. Amrouche, C. Bernardi, M. Dauge, and V. Girault. Vector potentials in three-dimensional nonsmooth domains. *Math. Methods Appl. Sci.*, 21:823–864, 1998.

[2] F. Assous, P. Ciarlet, Jr., S. Labruine, and S. Lohrengel. The singular complement method. Unpublished.

[3] R. Bergström, M.G. Larson, and K. Samuelsson. The $\mathcal{LL}^*$ finite element method and multigrid for the magnetostatic problem. Preprint 2, Chalmers Finite Element Center, Chalmers University of Technology, 2001.

[4] P. Bochev. Analysis of least-squares finite element methods for the Navier-Stokes equations. *SIAM J. Numer. Anal.*, 34:1817–1844, 1997.

[5] P. Bochev and M. Gunzburger. Analysis of least-squares finite element methods for for the Stokes equations. *Math. Comp.*, 63:479–506, 1994.

[6] P.B. Bochev and M.D. Gunzburger. Finite element methods of least-squares type. *SIAM Rev.*, 40(4):789–837, 1998.

[7] J.H. Bramble, R.D. Lazarov, and J.E. Pasciak. A least-squares approach based on a discrete minus one inner product for first order systems. *Math. Comp.*, 66(219):935–955, 1997.

[8] J.H. Bramble, R.D. Lazarov, and J.E. Pasciak. Least-squares for second order elliptic problems. *Comput. Methods in Appl. Mech. Engrg.*, 152:195–210, 1998.

[9] S.C. Brenner and L.R. Scott. *The Mathematical Theory of Finite Element Methods.* Springer-Verlag, 1994.

[10] F. Brezzi and M. Fortin. *Mixed and Hybrid Finite Element Methods.* Springer-Verlag, 1991.

[11] Z. Cai, T.A. Mantueffel, S.F. McCormick, and S. Parter. First-order system least squares for planar linear elasticity: pure traction. *SIAM J. Numer. Anal.*, (35):320–335, 1998.

[12] Y. Cao and M.D. Gunzberger. Least-squares finite element approximations to solutions of interface problems. *SIAM J. Numer. Anal.*, 35(1):393–405, 1998.

[13] M. Costabel and M. Dauge. Weigthed regularization of Maxwell equations in polyhedral domains. Unpublished.

[14] C.L. Cox and G.J. Fix. On the accuaracy of least squares methods in the presence of corner singularities. *Comp. & Maths. with Appls.*, 10(6):463–475, 1984.

[15] M. Dauge. *Elliptic Boundary Value Problems on Corner Domains.* Lecture Notes in Mathematics. Springer-Verlag, 1980.

[16] L. Formaggia and S. Perotto. Anisotropic error estimates for elliptic problems. Technical Report 18.2000, Dept. of Mathematics, Lausanne, 2000.

[17] P. Grisvard. *Elliptic Problems in Nonsmooth Domains.* Pitman Publishing Inc., 1985.

[18] J.D. Jackson. *Classical Electrodynamics.* John Wiley & Sons, 2nd edition, 1975.

[19] B.-N. Jiang, J. Wu, and L.A. Povinelli. The origin of spurious solutions in computational electromagnetics. *J. Comp. Phys.*, 125:104–123, 1996.

[20] T.A. Manteuffel, S.F. McCormick, and G. Starke. First-order system of least-squares for second order elliptic problems with discontinuous coefficients. To appear.

[21] P. Monk and D.-Q. Wang. A least-squares method for the Helmholtz equation. *Comput. Metods Appl. Mech. Engrg.*, 175:121–136, 1999.

[22] A.I. Pehlivanov, G.F. Carey, and P.S. Vassilevski. Least-squares mixed finite element methods for non-selfadjoint problems: I. error estimates. *Numer. Math.*, 72:501–522, 1996.

[23] L.R. Scott and S. Zhang. Finite element interpolation of nonsmooth functions satisfying bundary conditions. *Math. Comp.*, 54:483–493, 1990.

[24] K.G. Siebert. An a posteriori error estimator for anisotropic refinement. *Numer. Math.*, 73(3):373–398, 1996.

[25] S.-Y. Yang and J.-L. Liu. A unified analysis of a weighted least squares method for first-order systems. *Appl. Math. Comput.*, 92:9–27, 1998.

[13] M. Costabel and M. Dauge. Weigthed regularization of Maxwell equations in polyhedral domains. Unpublished.

[14] C.L. Cox and G.J. Fix. On the accuaracy of least squares methods in the presence of corner singularities. *Comp. & Maths. with Appls.*, 10(6):463–475, 1984.

[15] M. Dauge. *Elliptic Boundary Value Problems on Corner Domains.* Lecture Notes in Mathematics. Springer-Verlag, 1980.

[16] L. Formaggia and S. Perotto. Anisotropic error estimates for elliptic problems. Technical Report 18.2000, Dept. of Mathematics, Lausanne, 2000.

[17] P. Grisvard. *Elliptic Problems in Nonsmooth Domains.* Pitman Publishing Inc., 1985.

[18] J.D. Jackson. *Classical Electrodynamics.* John Wiley & Sons, 2nd edition, 1975.

[19] B.-N. Jiang, J. Wu, and L.A. Povinelli. The origin of spurious solutions in computational electromagnetics. *J. Comp. Phys.*, 125:104–123, 1996.

[20] T.A. Manteuffel, S.F. McCormick, and G. Starke. First-order system of least-squares for second order elliptic problems with discontinuous coefficients. To appear.

[21] P. Monk and D.-Q. Wang. A least-squares method for the Helmholtz equation. *Comput. Metods Appl. Mech. Engrg.*, 175:121–136, 1999.

[22] A.I. Pehlivanov, G.F. Carey, and P.S. Vassilevski. Least-squares mixed finite element methods for non-selfadjoint problems: I. error estimates. *Numer. Math.*, 72:501–522, 1996.

[23] L.R. Scott and S. Zhang. Finite element interpolation of nonsmooth functions satisfying bundary conditions. *Math. Comp.*, 54:483–493, 1990.

[24] K.G. Siebert. An a posteriori error estimator for anisotropic refinement. *Numer. Math.*, 73(3):373–398, 1996.

[25] S.-Y. Yang and J.-L. Liu. A unified analysis of a weighted least squares method for first-order systems. *Appl. Math. Comput.*, 92:9–27, 1998.

Paper III

Discontinuous Least-Squares Finite Element Methods for the Div-Curl Problem *

Rickard Bergström† and Mats G. Larson‡

Abstract

In this paper, we consider the div-curl problem posed on nonconvex polyhedral domains. We propose a least-squares method based on discontinuous elements with normal and tangential continuity across interior faces, as well as boundary conditions, weakly enforced through a properly designed least-squares functional. Discontinuous elements make it possible to take advantage of regularity of given data (divergence and curl of the solution) and obtain convergence also on nonconvex domains. In general, this is not possible in the least-squares method with standard continuous elements. We show that our method is stable, derive a priori error estimates, and present numerical examples illustrating the method.

1 Introduction

The least squares finite element method is a general technique for finding the approximate solution of first order partial differential equations based on minimization of the L^2-norm of the residual over a suitable finite element space. Second order problems are first written as first order systems by introducing additional, often physically motivated, variables. The method manufactures symmetric positive definite algebraic systems which are suitable for applying iterative techniques to find the solution, for instance multigrid. For an overview of least-squares finite element methods, we refer to [7] and the references therein.

*Research supported by ABB Corporate Research, Sweden

†Supported by the Swedish Foundation for Strategic Research through the National Graduate School in Scientific Computing and the National Network in Applied Mathematics

‡Supported by Swedish Research Council for Engineering Sciences

In this paper, we develop a least-squares method for the div-curl problem posed on a nonconvex polyhedral domain with discontinuous piecewise constant coefficients and a right hand side, defined on a partition of the domain into (possibly nonconvex) subdomains, which is piecewise sufficiently smooth ($H^\alpha, \alpha \geq 0$). This problem serves as an important model problem in electromagnetics and also arises when a curl-term is added as stabilization when solving the second order elliptic problem, see, e.g., [10] and [21].

Standard least-squares finite element methods typically require rather strong regularity on the exact solution. For instance, in most works a convex domain is required. This problem has been studied and at least two different solution approaches have been presented, both based on weaker measurements of the residual. The first uses a weighted norm with a radial weight in the vicinity of corners, see Cox and Fix [13] and Manteuffel *et al.* [19]. The second approach is to replace the L^2-norm by a discrete approximation of the H^{-1}-norm, see Bramble *et al.* [9]. Both these methods are somewhat complicated to implement; the first requires knowledge of a local weight of suitable strength at each corner or line singularity and in the second, an implementation of the discrete version of the H^{-1}-norm is needed.

Instead, we propose using discontinuous approximation spaces where tangential and normal continuity, as well as boundary conditions, are weakly enforced through a properly defined least-squares functional. Such spaces make it possible to take advantage of the regularity of the given right hand side and obtain convergence also in the nonconvex case. For efficiency reasons we formulate a hybrid scheme, where discontinuous elements only are employed in the vicinity of corners where it is necessary. Away from the singularities, the solution is regular and continuous, typically higher order, polynomials may be used.

In the analysis we consider the simplified case when the coefficient equals the identity, and comment on the extension to space varying data. We prove coercivity with respect to the H(div,curl)-norm and a priori error estimates of optimal order.

We also present numerical results for model problems in three spatial dimensions. The problems include a line singularity, a point singularity and a magnetostatic interface problem, where the coefficient exhibits a large jump across the interface.

The paper is organized as follows. In Section 2, we present the div-curl problem and the least-squares method; in Section 3, we prove coercivity of the bilinear form with respect to the H(div, curl)-norm for simplified model problems and a priori error estimates; in Section 4, we introduce a hybrid

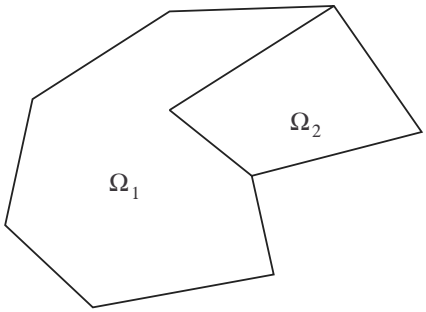

Figure 1: A polygonal domain with two subdomains.

formulation suitable for efficient computations together with the natural mesh refinement indicator; in Section 5, we present numerical results.

2 The least-squares finite element method

2.1 Model problem

We consider the problem: find $u : \Omega \to \mathbf{R}^3$ such that

$$\nabla \times Au = \omega \quad \text{in } \Omega, \tag{2.1a}$$
$$\nabla \cdot u = \rho \quad \text{in } \Omega, \tag{2.1b}$$
$$n \times Au = 0 \quad \text{on } \Gamma_T, \tag{2.1c}$$
$$n \cdot u = 0 \quad \text{on } \Gamma_N, \tag{2.1d}$$

where $\Omega \subset \mathbf{R}^3$ is a polyhedral domain with boundary $\Gamma = \Gamma_T \cup \Gamma_N$, see Grisvard [16] for a definition. By subscripts T and N we refer to the tangential and normal traces, ω and $\rho \in [L^2(\Omega)]^3$ are given functions, n is the exterior unit normal to Γ, A is a piecewise constant function $A = A^i$ for $x \in \Omega^i$, with $\{\Omega^i\}$ a partition of Ω into polyhedral subdomains Ω^i.

Natural spaces for this problem are

$$H(\mathrm{div};\Omega) = \{v \in [L^2(\Omega)]^3 : \nabla \cdot v \in L^2(\Omega)\}, \tag{2.2a}$$
$$H(\mathrm{curl}A;\Omega) = \{v \in [L^2(\Omega)]^3 : \nabla \times Av \in [L^2(\Omega)]^3\}, \tag{2.2b}$$
$$H(\mathrm{div},\mathrm{curl}A;\Omega) = H(\mathrm{div};\Omega) \cap H(\mathrm{curl}A;\Omega), \tag{2.2c}$$

which are Sobolev spaces with their respective product norms,

$$\|v\|^2_{H(\mathrm{div})} = \|\nabla \cdot v\|^2 + \|v\|^2, \tag{2.3a}$$

$$\|v\|^2_{H(\mathrm{curl})} = \|\nabla \times v\|^2 + \|v\|^2, \tag{2.3b}$$

$$\|v\|^2_{H(\mathrm{div,curl})} = \|\nabla \cdot v\|^2 + \|\nabla \times v\|^2 + \|v\|^2. \tag{2.3c}$$

Under our assumptions on data, the solution u to (2.1) resides in at least $[H^{1/2}(\Omega)]^3$, since the subspace of $H(\mathrm{div}, \mathrm{curl}; \Omega)$ restricted to functions with traces that fulfil (2.1c)-(2.1d), are embedded in $[H^s(\Omega)]^3$, with $s > 1/2$, see [1] and [12]. For convex domains, we have $s = 1$.

2.2 Finite element spaces

Let $\mathcal{K}$ be a triangulation of Ω into shape regular tetrahedra K which respects the subdomains, i.e., all $K \subset \Omega^i$ for some i. Denote the set of all faces F by $\mathcal{F}$ and divide $\mathcal{F}$ into three disjoint sets,

$$\mathcal{F} = \mathcal{F}_I \cup \mathcal{F}_T \cup \mathcal{F}_N, \tag{2.4}$$

where $\mathcal{F}_I$ is the set of all faces in the interior of Ω, $\mathcal{F}_T$ the faces on Γ_T, and $\mathcal{F}_N$ the faces on Γ_N. We let $h : \Omega \to \mathbf{R}$ denote the mesh function such that $h|_K = h_K = \mathrm{diam}(K)$ and $h|_F = h_F = \mathrm{diam}(F)$, i.e., a measure of the size of the face F. Finally, we define the discontinuous piecewise polynomial space

$$\mathcal{V}_h = [\mathcal{DP}_p]^3, \tag{2.5}$$

where

$$\mathcal{DP}_p = \bigoplus_{K \in \mathcal{K}} \mathcal{P}_p(K), \tag{2.6}$$

and $\mathcal{P}_p(K)$ is the space of all polynomials of degree less than or equal to p defined on K. The degree of the polynomials, as well as the meshsize, may vary from element to element so that $p|_K = p_K$, thus allowing h-p adaptivity.

2.3 The discontinuous least-squares finite element method

DLSFEM, the discontinuous least-squares finite element method, reads: find $u_h \in \mathcal{V}_h$ such that

$$I(u_h) = \inf_{v \in \mathcal{V}_h} I(v), \tag{2.7}$$

where the least-squares functional $I(\cdot)$ is defined by

$$I(v) = \sum_{K\in\mathcal{K}} \Big(\|A^{-1/2}(\nabla\times Av - \omega)\|_K^2 + \|A^{1/2}(\nabla\cdot v - \rho)\|_K^2 \Big) \tag{2.8}$$
$$+ \sum_{F\in\mathcal{F}_I\cup\mathcal{F}_T} \Big(\|h^{1/2}A_T^{-1/2}Q_0[n\times Av]\|_F^2 + \|h^{-1/2}A_T^{1/2}P_0[n\times v]\|_F^2 \Big)$$
$$+ \sum_{F\in\mathcal{F}_I\cup\mathcal{F}_N} \Big(\|h^{1/2}A_N^{1/2}Q_0[n\cdot v]\|_F^2 + \|h^{-1/2}A_N^{1/2}P_0[n\cdot v]\|_F^2 \Big).$$

Here we used the following notation: P_0 is the L^2-projection on constant functions on each face F and $Q_0 = I - P_0$ with I the identity operator; n is a fixed unit normal to $F \in \mathcal{F}_I$ and the exterior unit normal for $F \in \mathcal{F}_T \cup \mathcal{F}_N$; $[v] = v^+ - v^-$ for $F \in \mathcal{F}_I$ and $[v] = v^+$ for $F \in \mathcal{F}_T \cup \mathcal{F}_N$, where $v^\pm(x) = \lim_{s\to 0, s>0} v(x \mp sn)$ for $x \in F$; $A_N = 2A^+A^-/(A^+ + A^-)$ and $A_T = (A^+ + A^-)/2$. Note that both differential equations (2.1a) and (2.1b) and boundary conditions (2.1c) and (2.1d), as well as tangential and normal continuity on interior faces, are imposed weakly through the least-squares functional.

Remark 2.1 We may use weighting of the different terms in the least-squares functional by inserting a positive constant in front of each term, see [11]. Weighting leads to a different, but equivalent, discrete approximation. To simplify the notation, we have not included these weights.

The corresponding variational equation takes the form: find $u_h \in \mathcal{V}_h$ such that

$$a(u_h, v) = l(v), \tag{2.9}$$

for all $v \in \mathcal{V}_h$. Here $a(\cdot,\cdot)$ is a bilinear form and $l(\cdot)$ a linear functional, defined by

$$a(u,v) = \sum_{K\in\mathcal{K}} (A^{-1}\nabla\times Au, \nabla\times Av)_K + (A\nabla\cdot u, \nabla\cdot v)_K \tag{2.10a}$$
$$+ \sum_{F\in\mathcal{F}_I\cup\mathcal{F}_T} \big((hA_T^{-1}Q_0[n\times Au], Q_0[n\times Av])_F$$
$$+ (h^{-1}A_T^{-1}P_0[n\times Au], P_0[n\times Av])_F \big)$$
$$+ \sum_{F\in\mathcal{F}_I\cup\mathcal{F}_N} \big((hA_N Q_0[n\cdot u], Q_0[n\cdot v])_F$$
$$+ (h^{-1}A_N P_0[n\cdot u], P_0[n\cdot v])_F \big),$$
$$l(v) = \sum_{K\in\mathcal{K}} (A^{-1}\omega, \nabla\times Av)_K + (A\rho, \nabla\cdot v)_K. \tag{2.10b}$$

3 Error estimates

Throughout this section, we assume that $A = I$, with I the identity matrix, Ω is a nonconvex polyhedral domain, and $\Gamma = \Gamma_N$. Based on the decompositions by Bonnet-Ben Dhia *et al.*[8], our analysis can directly be extended to the case $\Gamma = \Gamma_T$ and, with sufficiently smooth interface boundaries, $A \neq I$. These assumptions are necessary to prove the coercivity of Theorem 3.1, while the error estimate in the least-squares norm in Theorem 3.5 holds for the general problem (2.1).

3.1 The least-squares norm

We define the natural least-squares norm, or energy norm,

$$|||v|||^2 = a(v, v), \tag{3.1}$$

for all $v \in \mathcal{V}_h + H(\mathrm{div}, \mathrm{curl}; \Omega) \cap H^{1/2}(\Omega)$. We then have the following result which shows that $|||\cdot|||$ is indeed a norm on this space.

Theorem 3.1 *There is a constant C, independent of h, such that*

$$\|v\| \leq C|||v|||, \tag{3.2}$$

for all $v \in \mathcal{V}_h + H(div, curl; \Omega) \cap H^{1/2}(\Omega)$.

In order to prove this estimate we first establish a suitable Helmholtz decomposition of $[L^2(\Omega)]^3$.

Lemma 3.2 *For each $v \in [L^2(\Omega)]^3$ there is $\chi \in [H^1]^3(\Omega)$ and $\phi \in H^1(\Omega)$ such that*

$$v = \nabla \times \chi + \nabla\phi. \tag{3.3}$$

Furthermore, the stability estimates

$$\|\chi\|_1 \leq C\|v\|, \tag{3.4a}$$
$$\|\phi\|_1 \leq C\|v\|, \tag{3.4b}$$

hold.

Proof. Let ϕ be the solution of the Neumann problem: find $\phi \in H^1(\Omega)$ such that

$$(\nabla\phi, \nabla w) = -(\nabla \cdot v, w) + (n \cdot v, w)_\Gamma, \tag{3.5}$$

for all $w \in H^1(\Omega)$. Then $\nabla \cdot (v - \nabla\phi) = 0$ and $n \cdot (v - \nabla\phi) = 0$ on Γ. Thus there exists $\chi_0 \in H(\mathrm{curl}; \Omega)$ such that $\nabla \times \chi_0 = v - \nabla\phi$ and $n \times \chi_0 = 0$ on Γ [15]. Note that the boundary condition $n \times \chi_0 = 0$ implies $n \cdot \nabla \times \chi_0 = n \cdot (v - \nabla\phi) = 0$.

Using Lemma 2.1 in Pasciak and Zhao [20] there exists $\chi \in [H^1(\Omega)]^3$ with $n \times \chi = 0$ on Γ and $\nabla \times \chi = \nabla \times \chi_0$. Furthermore, the stability estimate

$$\|\chi\|_1 \leq C\|\nabla \times \chi_0\|, \tag{3.6}$$

holds.

The decomposition (3.3) is thus established. Finally, we note that

$$\|v\|^2 = \|\nabla \times \chi_0\|^2 + \|\nabla\phi\|^2. \tag{3.7}$$

Then (3.4b) follows immediately and (3.4a) follows by using (3.6). □

Proof of Theorem 3.1. Using Lemma 3.2, we write

$$v = \nabla \times \chi + \nabla\phi. \tag{3.8}$$

Multiplying with v, integrating, and using integration by parts, gives

$$\|v\|^2 = \sum_{K \in \mathcal{K}} (v, \nabla \times \chi)_K + (v, \nabla\phi)_K \tag{3.9}$$

$$= \sum_{K \in \mathcal{K}} (\nabla \times v, \chi)_K - (\nabla \cdot v, \phi)_K + \sum_{F \in \mathcal{F}_I} ([n \times v], \chi)_F + \sum_{F \in \mathcal{F}} ([n \cdot v], \phi)_F. \tag{3.10}$$

Using the Cauchy-Schwarz inequality, definition of the $|||\cdot|||$-norm , and stability estimates (3.4), we get

$$\sum_{K \in \mathcal{K}} (\nabla \times v, \chi)_K \leq \sum_{K \in \mathcal{K}} \|\nabla \times v\|_K \|\chi\|_K \leq C|||v||| \, \|v\|, \tag{3.11}$$

$$\sum_{K \in \mathcal{K}} (\nabla \cdot v, \phi)_K \leq \sum_{K \in \mathcal{K}} \|\nabla \cdot v\|_K \|\phi\|_K \leq C|||v||| \, \|v\|. \tag{3.12}$$

Next we turn to the edge terms. Writing $v = Q_0 v + P_0 v$, we have

$$|([n \times v], \chi)_F| \leq \|h^{1/2}[n \times Q_0 v]\|_F h_K^{-1/2} \|Q_0 \chi\|_F + \|h^{-1/2}[n \times P_0 v]\|_F h_K^{1/2} \|\chi\|_F. \tag{3.13}$$

We recall the trace inequality $\|w\|_F \leq C(h_K^{-1/2}\|w\|_K + h_K^{1/2}\|\nabla w\|_K)$, with F a face on ∂K. To estimate $\|Q_0\chi\|_F$, we first write $Q_0\chi = (I - P_0)\chi$ on F and then use the trace inequality

$$h_K^{-1/2}\|Q_0\chi\|_F \leq Ch_K^{-1/2}\big(h_K^{-1/2}\|\chi - P_{0,K}\chi\|_K + h_K^{1/2}\|\nabla(\chi - P_{0,K}\chi)\|_K\big) \tag{3.14}$$

$$\leq C\|\nabla\chi\|_K, \tag{3.15}$$

where $P_{0,K}$ is the $L^2(K)$ projection on $\mathcal{P}_0(K)$ and we applied the standard estimate $\|\chi - P_{0,K}\chi\|_K \leq Ch_K\|\nabla\chi\|$.

Next we have

$$h_K^{1/2}\|\chi\|_F \leq Ch_K^{1/2}\big(h_K^{-1/2}\|\chi\|_K + h_K^{1/2}\|\nabla\chi\|_K^2\big) \tag{3.16}$$

$$\leq C\|\chi\|_{1,K}. \tag{3.17}$$

Collecting these estimates and using stability estimate (3.4a), we arrive at

$$|([n \times v], \chi)_F| \leq C|||v|||\,\|v\| \tag{3.18}$$

The remaining boundary term is estimated in the same way. Finally, dividing by $\|v\|$, the desired estimate follows. □

3.2 Interpolation error estimates

We begin by introducing the interpolation operator $\pi : H(\mathrm{div}, \mathrm{curl}; \Omega) \cap [H^{1/2}(\Omega)]^3 \to \mathcal{V}_h$, such that $\pi u|_K = \pi_K u$ where $\pi_K : H(\mathrm{div}, \mathrm{curl}; K) \cap [H^{1/2}(K)]^3 \to [\mathcal{P}_1(K)]^3$ is defined by

$$\int_F u \cdot v \; dS = \int_F \pi_K u \cdot v \; dS, \tag{3.19}$$

for each face $F \subset \partial K$ and all $v \in [\mathcal{P}_0(F)]^3$. From this definition we derive the following two identities

$$\nabla \times \pi_K u = P_{0,K}\nabla \times u, \tag{3.20a}$$

$$\nabla \cdot \pi_K u = P_{0,K}\nabla \cdot u, \tag{3.20b}$$

where $P_{0,K}$ is the $L^2(K)$-projection on $[\mathcal{P}_0(K)]^3$. For instance, we have

$$\int_K \nabla \times (u - \pi_K u) \cdot v \; dx = \int_{\partial K} n \times (u - \pi_K u) \cdot v \; dS = 0, \tag{3.21}$$

for all $v \in [\mathcal{P}_0(K)]^3$. Using (3.20), we arrive at

$$\nabla \times u - \nabla \times \pi_K u = (I - P_{0,K}) \nabla \times u. \tag{3.22}$$

Applying standard estimates for the L^2-projection, we can deduce the following lemma.

Lemma 3.3 *Let K be an affine element. Then there is a constant C depending only on the shape of K, such that*

$$\|\nabla \times (u - \pi u)\|_K \leq C h_K^{\beta} |\nabla \times u|_{\beta,K}, \tag{3.23}$$

$$\|\nabla \cdot (u - \pi u)\|_K \leq C h_K^{\beta} |\nabla \cdot u|_{\beta,K}, \tag{3.24}$$

with $0 \leq \beta \leq 1$.

We then have the following interpolation error estimate.

Lemma 3.4 *For $u \in [H^{\alpha}(\Omega)]^3$, $\alpha \geq 1/2$, with $\nabla \times u \in [H^{\beta}(\Omega)]^3$ and $\nabla \cdot u \in H^{\beta}(\Omega)$, $\beta \geq 0$, it holds*

$$|||u - \pi u|||^2 \leq C \sum_{K \in \mathcal{K}} h_K^{2\alpha} \|u\|_{\alpha,K}^2 + h_K^{2\beta} \big(\|\nabla \times u\|_{\beta,K}^2 + \|\nabla \cdot u\|_{\beta,K}^2 \big), \tag{3.25}$$

with the constant C independent of h.

Proof. Using the interpolation error estimates in Lemma 3.3, we get

$$\|\nabla \times (u - \pi u)\|_K \leq C h_K^{\beta} \|\nabla \times u\|_{K,\beta}, \tag{3.26}$$

$$\|\nabla \cdot (u - \pi u)\|_K \leq C h_K^{\beta} \|\nabla \cdot u\|_{K,\beta}. \tag{3.27}$$

We now turn to the face contributions. Using the triangle inequality we have

$$\|Q_0[n \times (u - \pi u)]\|_F \leq \|Q_0 n \times (u - \pi u^+)\|_F + \|Q_0 n \times (u - \pi u^-)\|_F, \tag{3.28}$$

where face $F = \bar{K^+} \cap \bar{K^-}$ is shared by elements K^+ and K^-, and $\pi u^{\pm} = \pi u|_{K^{\pm}}$. Each term on the right hand side of (3.28) can now be estimated as

$$\begin{aligned} h_F \|Q_0 n \times (u - \pi u)\|_F^2 + h_F \|Q_0 n \cdot (u - \pi u)\|_F^2 &= h_F \|Q_0 (u - \pi u)\|_F^2 \\ &\leq C h_F \|u - \pi u\|_{K,1/2}^2 \leq C h_K^{2\alpha} \|u\|_{K,\alpha}^2, \end{aligned} \tag{3.29}$$

with $\alpha \geq 1/2$, $K = K^{\pm}$, and $\pi u = \pi u^{\pm}$. For the second face contribution we have the identity

$$h_F^{-1} \|P_0 n \times (u - \pi u)\|_F^2 + h_F^{-1} \|P_0 n \cdot (u - \pi u)\|_F^2 = h_F^{-1} \|P_0 (u - \pi u)\|_F^2 = 0, \tag{3.30}$$

where we used the definition of the interpolant in the last equality. □

3.3 A priori error estimate

Now, we are ready to state the following main result:

Theorem 3.5 *Let $u \in [H^\alpha(\Omega)]^3$, $\alpha \geq 1/2$, with $\nabla \times u \in [H^\beta(\Omega)]^3$ and $\nabla \cdot u \in H^\beta(\Omega)$, $\beta \geq 0$, be the exact solution to (2.1) and $u_h \in \mathcal{V}_h$ the approximate solution defined by (2.9). Then it holds*

$$|||u - u_h|||^2 \leq C \sum_{K \in \mathcal{K}} h_K^{2\alpha} \|u\|_{\alpha,K}^2 + h_K^{2\beta} \big(\|\nabla \times u\|_{\beta,K}^2 + \|\nabla \cdot u\|_{\beta,K}^2 \big), \quad (3.31)$$

with constant C independent of the meshsize h.

Proof. By the definition of the least squares method we have

$$|||u - u_h||| \leq |||u - \pi u|||, \quad (3.32)$$

and thus estimate (3.31) follows immediately from the interpolation error estimate. □

Combining Theorems 3.1 and 3.5 we get the following corollary.

Corollary 3.1 *Under the same assumptions as in Theorem 3.5 it holds*

$$\sum_{K \in \mathcal{K}} \|u - u_h\|_{H(K,div,curl)}^2 \leq C \sum_{K \in \mathcal{K}} h_K^{2\alpha} \|u\|_{\alpha,K}^2 + h_K^{2\beta} \big(\|\nabla \times u\|_{\beta,K}^2 + \|\nabla \cdot u\|_{\beta,K}^2 \big). \quad (3.33)$$

4 A hybrid formulation

Since the solution is of low regularity only close to the singularities, it is natural to use the computationally expensive discontinuous elements only in this region and use continuous elements in the smooth region. Denote by Ω_D a region, conforming with the triangulation $\mathcal{K}$, surrounding the geometric singularities, where we have to use DLSFEM, and let $\Omega_C = \Omega \backslash \Omega_D$. In Ω_C we have the solution $u \in [H^{s_C}]^3$, with $s_C \geq 1$, and may use continuous LSFEM, with polynomials of degree p_C. If the decomposition $\Omega = \Omega_C \cup \Omega_D$ is chosen such that s_C is considerably larger than s, we can also benefit from this by using high order polynomials in Ω_C. Further, let $\mathcal{K}_D = \{K \in \mathcal{K} : K \subset \Omega_D\}$ be the elements covering Ω_D, and define $\mathcal{K}_C$ analogously. An interpolation operator of Scott-Zhang type [22] is used for the continuous approximation.

We then have the following extension of our earlier a priori error estimate:

Corollary 4.1 *Under the same assumptions as in Theorem 3.5 it holds*

$$\sum_{K\in\mathcal{K}}\|u-u_h\|^2_{H(div,curl,K)} \le C\sum_{K\in\mathcal{K}_D} h_K^{2\alpha}\|u\|^2_{\alpha,K} + h_K^{2\beta}\left(\|\nabla\times u\|^2_{\beta,K} + \|\nabla\cdot u\|^2_{\beta,K}\right) + C\sum_{K\in\mathcal{K}_C} h_K^{2\alpha_C}\|u\|^2_{\alpha_C+1,K}. \tag{4.1}$$

with $\alpha_C = \min(p_C+1, s_C)$.

5 Numerical examples

We present in this section examples in domains in three spatial dimensions having corners, or subdomains with corners. We use the least-squares functional as mesh refinement indicator, since it exactly represents the error measured in energy norm $|||\cdot|||$ [18]. Moreover, we use an isotropic mesh refinement algorithm, splitting each element marked for refinement into two to eight new elements by successively dividing the longest edge, see [6] for more details. For these singular problem, it is however clear that we would gain from using an anisotropic error estimator and mesh refinement, see for instance [2], [14], and [23].

5.1 First order Poisson system

Here we consider the Poisson system: find p such that

$$-\Delta p = f \quad \text{in } \Omega, \tag{5.1a}$$
$$n\cdot\nabla p = g_N \quad \text{on } \Gamma_N, \tag{5.1b}$$
$$p = g_D \quad \text{on } \Gamma_D. \tag{5.1c}$$

Introducing the flux

$$u = \nabla p, \tag{5.2}$$

we may write problem (5.1) as a first order system: find (p,u) such that

$$-\nabla\cdot u = f \quad \text{in } \Omega, \tag{5.3a}$$
$$u-\nabla p = 0 \quad \text{in } \Omega, \tag{5.3b}$$
$$\nabla\times u = 0 \quad \text{in } \Omega, \tag{5.3c}$$
$$n\cdot u = g_N \quad \text{on } \Gamma_N, \tag{5.3d}$$
$$n\times u = n\times\nabla g_D \quad \text{on } \Gamma_D, \tag{5.3e}$$
$$p = g_D \quad \text{on } \Gamma_D. \tag{5.3f}$$

The curl-constraint (5.3c) is added since we then, on a convex domain, achieve H^1-coercivity for the system [10]. It arises from equation (5.2) and the fact that the curl of a gradient is identically zero.

We note that (5.3a), (5.3c), (5.3d), and (5.3e) completely define u, which thus can be solved independently of p in a first step. The latter is computed in a second step, by solving (5.3b) and (5.3f) with u as data.

We have applied the method described in this paper to solve the div-curl system of the first step on two problems posed on nonconvex domains, and then computed p by standard LSFEM [19].

5.1.1 Line singularity

We solve problem (5.3) and Ω the L-shaped domain displayed in Figure 2 with $z \in (0, 0.2)$, $\Gamma_N = \{x \in \Omega; z = 0.0 \text{ or } z = 0.2\}$ and $\Gamma_D = \partial\Omega \backslash \Gamma_N$, $f = 0$, and g_D chosen so that the exact solution p is

$$p(\rho, \theta, z) = \rho^{2/3} \sin(2\theta/3 + \pi/3). \tag{5.4}$$

The error, measured in $H^1(\Omega) \times H(\mathrm{div}, \mathrm{curl}; \Omega)$-norm, is plotted in Figure 3. In this figure, also the least-squares functional is plotted. We note that the behaviour of our modified method is the same as reported in [5] when the stabilizing curl-term was not included. The convergence of the algebraic solver is however much better when considering this compatibility constraint. In Figure 4(b) we can see the solution in the corner, displaying correctly the singularity and with the flux orthogonal to the boundary. On the contrary, standard LSFEM does not work in this setting. Instead we note that, in order to satisfy the conflicting constraints, the flux tends to zero in the corner, see Figure 4(a).

5.1.2 Point singularity

In this section, the domain where we solve (5.3) is $\Omega = \{(r, \theta, \phi) : r \in [0, 1), \theta \in (\beta, \pi], \phi \in [0, 2\pi)\}$ with $\beta = \pi/16$, described in spherical coordinates.

Also here $f = 0$, and we choose $g_D = P_\nu$, where P_ν is the first class Legendre function of order ν, and $\Gamma_D = \partial\Omega$. The exact solution p to this problem is

$$p(r, \theta) = r^\nu P_\nu(\cos(\theta)), \tag{5.5}$$

with ν depending on β; in our case we have $\nu \simeq 0.215$ for $\beta = \pi/16$, see [17]. A plot of the error is shown in Figure 6. The behaviour is similar as for the previous case, and also here the use of continuous elements fails.

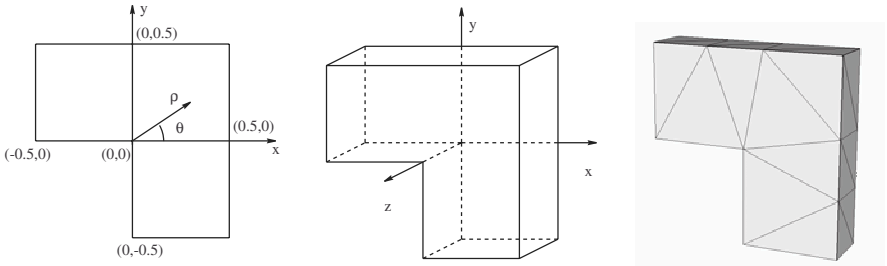

(a) *The x-y plane* (b) *The domain* (c) *Initial mesh*

Figure 2: The L-shaped domain with a line singularity.

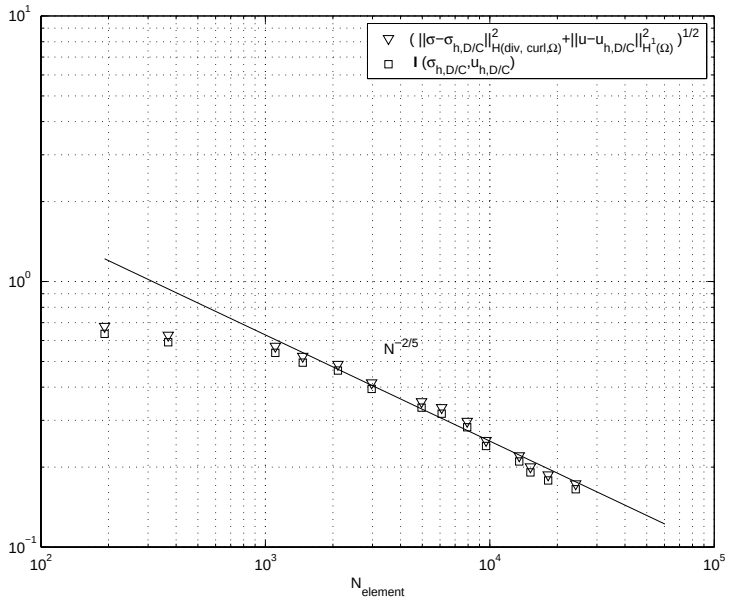

Figure 3: Error for DLSFEM in the line singularity problem. Triangles denote the error measured in the $H^1(\Omega) \times H(\mathrm{div}, \mathrm{curl}; \Omega)$-norm and squares denote the least-squares residual.

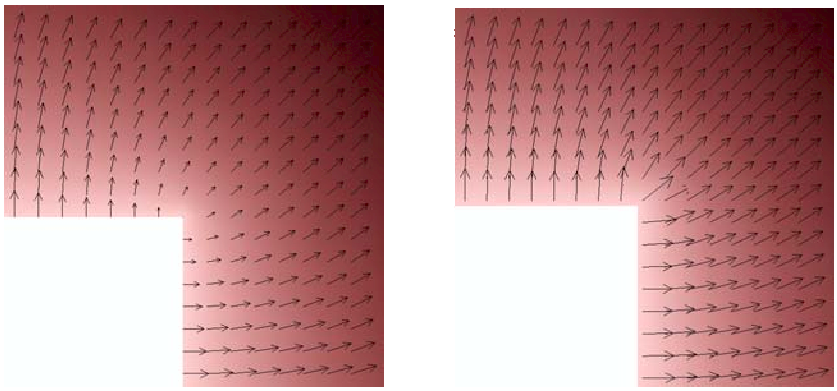

(a) *Standard LSFEM* (b) *Discontinuous LSFEM*

Figure 4: The computed flux in the vicinity of the corner of the L-shaped domain. Note that for standard LSFEM, the flux incorrectly tends to zero in the corner.

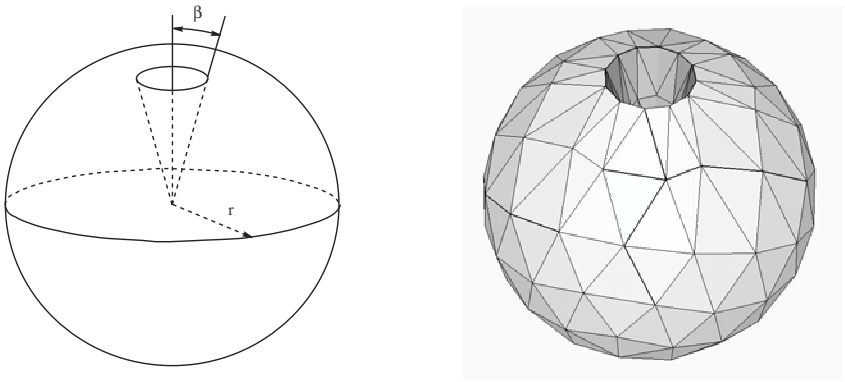

(a) *Geometry* (b) *Initial mesh*

Figure 5: The cone problem with a point singularity.

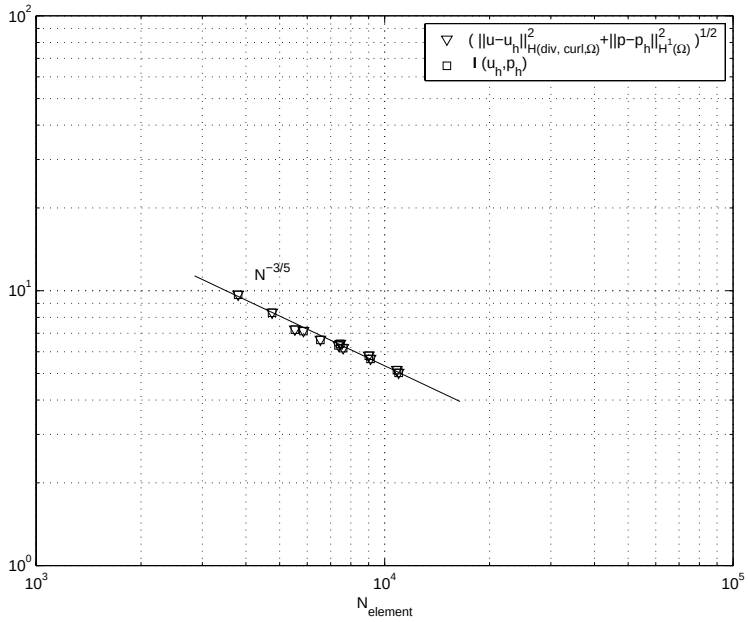

Figure 6: Error for DLSFEM in the point singularity problem. Triangles denote the error measured in the $H^1(\Omega) \times H(\mathrm{div}, \mathrm{curl}; \Omega)$-norm and squares denote the least-squares residual.

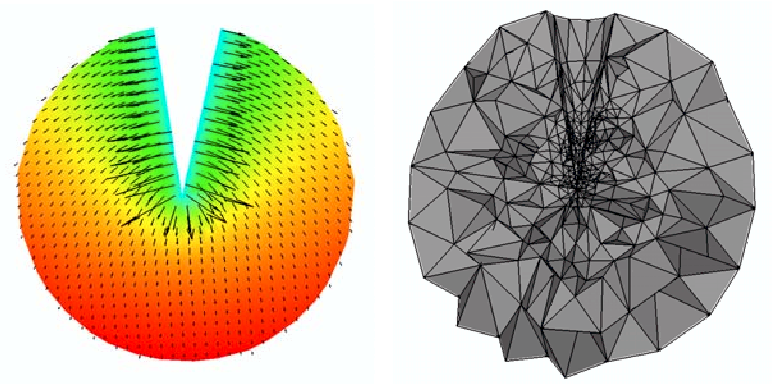

(a) *Solution* (b) *Refined mesh*

Figure 7: The solution and the refined mesh for the point singularity problem.

5.2 The magnetostatic equations

The equations that define static magnetic fields are

$$\nabla \times H = J, \tag{5.6a}$$

$$\nabla \cdot B = 0, \tag{5.6b}$$

where H is the magnetic field intensity, B is the magnetic flux density, and J the imposed current density. The two fields H and B are related through the constitutive relation

$$B = \mu H, \tag{5.7}$$

where $\mu = \mu_r \mu_0$ is the magnetic permeability with $\mu_0 = 4\pi \times 10^{-7}$ H/m and $\mu_r > 0$. At the interface between two materials, equations (5.6) imply the continuity conditions

$$[H] \times n = 0, \tag{5.8a}$$

$$[B] \cdot n = 0, \tag{5.8b}$$

stating that the tangential components of H are continuous, as well as the normal component of B. In view of equation (5.7), the normal component $H \cdot n$ and the tangential components $B \times n$ will thus be discontinuous across an interface of discontinuity of μ. At the boundary, we have either a prescribed field, a symmetry condition or a perfectly conducting wall, $B \cdot n = 0$.

5.2.1 Model problem

We have previously reported problems in applying LSFEM to magnetostatic problems with realistic data [5]. Applying the discontinuous least-squares method to system (5.6), we have however successfully solved a model problems of this kind. Never the less, the mesh refinement indicator does not seem to yield optimal convergence. The problem is axisymmetric in order to make two dimensional reference computations possible, and is also reported in [3] and [4].

The geometry of this problem is described in Figure 10(a). A three dimensional view can be seen in Figure 10(b). The model consists of an iron cylinder core encircled by a copper winding. The configuration is enclosed in air and surrounded by a box with perfectly magnetic surfaces. The winding is modeled as a homogeneous copper coil.

Data for this problem are relative magnetic permeabilities $\mu_{r,Fe} = 10^4$ and $\mu_{r,Cu} = \mu_{r,air} = 1$, and the current density J is constant over the cross section of the coil with a total current of 1 A.

	DLSFEM	Reference
No of elements	348 373	-
No of nodes	59 970	-
W_{air} (J)	$8.322 \times 10^{-7}(0.08)$	9.089×10^{-7}
W_{cu} (J)	$3.434 \times 10^{-8}(0.05)$	3.614×10^{-8}
W_{fe} (J)	$5.358 \times 10^{-10}(0.13)$	4.731×10^{-10}

Table 1: The computed magnetic energies compared with reference values using DLSFEM; the relative error is given in parenthesis. The reference values are from two dimensional computations done at ABB [4].

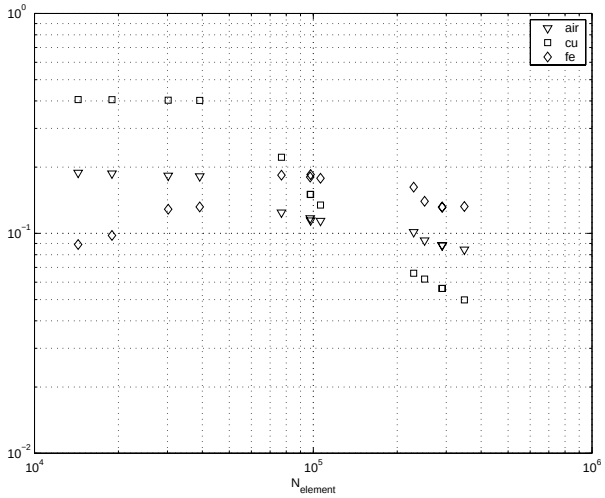

Figure 8: Relative error in the energy for DLSFEM in the magnetostatic problem. Triangles denote the error in the air region, squares represent the copper region, and diamonds the iron core.

Reference computations in two dimensions done by ABB and reported in [4], gave the values of the magnetic energies in the different materials as listed in Table 1, where the magnetic energy is defined by

$$W_{\Omega^i} = \frac{1}{2} \int_{\Omega^i} B \cdot H \, dx. \tag{5.9}$$

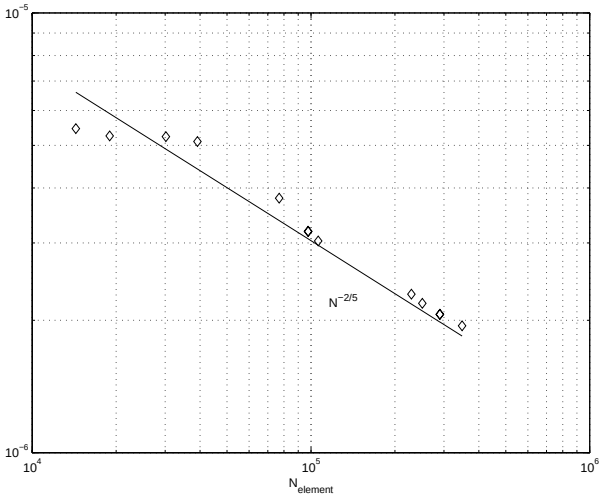

Figure 9: The least-squares residual for the magnetostatic example.

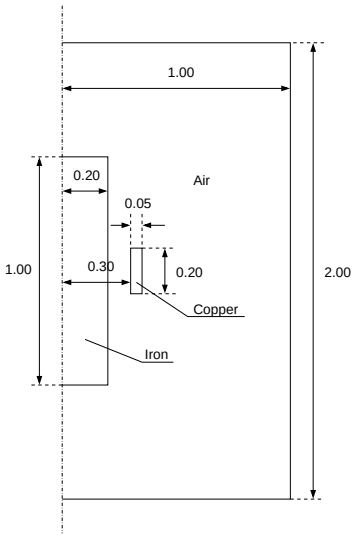

(a) *Geometry of the magnetostatic example*

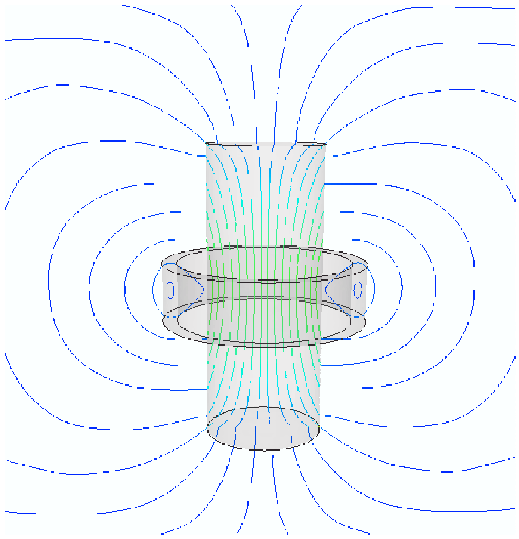

(b) *Field lines of the solution*

Figure 10: Geometry and the solution for the magnetostatic example.

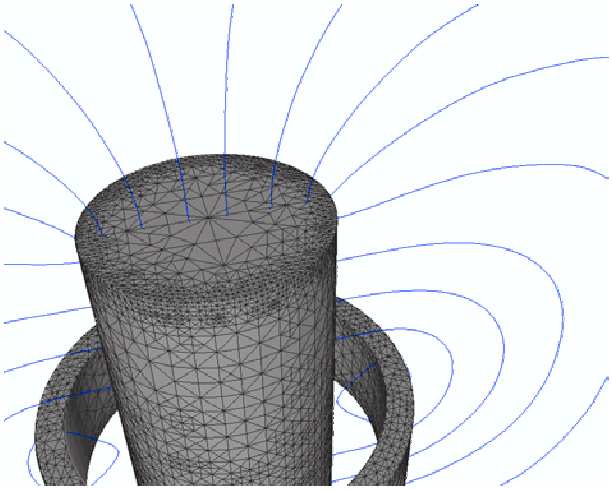

Figure 11: Detail of the mesh.

References

[1] C. Amrouche, C. Bernardi, M. Dauge, and V. Girault. Vector potentials in three-dimensional nonsmooth domains. *Math. Methods Appl. Sci.*, 21:823–864, 1998.

[2] T. Apel, S. Nicaise, and J. Schöberl. Crouzeix-Raviart type finite elements on anisotropic meshes. *Numer. Math.*, 89(2):193–223, 2001.

[3] R. Bergström. Least-squares finite element method with applications in electromagnetics. Preprint 10, Chalmers Finite Element Center, Chalmers University of Technology, 2002.

[4] R. Bergström, A. Bondeson, C. Johnson, M.G. Larson, Y. Liu, and K. Samuelsson. Adaptive finite element methods in electromagnetics. Technical Report 2, Swedish Institute of Applied Mathematics (ITM), 1999.

[5] R. Bergström and M.G. Larson. Discontinuous/continuous least-squares finite element methods for elliptic problems. Preprint 11, Chalmers Finite Element Center, Chalmers University of Technology, 2002. To appear in Math. Models Methods Appl. Sci.

[6] R. Bergström, M.G. Larson, and K. Samuelsson. The $\mathcal{LL}^*$ finite element method and multigrid for the magnetostatic problem. Preprint 2, Chalmers Finite Element Center, Chalmers University of Technology, 2001.

[7] P.B. Bochev and M.D. Gunzburger. Finite element methods of least-squares type. *SIAM Rev.*, 40(4):789–837, 1998.

[8] A.-S. Bonnet-Ben Dhia, C. Hazard, and S. Lohrengel. A singular field method for the solution of Maxwell's equations in polyhedral domains. *SIAM J. Appl. Math.*, 59(6):2028–2044, 1999.

[9] J.H. Bramble, R.D. Lazarov, and J.E. Pasciak. A least-squares approach based on a discrete minus one inner product for first order systems. *Math. Comp.*, 66(219):935–955, 1997.

[10] Z. Cai, T.A. Manteuffel, and S.F. McCormick. First-order system least squares for second-order partial differential equations. II. *SIAM J. Numer. Anal.*, 34(2):425–454, 1997.

[11] Y. Cao and M.D. Gunzberger. Least-squares finite element approximations to solutions of interface problems. *SIAM J. Numer. Anal.*, 35(1):393–405, 1998.

[12] Z.M. Chen, Q. Du, and J. Zou. Finite element methods with matching and nonmatching meshes for Maxwell equations with discontinuous coefficients. *SIAM J. Numer. Anal.*, 37:1542–1570, 2000.

[13] C.L. Cox and G.J. Fix. On the accuaracy of least squares methods in the presence of corner singularities. *Comp. & Maths. with Appls.*, 10(6):463–475, 1984.

[14] L. Formaggia and S. Perotto. New anisotropic a priori estimates. *Numer. Math.*, 89:641–667, 2001.

[15] V. Girault and P.A. Raviart. *Finite Element Methods for Navier-Stokes Equations.* Springer-Verlag, 1986.

[16] P. Grisvard. *Elliptic Problems in Nonsmooth Domains.* Pitman Publishing Inc., 1985.

[17] J.D. Jackson. *Classical Electrodynamics.* John Wiley & Sons, 2nd edition, 1975.

[18] J.-L. Liu. Exact a posteriori error analysis of the least-squares finite element method. *Appl. Math. Comput.*, 116:297–305, 2000.

[19] T.A. Manteuffel, S.F. McCormick, and G. Starke. First-order system of least-squares for second order elliptic problems with discontinuous coefficients. To appear.

[20] J.E. Pasciak and J. Zhao. Overlapping schwarz methods in $h(\mathrm{curl})$ on nonconvex domains.

[21] A.I. Pehlivanov, G.F. Carey, and P.S. Vassilevski. Least-squares mixed finite element methods for non-selfadjoint problems: I. error estimates. *Numer. Math.*, 72:501–522, 1996.

[22] L.R. Scott and S. Zhang. Finite element interpolation of nonsmooth functions satisfying bundary conditions. *Math. Comp.*, 54:483–493, 1990.

[23] K.G. Siebert. An a posteriori error estimator for anisotropic refinement. *Numer. Math.*, 73(3):373–398, 1996.

Paper IV

The $\mathcal{LL}^*$ Finite Element Method and Multigrid for the Magnetostatic Problem *

Rickard Bergström†, Mats G. Larson‡ and Klas Samuelsson

Abstract

We develop the $\mathcal{LL}^*$-method for a magnetostatic model problem with large jumps in material parameters in three spatial dimensions. A priori and a posteriori error estimates are presented as well as an adaptive algorithm. We employ a multigrid method to solve the resulting algebraic equations. Finally, we present numerical results.

1 Introduction

In this paper we are concerned with finite element approximation of first order elliptic partial differential equations of the form $\mathcal{L}u = f$. More precisely, we study a model problem from magnetostatics in three spatial dimensions with large jumps in the material coefficients. Typically, due to corners in the geometry, the solution develops singularities and does not reside in H^1, and thus cannot be accurately approximated in spaces of continuous piecewise polynomials. As a remedy, we instead introduce the dual variable v such that $u = \mathcal{M}\mathcal{L}^*v$, where $\mathcal{M}$ is a bounded symmetric operator with bounded inverse. Substituting into the equation $\mathcal{L}u = f$, we obtain the symmetric second order problem $\mathcal{L}\mathcal{M}\mathcal{L}^*v = f$, which can be approximated by standard continuous polynomials, since $v \in H^1$. Choosing $\mathcal{M}$ properly, the energy minimized is the physical energy, which is a desirable property. We refer to this approach as the $\mathcal{LL}^*$-method. The resulting algebraic system is symmetric positive definite and can be efficiently solved by a multigrid method.

*This research is supported by ABB Corporate Research

†Supported by the Swedish Foundation for Strategic Research through the National Graduate School in Scientific Computing and the National Network in Applied Mathematics

‡Supported by Swedish Research Council for Engineering Sciences

The $\mathcal{LL}^*$-method was recently suggested by Cai *et al.* [11] for solving a second order elliptic problem by first rewriting it as a first order system of equations and then applying the aforementioned approach. Here the method is viewed as a remedy of the difficulties which the least-squares finite element method exhibits on problems which are not sufficiently regular. The least-squares method, see for instance [3], [5], [6], [14], and the references therein, determines an approximate solution u_h which minimizes the L^2-norm of the residual $\|\mathcal{L}u_h - f\|^2$. Thus u is required to be in H^1 for the residual to be well defined. It is also shown that $\mathcal{LL}^*$-method is closely related to least-squares methods based on dual norms of the residual, see Bramble *et al.* [7] and Cai *et al.* [10].

We may also view the $\mathcal{LL}^*$-method as a generalization of the classical potential methods in electromagnetics, see for instance Jin [16] for a general introduction to such techniques. In the case of the $\mathcal{LL}^*$-method, we allow for a more general potential v defined by $u = \mathcal{ML}^*v$.

We prove optimal a priori and a posteriori error estimates, and based on the later we develop an adaptive algorithm for refinement of the mesh. We also discuss implementation details of the mesh refinement algorithm.

The remainder of the paper is organized as follows: in Section 2 we introduce the model problem and derive the $\mathcal{LL}^*$-method; in Section 3 we prove a priori and a posteriori error estimates and describe the adaptive algorithm together with some details on the mesh refinement procedure; in Section 4 we formulate the multigrid algorithm; in Section 5 we present some numerical results.

2 The $\mathcal{LL}^*$ formulation

2.1 A magnetostatic model problem

Assume that $\Omega = \bigcup_{i=1}^n \Omega^i \in \mathbf{R}^3$ with boundary Γ, and denote the interface between regions Ω^i and Ω^j by Γ^{ij}, with $i < j$, see Figure 1. We allow Ω^i to be nonconvex and have corners, while Ω is assumed to be convex or have sufficiently smooth boundary. In applications, this is in general not a restrictive assumption. Assume that each subdomain have the magnetic permeability $\mu|_{\Omega^i} = \mu_r^i \, \mu_0$. The magnetostatic system then takes the form:

$$\nabla \times \mu^{-1} B = J \quad \text{in } \Omega^i, \tag{2.1a}$$

$$\nabla \cdot B = 0 \quad \text{in } \Omega^i, \tag{2.1b}$$

$$n \cdot B = 0 \quad \text{on } \Gamma, \tag{2.1c}$$

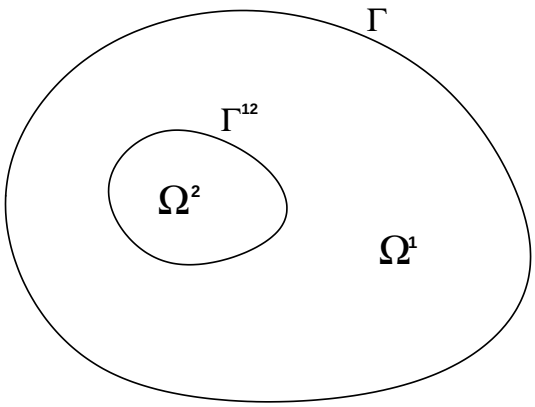

Figure 1: The notation used when a region is split into subregions.

and the interface conditions

$$[\mu^{-1}B] \times n = 0 \quad \text{on } \Gamma^{ij}, \tag{2.2a}$$

$$[B] \cdot n = 0 \quad \text{on } \Gamma^{ij}. \tag{2.2b}$$

hold. Here, n is the exterior unit normal on the boundary Γ and a fixed unit normal on each interior interface Γ^{ij}, and $[u(x)] = \lim_{s\to 0^+} u(x+sn) - u(x-sn)$ with $x \in \Gamma^{ij}$, denotes the jump in u across the interface Γ^{ij}. Furthermore, it is necessary that

$$\nabla \cdot J = 0, \tag{2.3}$$

for (2.1) to have a solution.

2.2 An associated first order operator

By adding a slack variable b to (2.1) we can show ellipticity of this system [15]. This extra variable is in fact zero in the continuous problem as we show below, but this is not necessarily the case in the discrete problem. Furthermore, adding the slack variable creates a suitable Hilbert space setting for the analysis.

The extended system thus becomes

$$\nabla \times \mu^{-1} B - \nabla b = J \quad \text{in } \Omega, \tag{2.4a}$$
$$\nabla \cdot B = 0 \quad \text{in } \Omega, \tag{2.4b}$$
$$n \cdot B = 0 \quad \text{on } \Gamma, \tag{2.4c}$$
$$b = 0 \quad \text{on } \Gamma, \tag{2.4d}$$
$$[\mu^{-1} B] \times n = 0 \quad \text{on } \Gamma^{ij}, \tag{2.4e}$$
$$[B] \cdot n = 0 \quad \text{on } \Gamma^{ij}. \tag{2.4f}$$

The slack variable b is identically zero, since by taking the divergence of (2.4a) we get the following Poisson problem for b:

$$-\Delta b = \nabla \cdot J - \nabla \cdot (\nabla \times \mu^{-1} B) \quad \text{in } \Omega, \tag{2.5}$$

together with the boundary condition (2.4d). From equations (2.1), (2.2) and (2.3) we see that the right hand side of (2.5) is zero, thus b is indeed zero and hence system (2.4) is equivalent to (2.1).

We introduce the Hilbert space

$$\mathcal{V} = [L^2(\Omega)]^3 \times L^2(\Omega), \tag{2.6}$$

and employ the notation $\boldsymbol{V} = [V\, v]^T \in \mathcal{V}$, with $V \in [L^2(\Omega)]^3$ and $v \in L^2(\Omega)$. We also define

$$\mathcal{V}_0 = \{\boldsymbol{V} \in \mathcal{V} : v = 0 \text{ on } \Gamma\}. \tag{2.7}$$

Next we define the first order operator $\mathcal{L}$ and its formal adjoint $\mathcal{L}^*$ as follows

$$\mathcal{L}\boldsymbol{V} = \begin{pmatrix} \nabla \times \mu^{-1} V - \nabla v \\ \nabla \cdot V \end{pmatrix}, \quad \mathcal{L}^*\boldsymbol{W} = \begin{pmatrix} \mu^{-1} \nabla \times W - \nabla w \\ \nabla \cdot W \end{pmatrix}, \tag{2.8}$$

for $\boldsymbol{V}, \boldsymbol{W} \in \mathcal{V}$.

To derive the boundary conditions associated with $\mathcal{L}^*$ we compute

$$(\mathcal{L}\boldsymbol{V}, \boldsymbol{W}) = (\boldsymbol{V}, \mathcal{L}^*\boldsymbol{W}) + \int_\Gamma n \times (\mu^{-1} V) \cdot W + \int_\Gamma v\ n \cdot W + \int_\Gamma n \cdot V\ w \tag{2.9}$$
$$= (\boldsymbol{V}, \mathcal{L}^*\boldsymbol{W}) + \int_\Gamma n \times (\mu^{-1} V) \cdot W,$$

where we used (2.4c) and (2.4d). Using the scalar triple product, $n \times (\mu^{-1} V) \cdot W = -(\mu^{-1} V) \cdot n \times W$ and thus the remaining boundary term vanishes if and only if the condition

$$n \times W = 0 \quad \text{on } \Gamma, \tag{2.10}$$

holds.

The domains of $\mathcal{L}$ and $\mathcal{L}^*$ are,

$$\mathcal{D}(\mathcal{L}) = \{\boldsymbol{V} \in H(\nabla \times \mu^{-1}, \Omega) \cap H(\nabla\cdot, \Omega) \times H^1(\Omega) : \quad n \cdot V = 0, v = 0 \text{ on } \Gamma\}, \tag{2.11a}$$

$$\mathcal{D}(\mathcal{L}^*) = \{\boldsymbol{V} \in H(\nabla\times, \Omega) \cap H(\nabla\cdot, \Omega) \times H^1(\Omega)/\ \mathbf{R} : n \times V = 0 \text{ on } \Gamma\}, \tag{2.11b}$$

where

$$H(\nabla \times \mu^{-1}, \Omega) = \{V \in [L^2(\Omega)]^3 : \nabla \times \mu^{-1} V \in [L^2(\Omega)]^3\}, \tag{2.12a}$$

$$H(\nabla\cdot, \Omega) = \{V \in [L^2(\Omega)]^3 : \nabla \cdot V \in L^2(\Omega)\}, \tag{2.12b}$$

are Hilbert spaces with the norms

$$\|V\|^2_{H(\nabla\times\mu^{-1},\Omega)} = \|V\|^2 + \|\nabla \times \mu^{-1} V\|^2, \tag{2.13a}$$

$$\|V\|^2_{H(\nabla\cdot,\Omega)} = \|V\|^2 + \|\nabla \cdot V\|^2. \tag{2.13b}$$

$H(\nabla\times, \Omega)$ corresponds to (2.12a) with $\mu = 1$. Thus, $\mathcal{D}(\mathcal{L})$ and $\mathcal{D}(\mathcal{L}^*)$ are Hilbert spaces, dense in $\mathcal{V}_0$ and $\mathcal{V}$ respectively, with the product norm

$$\|\boldsymbol{V}\|^2_{\mathcal{D}(\mathcal{L})} = \|V\|^2 + \|\nabla \times \mu^{-1} V\|^2 + \|\nabla \cdot V\|^2_0 + \|v\|^2_{H^1_0(\Omega)}, \tag{2.14}$$

and similarly for $\mathcal{D}(\mathcal{L}^*)$.

2.3 The $\mathcal{L}\mathcal{L}^*$ variational formulation

We can now in a standard manner derive a variational problem for (2.1) by integrating by parts: find $\boldsymbol{B} \in \mathcal{D}(\mathcal{L})$ such that

$$(\boldsymbol{J}, \boldsymbol{V}) = (\mathcal{L}\boldsymbol{B}, \boldsymbol{V}) = (\boldsymbol{B}, \mathcal{L}^*\boldsymbol{V}), \tag{2.15}$$

for all $\boldsymbol{V} \in \mathcal{D}(\mathcal{L}^*)$.

Next we introduce dual variables $\boldsymbol{U}$ such that

$$\boldsymbol{B} = \mathcal{M}\mathcal{L}^*\boldsymbol{U}, \tag{2.16}$$

where $\mathcal{M}$ denotes a symmetric positive definite bounded operator with bounded inverse. A suitable choice of $\mathcal{M}$ is presented below. Thus, we obtain the weak problem: find $\boldsymbol{U} \in \mathcal{D}(\mathcal{L}^*)$ such that

$$a(\boldsymbol{U}, \boldsymbol{V}) = l(\boldsymbol{V}), \tag{2.17}$$

for all $\boldsymbol{V} \in \mathcal{D}(\mathcal{L}^*)$. Here the bilinear form and functional are defined by

$$a(\boldsymbol{U}, \boldsymbol{V}) = (\mathcal{M}\mathcal{L}^*\boldsymbol{U}, \mathcal{L}^*\boldsymbol{V}), \tag{2.18}$$

$$l(\boldsymbol{V}) = (J, V). \tag{2.19}$$

We now turn to the operator $\mathcal{M}$. For our application, we assume that $\mathcal{M} : v \mapsto Mv$ where M is a 4×4 diagonal matrix with diagonal $[m_1\, m_1\, m_1\, m_2]$. To determine the parameters m_1 and m_2 we note that the energy of the bilinear form is

$$a(\boldsymbol{U}, \boldsymbol{U}) = (\mathcal{M}\mathcal{L}^*\boldsymbol{U}, \mathcal{L}^*\boldsymbol{U}) \tag{2.20}$$

$$= (\boldsymbol{B}, \mathcal{M}^{-1}\boldsymbol{B}) \tag{2.21}$$

$$= (m_1^{-1}B, B) + (m_2^{-1}b, b). \tag{2.22}$$

For the exact solution $b = 0$, and we should preferably obtain proportionality to the physical energy

$$\frac{1}{2}(B, H) = \frac{1}{2}(B, \mu^{-1}B), \tag{2.23}$$

and thus $m_1 = \mu$. Next, to determine m_2 we note that

$$a(\boldsymbol{U}, \boldsymbol{U}) = (\mu(\mu^{-1}\nabla \times U - \nabla u), \mu^{-1}\nabla \times U - \nabla u) + (m_2 \nabla \cdot U, \nabla \cdot U). \tag{2.24}$$

Balancing the terms involving U, we are led to choosing $m_2 = \mu^{-1}$.

Using Lemma 2.1 below, the bilinear form finally simplifies to

$$a(\boldsymbol{U}, \boldsymbol{U}) = (\mu^{-1}\nabla \times U, \nabla \times U) + (\mu^{-1}\nabla \cdot U, \nabla \cdot U) + (\mu \nabla u, \nabla u). \tag{2.25}$$

Lemma 2.1 *For* $\boldsymbol{V} \in \mathcal{D}(\mathcal{L}^*)$,

$$(\nabla \times V, \nabla v) = 0. \tag{2.26}$$

Proof. The identity follows using Green's formula,

$$(\nabla \times V, \nabla v) = (V, \nabla \times \nabla v) + (n \times V, \nabla v)_\Gamma, \tag{2.27}$$

since $n \times V = 0$ on Γ for $\boldsymbol{V} \in \mathcal{D}(\mathcal{L}^*)$. □

We are now ready to state the following theorems.

Theorem 2.2 *There are constants c and C, which depend only on μ, such that*

$$c\|\boldsymbol{V}\|_1^2 \leq a(\boldsymbol{V},\boldsymbol{V}) \leq C\|\boldsymbol{V}\|_1^2, \tag{2.28}$$

for all $\boldsymbol{V} \in \mathcal{V}$. Furthermore, there exists a unique solution $\boldsymbol{U}$ to (2.17) and the a priori estimate

$$\|\boldsymbol{U}\|_1 \leq c\|\boldsymbol{J}\|_{-1}, \tag{2.29}$$

holds.

Proof. To prove the lower bound we note that

$$\begin{aligned} a(\boldsymbol{V},\boldsymbol{V}) &= (\mu^{-1}\nabla\times V, \nabla\times V) + (\mu^{-1}\nabla\cdot V, \nabla\cdot V) + (\mu\nabla v, \nabla v) \\ &\geq C\min(\mu^{-1})\|V\|_1^2 + C\min(\mu)\|v\|_1^2, \end{aligned} \tag{2.30}$$

since Ω is assumed to have smooth boundary [13]. This concludes the proof of the coercivity. The upper bound is an obvious consequence of the Cauchy-Schwarz and triangle inequalities. The existence and uniqueness of the solution to (2.17) follows from the Lax-Milgram lemma and the a priori estimate is straightforward. □

Theorem 2.3 *There is a unique solution $\boldsymbol{B} \in \mathcal{D}(\mathcal{L})$ to (2.4), and $\boldsymbol{B} = \mathcal{M}\mathcal{L}^*\boldsymbol{U}$ is the unique solution to (2.15).*

Proof. We need to show that $\boldsymbol{B} = \mathcal{M}\mathcal{L}^*\boldsymbol{U} \in \mathcal{D}(\mathcal{L})$. Then $\boldsymbol{B}$ satisfies (2.15) and the uniqueness of this solution follows from the stability estimate

$$(\boldsymbol{B}, \mathcal{L}^*\boldsymbol{V}) = (\boldsymbol{J},\boldsymbol{V}) \leq \|\boldsymbol{J}\|\|\boldsymbol{V}\|. \tag{2.31}$$

To do this, we first note that from Theorem 2.2 we can conclude that $\mathcal{L}^{-*}$ is continuous. Furthermore, we get continuity of $\mathcal{L}^{-1}$ if we can show

$$\|\boldsymbol{V}\|_{\mathcal{D}(\mathcal{L})}^2 \leq C\|\mathcal{L}\boldsymbol{V}\|_{\mathcal{V}}^2. \tag{2.32}$$

This is clear since for $\boldsymbol{V} \in \mathcal{D}(\mathcal{L})$,

$$\begin{aligned} \|\mathcal{L}\boldsymbol{V}\|_{\mathcal{V}}^2 &= (\nabla\times\mu^{-1}V, \nabla\times\mu^{-1}V) + (\nabla v, \nabla v) + (\nabla\cdot V, \nabla\cdot V) \\ &\geq C(\|V\|^2 + \|v\|^2) = C\|\boldsymbol{V}\|_{\mathcal{V}}^2, \end{aligned} \tag{2.33}$$

and

$$\|\boldsymbol{V}\|_{\mathcal{D}(\mathcal{L})}^2 \leq C(\|\mathcal{L}\boldsymbol{V}\|^2 + \|\boldsymbol{V}\|_{\mathcal{V}}^2). \tag{2.34}$$

From Lemma 2.2 in [11], we now know that $\mathcal{R}(\mathcal{L}) = \mathcal{V}$ and $\mathcal{R}(\mathcal{L}^*) = \mathcal{V}_0$, thus $\boldsymbol{B} \in \mathcal{V}_0 \supseteq \mathcal{D}(\mathcal{L})$. □

3 The $\mathcal{LL}^*$ finite element method

3.1 The finite element method

Let $\mathcal{K}$ be a decomposition of Ω into, e.g., tetrahedral, elements K, with diameter $h_K = \text{diam}(K)$. We assume a minimal angle condition on the triangulation, see Brenner and Scott [8]. Let

$$\mathcal{W}_h = \mathcal{D}(\mathcal{L}^*) \cap \{\boldsymbol{V} \in [C(\Omega)]^4 : \boldsymbol{V}|_K \in [\mathcal{P}_r(K)]^4\}, \tag{3.1}$$

where $\mathcal{P}_r$ is the vector space of all polynomials of degree less than or equal to r. Thus $\mathcal{W}_h$ is the set of all piecewise vector polynomial functions of degree r, which are continuous across element edges.

For the error analysis following below, we need the following approximation property of $\mathcal{W}_h$, see Scott and Zhang [17]. Given a function $\boldsymbol{V} \in \mathcal{D}(\mathcal{L}^*) \cap [H^\alpha(\Omega)]^4$, for $r \geq 1$, there is an interpolation operator $\pi : \mathcal{D}(\mathcal{L}^*) \to \mathcal{W}_h$ such that

$$\|\boldsymbol{V} - \pi\boldsymbol{V}\|_{K,1} \leq C h_K^{\alpha-1} |\boldsymbol{V}|_{N(K),\alpha}, \quad 1 \leq \alpha \leq r+1, \tag{3.2}$$

where $N(K)$ denotes the union of all elements bordering K.

The $\mathcal{LL}^*$ finite element method finally takes the form: find $\boldsymbol{U}_h \in \mathcal{W}_h$ such that

$$a(\boldsymbol{U}_h, \boldsymbol{V}) = l(\boldsymbol{V}), \tag{3.3}$$

for all $\boldsymbol{V} \in \mathcal{W}_h$.

In the computations, we can benefit from the fact that u_h is zero. This is clear since the equations for components U_h and u_h separate according to Lemma 2.1, and we have zero data for u_h. The bilinear form and the linear functional used in computations thus take the form

$$a_h(\boldsymbol{U}, \boldsymbol{V}) = (\mu^{-1}\nabla \times U, \nabla \times V) + (\mu^{-1}\nabla \cdot U, \nabla \cdot V), \tag{3.4a}$$

$$l_h(\boldsymbol{V}) = (J, V). \tag{3.4b}$$

Furthermore, functionals involving the magnetic field B should be computed via the variational form (3.4a). Hence the energy, e.g., is computed as

$$W_h = \frac{1}{2} a_h(\boldsymbol{U}_h, \boldsymbol{U}_h). \tag{3.5}$$

3.2 A priori error estimate

Using standard techniques we derive the following a priori error estimate.

Theorem 3.1 *Let $\boldsymbol{U} \in \mathcal{D}(\mathcal{L}^*) \cap [H^s(\Omega)]^4$ be a solution to (2.17) and $\boldsymbol{U}_h \in \mathcal{W}_h$ the approximate solution defined by (3.3). Then there is a constant C, independent of h, such that*

$$\|\boldsymbol{U} - \boldsymbol{U}_h\|_1^2 \leq C \sum_{K \in \mathcal{K}} h_K^{2(\alpha-1)} |\boldsymbol{U}|_{N(K),\alpha}^2, \tag{3.6}$$

with $\alpha = \min(r+1, s)$.

Proof. Let $\boldsymbol{E} = \boldsymbol{U} - \boldsymbol{U}_h$ denote the error. Then

$$\begin{aligned} c\|\boldsymbol{E}\|_1^2 &\leq a(\boldsymbol{E}, \boldsymbol{U} - \boldsymbol{U}_h) \\ &= a(\boldsymbol{E}, \boldsymbol{U} - \pi\boldsymbol{U} + \pi\boldsymbol{U} - \boldsymbol{U}_h) \\ &= a(\boldsymbol{E}, \boldsymbol{U} - \pi\boldsymbol{U}) \\ &\leq C\|\boldsymbol{E}\|_1^2 \|\boldsymbol{U} - \pi\boldsymbol{U}\|_1^2, \end{aligned} \tag{3.7}$$

where (3.3) was used in the last equality. Dividing by $\|\boldsymbol{E}\|_1$, and finally using the interpolation estimate (3.2) proves the estimate. □

3.3 A posteriori error estimate

Introducing the energy norm

$$|||\boldsymbol{V}|||^2 = a(\boldsymbol{V}, \boldsymbol{V}), \tag{3.8}$$

we can state the following a posteriori error estimate.

Theorem 3.2 *Let $\boldsymbol{U} \in \mathcal{D}(\mathcal{L}^*) \cap [H^1(\Omega)]^4$ be a solution to (2.17) and $\boldsymbol{U}_h \in \mathcal{W}_h$ the approximate solution defined by (3.3). Then there is a constant C, independent of h, such that*

$$|||\boldsymbol{U} - \boldsymbol{U}_h|||^2 \leq C \sum_{K \in \mathcal{K}} R_K(\boldsymbol{U}_h)^2, \tag{3.9}$$

where

$$R_K(\boldsymbol{U}_h)^2 = \omega_1 \|h\mathcal{M}^{-1/2}(\boldsymbol{J} - \mathcal{L}\mathcal{M}\mathcal{L}^*\boldsymbol{U}_h)\|_K^2 + \omega_2 \|h^{1/2} K[\lambda_n(\boldsymbol{U}_h)]\|_{\partial K}^2. \tag{3.10}$$

The boundary flux $\lambda_n(\boldsymbol{V})$ is defined by

$$\lambda_n(\boldsymbol{V}) = \begin{pmatrix} n \times (\mu^{-1}\nabla \times V) + n\mu^{-1}\nabla \cdot V \\ n \cdot (\mu \nabla v) \end{pmatrix}, \tag{3.11}$$

and K is a diagonal matrix with diagonal $[k_1 k_1 k_1 k_2]$ where

$$k_1 = \frac{(\mu^-)^{1/2}}{\mu^+ + \mu^-}, \tag{3.12a}$$

$$k_2 = \frac{(\frac{1}{\mu^-})^{1/2}}{\frac{1}{\mu^+} + \frac{1}{\mu^-}}. \tag{3.12b}$$

Remark 3.1 Note that the constant $C = C(\omega_1, \omega_2, C_{tr}, C_i)$. To achieve a constant free error estimator, one may instead solve local problems, see [2], in general at the cost of more expensive computations.

Remark 3.2 Note that

$$|||\boldsymbol{U} - \boldsymbol{U}_h||| = a(\boldsymbol{U} - \boldsymbol{U}_h, \boldsymbol{U} - \boldsymbol{U}_h) = a(\boldsymbol{U}, \boldsymbol{U}) - a(\boldsymbol{U}_h, \boldsymbol{U}_h) = 2(W - W_h). \tag{3.13}$$

Thus the error in the energy is directly related to the error in the energy norm of the dual variables, motivating adaptation of the grid with respect to the error measured in the energy norm .

Proof. Let $\boldsymbol{E} = \boldsymbol{U} - \boldsymbol{U}_h$ denote the error. Then

$$\begin{aligned} |||\boldsymbol{E}|||^2 &= a(\boldsymbol{U} - \boldsymbol{U}_h, \boldsymbol{E}) \\ &= a(\boldsymbol{U} - \boldsymbol{U}_h, \boldsymbol{E} - \pi\boldsymbol{E}) \\ &= (\mathcal{M}\mathcal{L}^*(\boldsymbol{U} - \boldsymbol{U}_h), \mathcal{L}^*(\boldsymbol{E} - \pi\boldsymbol{E})) \\ &= \sum_{K \in \mathcal{K}} (\boldsymbol{J} - \mathcal{L}\mathcal{M}\mathcal{L}^*\boldsymbol{U}_h, \boldsymbol{E} - \pi\boldsymbol{E})_K + (\lambda_n(\boldsymbol{U}) - \lambda_n(\boldsymbol{U}_h), \boldsymbol{E} - \pi\boldsymbol{E})_{\partial K} \\ &= \sum_{K \in \mathcal{K}} (\boldsymbol{J} - \mathcal{L}\mathcal{M}\mathcal{L}^*\boldsymbol{U}_h, \boldsymbol{E} - \pi\boldsymbol{E})_K + (\Lambda_n(\boldsymbol{U}_h) - \lambda_n(\boldsymbol{U}_h), \boldsymbol{E} - \pi\boldsymbol{E})_{\partial K}, \end{aligned} \tag{3.14}$$

where $\lambda_n(\boldsymbol{V})$ is defined above in (3.11) and $\Lambda_n(\boldsymbol{U}_h)$ is a discrete approximation of the true flux $\lambda_n(\boldsymbol{U})$. The replacement of $\lambda_n(\boldsymbol{U})$ with $\Lambda_n(\boldsymbol{U}_h)$ in the last equality is possible since on all internal edges, the boundary contributions from the neighbouring elements cancel for $\lambda_n(\boldsymbol{U})$, and this should be true for $\Lambda_n(\boldsymbol{U}_h)$ by construction. Also on external edges $\Lambda_n(\boldsymbol{U}_h)$ should satisfies the boundary conditions.

In a standard derivation of an energy norm a posteriori error estimate, e.g., as in Eriksson and Johnson [12], one constructs a discrete flux as the average of the approximate flux on each element side, i.e.,

$$\Lambda_n(\boldsymbol{U}_h) = \frac{1}{2}(\lambda_n(\boldsymbol{U}_h^+) + \lambda_n(\boldsymbol{U}_h^-)), \tag{3.15}$$

which leads to the standard jump terms $\frac{1}{2}[\lambda_n(\boldsymbol{U}_h)]$. However, in order to correctly distribute the error in the fluxes across interfaces with large discontinuities in μ, we here choose a weighted average

$$\Lambda_n(\boldsymbol{U}_h) = (M^+ + M^-)^{-1}(M^-\lambda_n(\boldsymbol{U}_h^+) + M^+\lambda_n(\boldsymbol{U}_h^-)), \tag{3.16}$$

which instead lead to a jump term similar to the one derived by Cai and Samuelsson [9].

We will now get

$$\begin{aligned}
|||\boldsymbol{E}|||^2 &= \sum_{K\in\mathcal{K}} (\boldsymbol{J} - \mathcal{L}\mathcal{M}\mathcal{L}^*\boldsymbol{U}_h, \boldsymbol{E} - \pi\boldsymbol{E})_K \\
&\quad + (\Lambda_n(\boldsymbol{U}_h) - \lambda_n(\boldsymbol{U}_h), \boldsymbol{E} - \pi\boldsymbol{E})_{\partial K} \\
&= \sum_{K\in\mathcal{K}} (\boldsymbol{J} - \mathcal{L}\mathcal{M}\mathcal{L}^*\boldsymbol{U}_h, \boldsymbol{E} - \pi\boldsymbol{E})_K \\
&\quad + ((M^+ + M^-)^{-1}M^-[\lambda_n(\boldsymbol{U}_h)], \boldsymbol{E} - \pi\boldsymbol{E})_{\partial K} \\
&\le C \sum_{K\in\mathcal{K}} \Big(\|h\mathcal{M}^{-1/2}(\boldsymbol{J} - \mathcal{L}\mathcal{M}\mathcal{L}^*\boldsymbol{U}_h)\|_K \|h^{-1}\mathcal{M}^{1/2}(\boldsymbol{E} - \pi\boldsymbol{E})\|_K \\
&\quad + \|h^{1/2}(M^+ + M^-)^{-1}(M^-)^{1/2}[\lambda_n(\boldsymbol{U}_h)]\|_{\partial K} \\
&\quad\quad \times \|h^{-1/2}M^{1/2}(\boldsymbol{E} - \pi\boldsymbol{E})\|_{\partial K} \Big) \\
&\le C \left(\sum_{K\in\mathcal{K}} R(\boldsymbol{U}_h)^2 \right)^{1/2} |||\boldsymbol{E}|||,
\end{aligned} \tag{3.17}$$

where we made use of the Cauchy-Schwarz inequality and the trace inequality $\|v\|_{\partial K}^2 \le C\|v\|_K(h_K^{-1}\|v\|_K + \|\nabla v\|_K)$. Finally the aforementioned approximation property

$$\|h^{-1}\mathcal{M}^{1/2}(\boldsymbol{V} - \pi\boldsymbol{V})\|^2 \le C|\mathcal{M}^{1/2}\boldsymbol{V}|_1^2 \le C\|\mathcal{M}^{1/2}\nabla\boldsymbol{V}\|^2 \le C|||V|||^2$$

was used. □

3.4 An adaptive algorithm

We start the adaptive algorithm from an initial coarse decomposition $\mathcal{K}_0$ consisting of tetrahedra. It is important that the interfaces between discontinuous materials are respected by the triangulation, i.e., the material interfaces consist of element sides.

The initial triangulation is then adaptively refined level by level. There are two main components in this process: the error estimator and the local grid refiner. The role of the error estimator is to locally determine which elements are to be bisected to construct a refined grid. It is not critical which refinement method is used, except that it should have the property that the refinement is stable, i.e., the refined grid should remain shape regular even after many adaptive local refinements.

We will briefly describe the refinement method used in our implementation. The refinement algorithm is also used in [9] and implemented in the adaptive module of [1].

- Compute for each element K of the triangulation an indicator value I_K, where a large value of I_K indicates a large error. Based on the a posteriori estimate (3.9) we use $I_K = R_K(\boldsymbol{U}_h)^2$.

- From the indicator values I_K , each tetrahedron K of $\mathcal{K}$ is assigned an integer $i_K \in \{0, 1, 2, 3, 4, 5, 6\}$. The integer i_K denotes the minimal number of edges of tetrahedron K where new nodes are inserted in the refinement.

  Given a parameter $\beta \in (0, 1)$ and the maximal indicator value $I_{max} = \max_{K \in \mathcal{K}} I_K$ the integer i_K is computed by

$$i_K = \begin{cases} 0 & \text{if} \quad I_K \leq \beta^6 I_{max}, \\ j & \text{if} \quad \beta^{7-j} I_{max} < I_K \leq \beta^{6-j} I_{max} \quad \text{for} \quad j = 1, \ldots 6. \end{cases}$$

- Mark the i_K longest edges in the elements for new node insertion. By the next step, the neighbour elements might need to mark additional edges to guarantee stability of the refinement.

- The following two rules are recursively applied to mark the neighbour elements: If any edge in a tetrahedron is marked, then the longest edge is also marked, and if any edge on a face of a tetrahedron is marked, then the longest edge of that face is also marked.

- The tetrahedra having any marked edges is refined by repeated bisection until there are no more marked edges. The length of the marked edges of the tetrahedron determines the order of tetrahedral bisection. The longest edge is bisected first which, together with the marking of edges in the previous step, guarantees that the refinement will be regular.

- Project nodes at the curved outer boundaries or internal interfaces to the correct geometry.

The method have the property that the sequence of grid refinements are nested and the minimum number of edges where new nodes are added to the refined grid is controlled. If the geometry model has curved outer boundaries or internal interfaces the refinement will not be strictly nested, due to that the newly introduced nodes need to conform to the curved geometry model. For more information on the geometry model and implementational issues we refer to [4].

4 The multigrid method

Let $\mathcal{K}_k, k = 0, \ldots, m$ be a sequence of decompositions of Ω and let $\mathcal{W}_{h,k}, k = 0, \ldots, m$, be the associated spaces of piecewise vector polynomial functions. We assume that the spaces are nested $\mathcal{W}_{h,0} \subset \mathcal{W}_{h,1} \subset \ldots \subset \mathcal{W}_{h,m}$.

The operator $A_k : \mathcal{W}_{h,k} \mapsto \mathcal{W}_{h,k}$ is defined by $(A_k \boldsymbol{U}_k, \boldsymbol{V}) = a(\boldsymbol{U}_k, \boldsymbol{V})$ for all $\boldsymbol{V} \in \mathcal{W}_{h,k}$ and $L_k = l(\boldsymbol{V})$ for all $\boldsymbol{V} \in \mathcal{W}_{h,k}$. The finite element discretization (3.3) on $\mathcal{K}_k$ then takes the form

$$A_k \boldsymbol{U}_k = L_k,$$

for $k = 0, \ldots, m$.

We define the projection operator $Q_k : \mathcal{W}_{h,k+1} \mapsto \mathcal{W}_{h,k}$ by

$$(Q_k \boldsymbol{U}, \boldsymbol{V}) = (\boldsymbol{U}, \boldsymbol{V}) \quad \text{for all } \boldsymbol{V} \in \mathcal{W}_{h,k}.$$

We denote one multigrid V-cycle with (n_1, n_2) pre- and post-smoothing operations by $T = T_k$ where $T_k : \mathcal{W}_{h,k} \mapsto \mathcal{W}_{h,k}$, $1 \leq k \leq m$, is defined recursively by $T_0 = A_0^{-1}$ and

$$T_k L_k \quad = \quad v^{n_1+n_2+1},$$

where

$$\begin{aligned}
v^0 &= \begin{cases} 0 & \text{if} \quad k < m \\ \boldsymbol{U}_{m-1} & \text{if} \quad k = m \end{cases} \\
v^j &= v^{j-1} + S_k(L_k - A_k v^{j-1}), \quad \text{for } j = 1, \ldots, n_1, \\
v^{n_1+1} &= T_{k-1} Q_{k-1}(L_k - A_k v^{n_1}), \\
v^j &= v^{j-1} + S_k(L_k - A_k v^{j-1}), \quad \text{for } j = n_1 + 2, \ldots, n_1 + n_2 + 1.
\end{aligned}$$

Here $S_k : \mathcal{W}_{h,k} \mapsto \mathcal{W}_{h,k}$ represents one smoothing operation which can consist of a step of a preconditioned Krylov method.

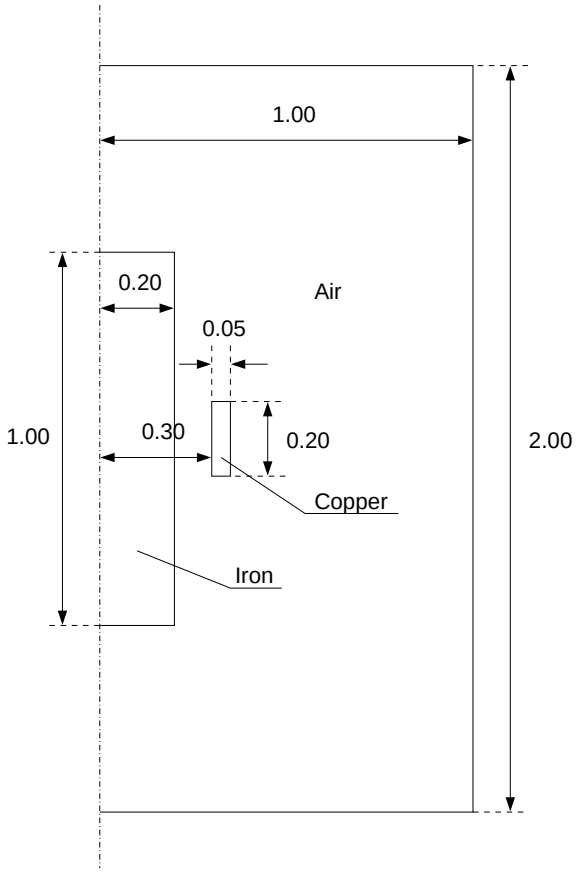

Figure 2: The geometry of the axisymmetric problem. The dimensions are given in meters.

5 Examples

The $\mathcal{LL}^*$ method described above was tested for problem (2.1) in three dimensions on an axisymmetric geometry that describes an electromagnet, see Figures 2 and 3. The model consists of an iron cylinder core inserted in a copper winding. The configuration is enclosed in air and surrounded by a box with perfectly conducting surfaces. The winding is modeled as a homogeneous copper coil.

Data for the problem are relative magnetic permeabilities of $\mu_{r,Fe} = 10^4$ and $\mu_{r,Cu} = \mu_{r,air} = 1$ and $\mu_0 = 4\pi \times 10^{-7}$ H/m and a current density J that is constant over the cross section of the coil with a total current of 1 A.

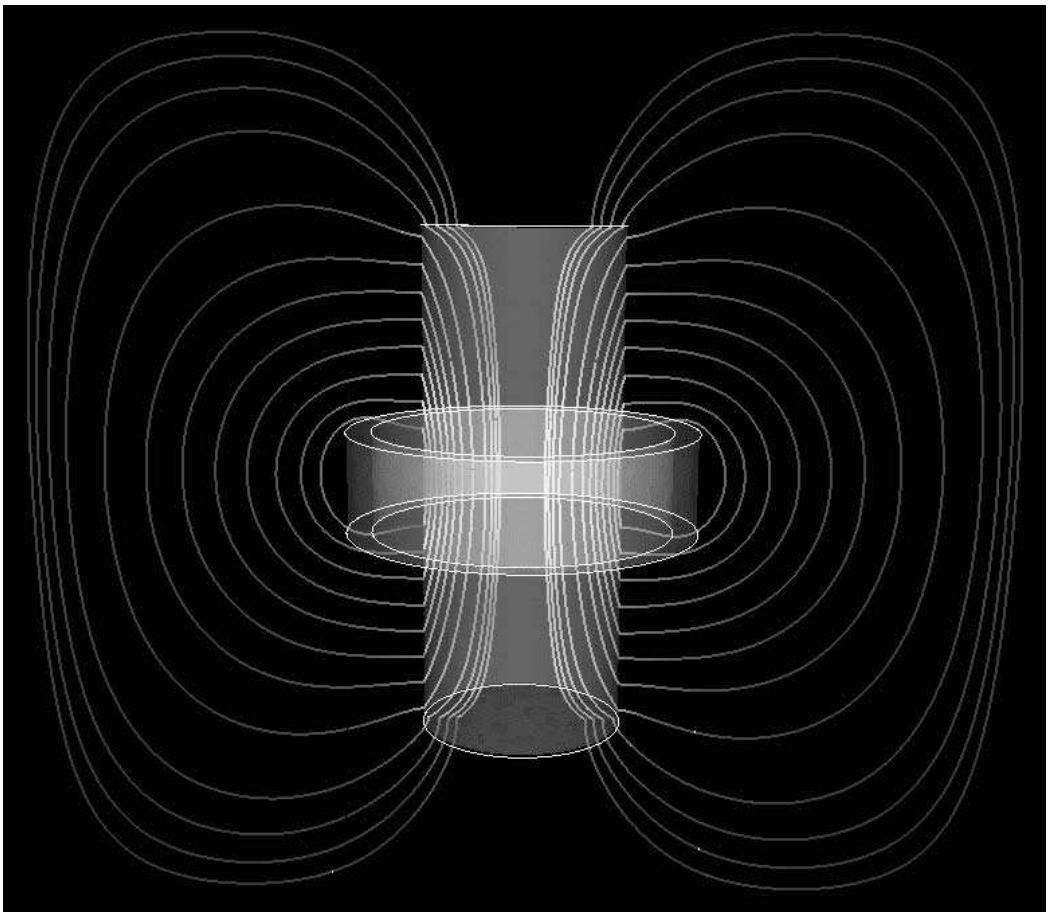

Figure 3: The magnetic field lines in a slice through the three dimensional solution of the axisymmetric problem.

The geometry and data for the problem was suggested by ABB Corporate Research, who also provided reference two dimensional axisymmetric solutions, reported in [4]. Note that the problem includes a large discontinuity in the coefficients of the problem, as well as edges where the field solution is singular.

The problem was solved using multigrid as described above, with three iterations of GMRES, preconditioned with one SSOR sweep at each level. The coarsest problem was solved using stabilized bi-conjugated gradient (BCGSTAB). Mesh adaptation was based on the energy norm a posteriori

$\text{No}_{elements}$	No_{nodes}	t_s [s]	$\epsilon_{r,air}$	$\epsilon_{r,Fe}$	$\epsilon_{r,Cu}$	$\epsilon_{r,total}$
14401	2580	4.1	0.23	0.47	0.47	0.24
32498	5938	41.29	0.14	0.33	0.29	0.15
104304	18868	172.56	0.07	0.18	0.13	0.07
294521	53417	967.69	0.04	0.09	0.07	0.04
645947	116506	3257.73	0.02	0.05	0.05	0.02
970767	175165	6331.57	0.02	0.04	0.03	0.02

Table 1: The time to solve the problem on each level and relative error in the computed magnetic energies using the $\mathcal{LL}^*$-method and piecewise linear polynomial elements. The reference values are from two dimensional computations done at ABB, see [4].

	Linear	Reference
W_{air} (J)	8.947e-7	9.089e-7
W_{Fe} (J)	4.539e-10	4.731e-10
W_{Cu} (J)	3.494e-8	3.614e-8
W_{total} (J)	9.301e-7	9.455e-7

Table 2: The computed magnetic energies compared with reference values using the $\mathcal{LL}^*$-method and piecewise linear polynomial elements. The mesh used to obtain these values had 970,767 elements and 175,165 nodes. The reference values are from two dimensional computations done at ABB, see [4].

error indicator derived above.

Table 1 gives the errors in energy, ϵ_r, and the solution times, t_s, on each level of the computation. The error is defined as

$$\epsilon_r = \frac{\|W_{ref} - W_h\|}{\|W_{ref}\|}, \tag{5.1}$$

where W_{ref} denotes the magnetic energies in the reference solution computed by ABB, and W_h denotes the ones computed from the $\mathcal{LL}^*$ solutions through (3.5). The actual computed energies are shown in Table 2 for the finest mesh.

Due to the use of unstructured grids together with non-uniform mesh refinement, asymptotic order of convergence is difficult to measure. However, in Figure 4 we show convergence of the error in energy compared with the

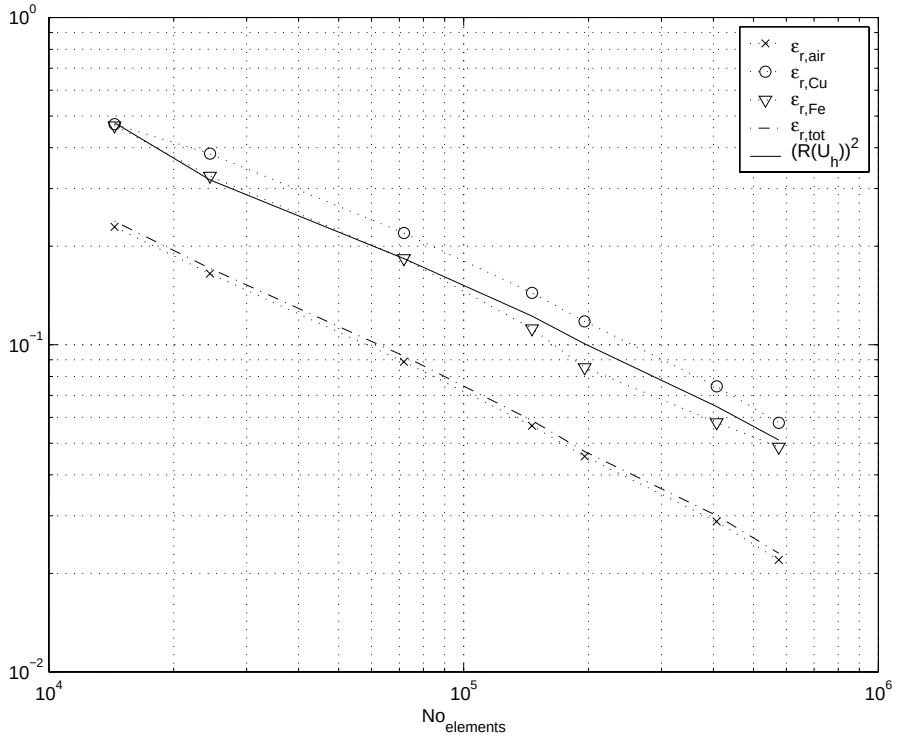

Figure 4: Convergence in error compared with the indicator derived in Section 3.3.

error indicator, and we can see that the error shows the same behaviour as the indicator. Thus, the convergence rate appears to be $O(h)$ as expected.

The convergence in multigrid is measured by the decrease in algebraic residual between two V-cycles on the same level in the grid hierarchy. In Table 3 these factors, called ρ, are given as the geometric mean value for all V-cycles on each level, and for different sizes of the discontinuity in material parameters. As expected, the convergence increases for smaller discontinuities.

$\frac{\mu_{Fe}}{\mu_{air}}$	$\text{No}_{elements}$	No_{nodes}	ρ
10000	14401	2580	2.43e-14
	32498	5938	1.42e-1
	104304	18868	3.59e-1
	294521	53417	6.13e-1
	645947	116506	7.21e-1
	970767	175165	7.07e-1
1000	14401	2580	2.36e-14
	32282	5898	9.86e-2
	104162	18850	2.87e-1
	294581	53430	4.92e-1
	582500	105255	5.86e-1
	1318174	237107	6.67e-1
100	14401	2580	2.26e-14
	31418	5741	4.90e-2
	102341	18515	1.65e-1
	266466	48356	2.33e-1
	594002	107212	2.89e-1
	1235205	222242	2.94e-1
10	14401	2580	1.66e-14
	25239	4583	9.74e-3
	84852	15395	2.86e-2
	193051	34983	3.25e-2
	492963	89041	3.38e-2
	1098954	197763	3.38e-2
1	14401	2580	7.66e-15
	21895	3982	6.69e-3
	55870	10095	8.64e-3
	96370	17475	9.53e-3
	290141	52226	1.18e-2
	516202	93285	1.03e-2

Table 3: Convergence factors for the multigrid iterations for different sizes of discontinuity. The factor ρ is the geometric mean of the decrease in the algebraic residual between two consecutive V-cycles for all V-cycles on each level.

References

[1] Diffpack home page. `http://www.nobjects.com/Products/Diffpack`.

[2] R.E. Banks and A. Weiser. Some a posteriori error estimators for elliptic partial differential equations. *Math. Comp.*, (44):283–301, 1985.

[3] R. Bergström. Least-squares finite element methods for electromagnetic applications. Preprint 5, Chalmers Finite Element Center, Chalmers University of Technology, 2000.

[4] R. Bergström, A. Bondeson, C. Johnson, M.G. Larson, Y. Liu, and K. Samuelsson. Adaptive finite element methods in electromagnetics. Technical Report 2, Swedish Institute of Applied Mathematics (ITM), 1999.

[5] M. Berndt, T.A. Manteuffel, and S.F. McCormick. Local error estimates and adaptive refinement for first-order system least squares (FOSLS). *Electron. Trans. Numer. Anal.*, pages 35–43, Dec 1997.

[6] P.B. Bochev and M.D. Gunzburger. Finite element methods of least-squares type. *SIAM Rev.*, 40(4):789–837, 1998.

[7] J.H. Bramble, R.D. Lazarov, and J.E. Pasciak. A least-squares approach based on a discrete minus one inner product for first order systems. *Math. Comp.*, 66(219):935–955, 1997.

[8] S.C. Brenner and L.R. Scott. *The Mathematical Theory of Finite Element Methods.* Springer-Verlag, 1994.

[9] X. Cai and K. Samuelsson. Parallel multilevel methods with adptivity on unstructerd grids. *Comput. Visual Sci.*, 3:133–146, 2000.

[10] Z. Cai, T.A. Mantueffel, S.F. McCormick, and S. Parter. First-order system least squares for planar linear elasticity: pure traction. *SIAM J. Numer. Anal.*, (35):320–335, 1998.

[11] Z. Cai, T.A. Mantueffel, S.F. McCormick, and J. Ruge. First-order system $\mathcal{LL}^*$ (FOSLL*):scalar elliptic partial differential equations. submitted, 2000.

[12] K. Eriksson and C. Johnson. Adaptive finite element methods for parabolic problems I: A linear model problem. *SIAM J. Numer. Anal*, 28:43–77, 1991.

[13] V. Girault and P.A. Raviart. *Finite Element Methods for Navier-Stokes Equations*. Springer-Verlag, 1986.

[14] B.-N. Jiang. *Least-squares finite element method : Theory and applications in computational fluid dynamics and electromagnetics*. Springer-Verlag, 1998.

[15] B.-N. Jiang, J. Wu, and L.A. Povinelli. The origin of spurious solutions in computational electromagnetics. *J. Comp. Phys.*, 125:104–123, 1996.

[16] J. Jin. *The Finite Element Method in Electromagnetics*. John Wiley & Sons, Inc., 1993.

[17] L.R. Scott and S. Zhang. Finite element interpolation of nonsmooth functions satisfying bundary conditions. *Math. Comp.*, 54:483–493, 1990.

Paper V

Eddy-Current Computations Using Adaptive Grids and Edge Elements

Yueqiang Liu, A. Bondeson, R. Bergström, C. Johnson, M. G. Larson, and K. Samuelsson

***Abstract*—Results are presented from eddy-current computations using adaptive techniques, based on rigorous *a posteriori* error estimates. The adaptivity restores the quadratic convergence with grid size of the magnetic energy, despite singularities occurring at corners. A new procedure is introduced to satisfy the solvability condition for the curl–curl equation. The methods are applied to a model of a hydrogenerator, with anisotropic conductivity and permeability. The ungauged formulation with both vector and scalar potentials gives very significant improvements in rate of convergence for this problem. Reasons for the improved convergence are discussed.**

***Index Terms*—Adaptivity, AV formulation, edge elements, hydrogenerator, ungauged.**

I. Introduction

THREE-DIMENSIONAL (3-D) eddy-current problems in realistic geometry are still demanding, and improvements in solution techniques are very valuable. In the present paper, we present results obtained using adaptive finite-element method (FEM) techniques based on a recent *a posteriori* error estimate [1]. We also demonstrate and discuss the advantages of the "ungauged" formulation with vector and scalar potentials [2]–[4] which significantly improves the convergence rate for iterative solvers.

The methods are applied to a simplified model of a hydrogenerator, assuming a time-harmonic field. The geometry is shown in Fig. 1. The simulated region contains an angular segment of the four stacks at the axial end of the hydrogenerator. In the circumferential direction of the generator, the simulation region includes a slot and half a tooth, and its physical dimensions are 50 mm × 749 mm × 400 mm. The geometry is described in detail in [5]. The material properties are listed in Table I. Both the electric conductivity and the magnetic permeability are anisotropic. The boundary conditions have been prescribed as vanishing normal magnetic flux density $B_n = 0$ on certain symmetry planes (essentially the surfaces facing the viewer in Fig. 1), and the tangential components of the magnetic field $\vec{H}$, as calculated from the Biot–Savart law for the currents in the rotor coil, on the remaining surfaces.

Manuscript received July 5, 2001; revised October 25, 2001. This work was supported in part by ABB Corporate Research and the Swedish Network for Applied Mathematics.

Y. Liu and A. Bondeson are with the Department of Electromagnetics, Chalmers University of Technology, S-412 96 Göteborg, Sweden (e-mail: elfliu@elmagn.chalmers.se; elfab@elmagn.chalmers.se).

R. Bergström, C. Johnson, M. G. Larson, and K. Samuelsson are with the Department of Mathematics, Chalmers University of Technology, S-412 96 Göteborg, Sweden (e-mail: ribe@math.chalmers.se; claes@math.chalmers.se; mgl@math.chalmers.se; klassam@math.chalmers.se).

Publisher Item Identifier S 0018-9464(02)02438-X.

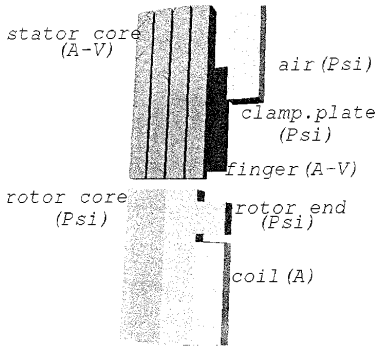

Fig. 1. Geometry of the hydrogenerator model. The simulation region is half a tooth and a slot of the generator. The region is elongated in the radial direction of the generator (y) and narrow in the azimuthal direction (x).

TABLE I
MATERIAL PARAMETERS IN DIFFERENT REGIONS. $\perp$ REFERS TO THE xy PLANE

	$\mu_{r,\perp\perp}$	$\mu_{r,zz}$	$\sigma_{\perp\perp}$ [S/m]	σ_{zz} [S/m]
Stator core	465	13.9	2×10^6	0
Finger	3	3	1×10^7	1×10^7
Plate	600	600	0	0
Rotor end	600	600	0	0
Rotor core	3255	14.1	0	0

II. Formulation

In simply connected regions where the current density vanishes, we use the magnetic scalar potential ψ, such that $\vec{H} = \nabla\psi$, and solve $\nabla \cdot \overline{\overline{\mu}} \cdot \nabla\psi = 0$. The permeability $\overline{\overline{\mu}}$ is in general a tensor.

In coil regions, the current density is specified, and the magnetic vector potential satisfies

$$\nabla \times \mu^{-1} \nabla \times \vec{A} = \vec{J}_s. \tag{1}$$

In conducting regions, the most efficient formulation uses both the vector and scalar potential, so that $\vec{E} = -j\omega\vec{A} - \nabla V$, and imposes no gauge [2]–[4]. Instead of a gauge condition, it is advantageous to impose the condition that the divergence of the conduction current vanish

$$\nabla \times \overline{\overline{\mu}}^{-1} \nabla \times \vec{A} + \overline{\overline{\sigma}} \cdot \left(j\omega\vec{A} + \nabla V \right) = 0 \tag{2}$$

$$-c\nabla \cdot \overline{\overline{\sigma}} \cdot \left(j\omega\vec{A} + \nabla V \right) = 0. \tag{3}$$

We call this the AV formulation. c is a parameter that can be chosen. The conductivity $\overline{\overline{\sigma}}$ is typically a tensor to model laminations. We have solved (1) together with (2) and (3) using the

lowest order edge elements for $\vec{A}$ and piecewise linear, nodal elements for V. The magnetic scalar potential ψ is also expanded in piecewise linear, nodal elements.

III. Solvability Conditions

The $\nabla \times \mu^{-1} \nabla \times$ operator in (1) has a large nullspace, to which the source-term $\vec{J}_s$ must be orthogonal, in order for the equation to have a solution. Within the space of the lowest order edge elements, the nullspace for the discretized curl–curl operator consists of gradients of piecewise linear functions. Thus, the right-hand side of (1) must be orthogonal to the gradients of all piecewise linear functions $\overline{U}$. Although the exact coil currents are divergence-free, the orthogonality will in general not be exact for the finite-element representation. To ensure $\nabla \cdot \vec{J}_s = 0$ numerically, we add a gradient as a correction to the prescribed current $\vec{J}$

$$\vec{J}_s = \vec{J} - \nabla U. \tag{4}$$

We assume that (1) holds in a region Ω with the boundary conditions $\hat{n} \times \vec{A} = \hat{n} \times \vec{A}_t$ (to specify B_n) on $\partial\Omega_A$ and $\hat{n} \times \mu^{-1} \nabla \times \vec{A} = \hat{n} \times \vec{H}$ on $\partial\Omega_H$. U is determined by multiplying (1) by all gradients $\nabla\overline{U}$ of piecewise linears, and integrating over Ω:

$$\int_{\partial\Omega_H} \nabla\overline{U} \cdot \left(\hat{n} \times \vec{H}\right) dS = \int_{\Omega} \nabla\overline{U} \cdot \left(\vec{J} - \nabla U\right) dv. \tag{5}$$

(U of course vanishes on all nodes on surfaces where $\vec{A}_t$ is specified). Equations (4) and (5) remove any projection of $\vec{J}_s$ on the null space of the curl–curl equation and guarantee that (1) has a solution. Iterative solvers converge also for singular systems of equations if the right-hand side is consistent.

Another procedure to achieve consistency was given by [6], who constructed a vector potential for the current. However, in addition to making the current divergence-free, the new procedure also provides a way of dealing with numerically generated boundary conditions for $\vec{H}_t$. The left-hand side of (5) vanishes if $\vec{H} = \nabla\psi$ on the entire boundary of Ω.

Solvability has to be considered also in connection with the divergence condition (3). Since we do not want (3) to add any new information that is inconsistent with Ampère's law (2), the weak form of (3) is constructed by projecting (2) on test functions $\nabla\overline{V}$ that span the null space of the curl–curl operator, giving:

$$\int_{\partial\Omega_H} \nabla\overline{V} \cdot \left(\hat{n} \times \vec{H}\right) dS + \int_{\Omega} \nabla\overline{V} \cdot \overline{\overline{\sigma}} \cdot \left(j\omega\vec{A} + \nabla V\right) dv = 0. \tag{6}$$

IV. Efficiency of Iterative Solvers

It has already been established for eddy-current problems that iterative solvers converge much faster in the ungauged AV formulation (2) and (3) than in the pure A formulation or other gauged formulations [2]–[4]. Our study confirms this. In fact, we find even larger improvement from the ungauged formulation than previous authors, presumably because the A formulation gives very badly conditioned matrices in the regions of anisotropic conductivity, as discussed in Section V.

TABLE II
Number of Iterations for Different Formulations in the Conducting and Nonconducting Regions for the Static and Time-Harmonic Hydrogenerator Problem

Repr. ($\sigma \neq 0$, $\sigma = 0$)	Frequency	Number of unknowns (complex)	Iterations
(A,A)	0	16590	49
		26786	81
(A,A)	50Hz	16590	4622
		26786	6943
(AV,A)	50Hz	18336	269
		22640	327
		59134	453
(AV,ψ)	50Hz	12987	67
		27948	163
		67542	221

We have used the PETSc package for preconditioned Krylov methods [7]. For these eddy-current problems, transpose-free quasi-minimized residuals (TFQMRs) are generally the most efficient solver. As preconditioner, we used the ILU decomposition of a matrix obtained from the system matrix by multiplying the diagonal elements for $\vec{A}$ by a factor $\simeq$1.1. Without such a multiplication, the preconditioning fails, apparently because of the null space of the curl–curl operator. The incomplete LU decomposition has been tried with different levels of fill in (ratio of the number of fill ins to the number of nonzero diagonal elements in the original matrix, indicated in parenthesis). Although the default ILU(1) works well for simple test problems, ILU(3) was considerably more efficient for the hydrogenerator problem. To reduce the memory requirement, we used ILU(2) for the largest grids, at the expense of a larger number of iterations.

Table II shows the number of iterations for the different grids, generated by adaptive mesh refinement, and different formulations in the conducting and nonconducting regions. In the coil region, we always use the A formulation in (1), with the source current modified according to (4) and (5).

Notably, the number of iterations is very high for the A formulation at 50 Hz, and the AV-formulation achieves a very significant reduction. The number of iterations is further reduced by using the magnetic scalar potential in the nonconducting regions. The combination of the A or AV formulations with the scalar magnetic potential was made following the standard Galerkin procedure. If the equations are combined in such a way that the boundary terms are symmetric, the matrix representing the highest derivatives is no longer definite.

V. Eigenvalue Distribution

Insights into why the AV formulation speeds up the convergence can be gained by considering the eigenvalue distribution for the different formulations. When the discretization is free of "spurious solutions" (as are the discretizations using edge elements for the vector potential), it is sufficient to consider the eigenvalues of the analytic operators applied to complex exponentials $\exp(j\vec{k} \cdot \vec{r})$, where $\pi/|k|$ ranges from the longest spatial scale of the problem to the smallest, i.e., the grid size.

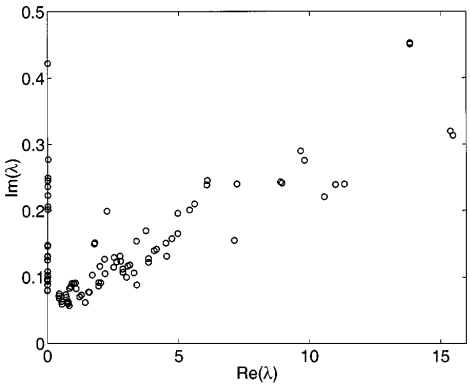

Fig. 2. Numerical spectrum in the complex plane for a discritized conducting cube with the A formulation. The side of the cube is 1 m, the frequency 50 Hz, the conductivity 10^4 S/m, $c = 1/(\mu\sigma)$, and the number of edges is 250.

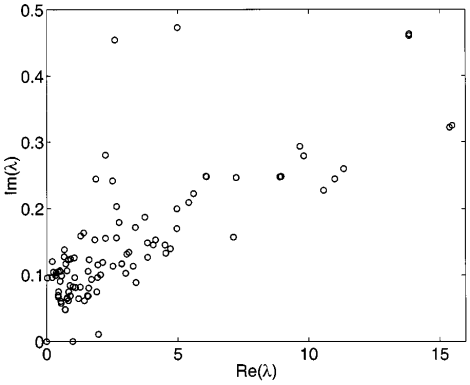

Fig. 3. Numerical spectrum in the complex plane for a discritized conducting cube with the AV formulation. The parameters are the same as in Fig. 2.

For isotropic σ and μ, the eigenvalues of the A formulation, where the operator is $\nabla \times \mu^{-1}\nabla \times + j\omega\sigma$, are $\lambda_{1,2} = k^2/\mu + j\omega\sigma$ (electromagnetic) and $\lambda_3 = j\omega\sigma$ (electrostatic $\vec{A} = \nabla\phi$).

For the AV operator in a homogeneous medium

$$\nabla \times \mu^{-1}\nabla \times \vec{A} + \overline{\overline{\sigma}} \cdot (j\omega A + \nabla V) = \lambda \vec{A} \tag{7}$$

$$-\nabla \cdot c\overline{\overline{\sigma}} \cdot (j\omega A + \nabla V) = \lambda V \tag{8}$$

the eigenvalues in the isotropic case are $\lambda_{1,2} = k^2/\mu + j\omega\sigma$ (electromagnetic), $\lambda_3 = c\sigma k^2 + j\omega\sigma$ (electrostatic) and $\lambda_4 = 0$ (gauge transformation). Thus, in addition to creating zero eigenvalues connected with gauge transformations, the AV formulation gives the electrostatic eigenvalues a real part. This brings them closer in the complex plane to the electromagnetic eigenmodes. Since all the nonzero eigenvalues have a part proportional to k^2, the AV formulation makes the problem elliptic (excepting the gauge transformations, of course). Since eigenvalues that are exactly zero do not affect iterative solvers if the right-hand side is consistent, and the nonzero spectrum for the AV formulation covers a smaller region of the complex plane, this formulation gives faster convergence. The gain from the AV formulation depends on the size of the imaginary part in comparison to the smallest and largest real parts, i.e., on the relation of the skin depth to the macroscopic scales and the grid size. Figs. 2 and 3 show the eigenvalue distributions for the test case of a discretized cube, with the A and AV formulations, respectively. Close examination shows that the separation between the electrostatic and electromagnetic eigenvalues of the matrix for the A formulation is not perfect (it would be if the normalization included the "mass matrix" $M_{ij} = \int \vec{N}_i \cdot \vec{N}_j \, dv$ where $\vec{N}$ denote the edge basis functions for the vector potential). However, when the number of elements is large enough to resolve the skin depth well, the eigenvalues separate as found analytically, and there is one "electrostatic" set very close to the imaginary axis.

For an anisotropic conductivity corresponding to laminations in the xy plane, $\overline{\overline{\sigma}} = \sigma(\hat{x}\hat{x} + \hat{y}\hat{y})$, the differences are even more significant. For the A formulation the eigenvalues are: $\lambda_1 = k^2/\mu + j\omega\sigma$ (electromagnetic), while $\lambda_{2,3}$ (mixed electromagnetic/electrostatic) satisfy the quadratic equation

$$\lambda^2 - \lambda\left(k^2/\mu + j\omega\sigma\right) + j\omega\sigma k_\perp^2/\mu = 0 \tag{9}$$

with $k_\perp^2 = k_x^2 + k_y^2$. Equation (9) shows that numerically small eigenvalues occur (for nearly electrostatic modes) when $k_z^2 \gg k_\perp^2$

$$\lambda_3 \simeq j\omega\sigma k_\perp^2/k^2.$$

Since the largest possible k is inversely proportional to the element size h, we see that the effective condition number (ratio of largest to smallest *nonzero* eigenvalue) of the A formulation, varies as h^{-4} to be compared with the h^{-2} scaling for the isotropic case. Thus, the A formulation gives an unfavorable scaling of the number of iterations when the grid is refined in the anisotropic case. This is confirmed by our numerical results.

For the AV formulation, the two mixed electromagnetic/electrostatic eigenvalues satisfy

$$\lambda^2 - \lambda\left(k^2/\mu + j\omega\sigma + k_\perp^2 c\sigma\right) + j\omega\sigma k_\perp^2/\mu + k_\perp^2 c\sigma k^2/\mu = 0 \tag{10}$$

[which reduces to (9) when $c = 0$]. These eigenvalues are well behaved when $k_z^2 \gg k_\perp^2$, in the sense that the small eigenvalues approach $k_\perp^2 c\sigma$, which is bounded from zero when the mesh is refined, and the condition number scales as h^{-2}. Thus, for laminated materials, the AV formulation strongly reduces the condition number in comparison with the A formulation.

VI. Adaptivity

We have implemented a scheme for adaptive mesh refinement, based on an error estimate in energy norm [1]. Which elements are to be refined is decided from their contributions to the total error. For the AV-formulation, the contribution $I(e)$ from element e is

$$I(e) = \sum_{f=1}^{4} \frac{h_f}{2}\left(\overline{\mu}\left|\delta\vec{H}_t\right|^2 + \frac{1}{\omega\overline{\sigma}}|\delta J_n|^2\right) A_f + h_e^2\overline{\mu}\left|\vec{J}_s + \vec{J}_\sigma\right|^2 V_e \tag{11}$$

where $\delta\vec{H}_t$ is the jump in tangential $\vec{H}$ across element boundaries, δJ_n the jump in the normal component of the conduction

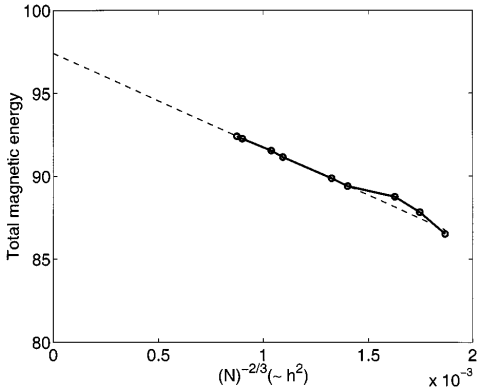

Fig. 4. Convergence of the magnetic energy with adaptive grid for the hydrogenerator at 50 Hz.

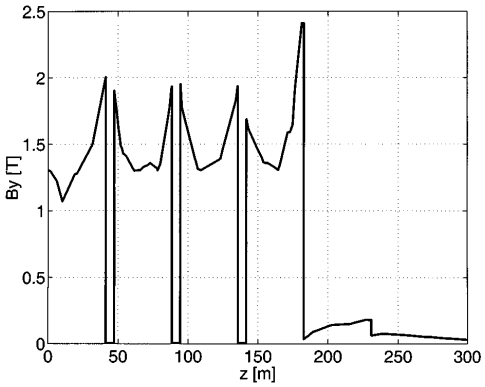

Fig. 5. The radial component of the flux density along an axial line, crossing the stacks of the generator.

current, A_f the area of face f, V_e the volume of the element, and bars refer to averages defined in [1]. Similar estimates have been applied previously, on more heuristic grounds [8]. For the ψ formulation, we used the error indicator [9]

$$I(e) = \sum_{f=1}^{4} \frac{h_f}{2} \mu^{-1} |\delta B_n|^2 A_f.$$

Fig. 4 shows that the energy $\int \vec{H} \cdot \vec{B}\, dv$ converges for the hydrogenerator problem as $O(h^2)$, where h is an average element size defined as $N^{-1/3}$, and N is the number of elements. Because of singular behavior at corners where the permeability is discontinuous, ($B \propto r^{-p}$, where r is the distance to the corner, and $p \simeq 1/3$ if μ has a large jump), computations with uniform grids only give $O(h^{4/3})$ convergence, so that adaptivity clearly improves the convergence. In addition to refining the grid at corners, the adaptivity also refines regions of the stacks where the skin effect makes the solution vary rapidly. Fig. 5 illustrates how the magnetic field along a stator pole varies in the direction across the stacks.

VII. Conclusion

For eddy-current computations with edge elements, the ungauged AV formulation gives much faster convergence than the pure A formulation, in particular when combined with a scalar magnetic potential in nonconducting regions. The improvement is explained by the eigenvalue distribution: the ungauged AV formulation moves the eigenvalues of the electrostatic components away from the imaginary axis, and closer to the electromagnetic eigenvalues. We have also introduced a procedure, that only requires the solution of a Poisson equation, to make both the source current and boundary conditions for $\vec{H}_t$ consistent, so that the singular, ungauged AV formulation has a solution. Finally, adaptive mesh refinement, based on a local error estimator recovers the nominal $O(h^2)$ convergence, despite the presence of singularities. These techniques have been tested successfully on a model of a generator, including anisotropy and large variations in material properties.

References

[1] R. Beck, R. Hiptmair, R. H. W. Hoppe, and B. Wohlmuth, "Residual based *a posteriori* error estimates for eddy-current computation," *ESAIM—Math. Model. Numer. Anal.*, vol. 34, pp. 159–182, Jan./Feb. 2000.

[2] K. Fujiwara, T. Nakata, and H. Ohashi, "Improvement of convergence of ICCG method for the A-ϕ method using edge elements," *IEEE Trans. Magn.*, vol. 32, pp. 804–806, May 1996.

[3] R. Dyczij-Edlinger and O. Biro, "A joint vector and scalar potential formulation for driven high frequency problems using hybrid edge and nodal finite elements," *IEEE Trans. Microwave Theory Tech.*, vol. 44, pp. 15–22, Jan. 1996.

[4] O. Biro, "Edge element formulations of eddy-current problems," *Comput. Meth. Appl. Mech. Eng.*, vol. 169, pp. 391–405, Feb. 1999.

[5] M. Tuoma Holmberg, "Three-dimensional finite element computation of Eddy-currents in synchronous machines," Ph.D. dissertation, Dept. Power Eng., Chalmers Univ. Tech., Göteborg, Sweden, 1998.

[6] Z. Ren, "Influence of the RHS on the convergence behavior of the curl–curl equation," *IEEE Trans. Magn.*, vol. 32, pp. 655–658, May 1996.

[7] S. Balay, W. D. Gropp, L. McInnes, and B. F. Smith. (2000) PETSc home page. [Online]. Available: http://www.mcs.anl.gov/petsc

[8] S. Y. Hahn, C. Calmels, G. Meunier, and J. L. Coulomb, "*A posteriori* error estimate for adaptive finite element mesh generation," *IEEE Trans. Magn.*, vol. 24, pp. 315–317, Jan. 1988.

[9] P. Fernandes, P. Girdinio, P. Molfino, and M. Repetto, "A posteriori estimates for adaptive mesh refinement," *IEEE Trans. Magn.*, vol. 24, pp. 299–302, Jan. 1988.

Paper VI

Edge Element Computations of Eddy Currents in Laminated Materials

Yueqiang Liu, A. Bondeson, R. Bergström, M. G. Larson, and K. Samuelsson

Abstract— **Results are shown from three-dimensional computations of the power dissipation in laminated conductors, using edge elements. It is found that the lowest order *hexahedral* edge elements, with Nédélec constraints, give much more accurate results than the corresponding *tetrahedral* elements. Whenever possible, the best choice is to use hexahedral grid aligned with the laminations. If this is not possible, the dissipation can still be accurately computed with the lowest order hexahedral elements, by using midpoint integration. Tetrahedral grids work well only with the complete basis, at the expense of doubled number of degrees of freedom in the conducting regions. Midpoint integration improves the convergence of the power dissipation also for the complete tetrahedral basis.**

Keywords— **Anisotropic conductivity, Hexahedral, Tetrahedral, Edge elements, Adaptivity.**

I. Introduction

EDDY current computations with anisotropic electric and magnetic material properties are needed to understand the power loss distributions in large electrical machines and generators.

Three-dimensional eddy current computations for laminated materials have been made with nodal based finite elements applied to different formulations, e.g., AV [1] and $T\Phi$ formulation [2], or a single-component electric vector potential [3][4]. Recently, edge elements for the electric vector potential or magnetic vector potential have also been implemented, but only with hexahedral grid and the laminations aligned with the grid [5][6].

In an eddy current computation [7] using the lowest order Nédélec *tetrahedral* elements, we found that it is very difficult to achieve reasonably accurate results for the power loss, even though the magnetic field converged well. The error of the computed power loss can readily exceed 50%, even for a simple cube test problem with well resolved skin layer. We found similar difficulties for hexahedral grids when the laminations are not aligned with the grid. In this paper, we point out the reason for this and show some possible solutions. We also show that adaptive techniques, with anisotropic refinement, can be used to improve the convergence on hexahedral grids.

II. Basis functions and notations

For a tetrahedral grid, we first use the lowest order Nédélec elements, denoted here as Tet-(1,0) elements. We follow the standard choice of the basis functions

$$\vec{N}_i = \xi_{i_1}\nabla\xi_{i_2} - \xi_{i_2}\nabla\xi_{i_1}, \qquad i = 1,...,6. \tag{1}$$

Manuscript submitted March 27, 2002. This work was supported in part by ABB Corporate Research and the Swedish Network for Applied Mathematics.

Yueqiang Liu and A. Bondeson are with the Department of Electromagnetics, Chalmers University of Technology, S-412 96 Göteborg, Sweden (e-mail {elfliu, elfab}@elmagn.chalmers.se).

R. Bergström, M. G. Larson, and K. Samuelsson are with the Department of Computational Mathematics, Chalmers University of Technology, S-412 96 Göteborg, Sweden (e-mail {ribe, mgl, klassam}@math.chalmers.se).

where $\xi_j, j = 1,...,4$ is the linear basis functions associated with the nodes of a tetrahedron.

For the complete basis, denoted as Tet-(1,1) elements, we add 6 more basis functions to (1)

$$\vec{N}_i = \xi_{i_1}\nabla\xi_{i_2} + \xi_{i_2}\nabla\xi_{i_1} = \nabla(\xi_{i_1}\xi_{i_2}), \qquad i = 1,...,6. \tag{2}$$

Thus, for Tet-(1,0) elements, we assign 1 degree of freedom (DOF) to each edge; and for Tet-(1,1) elements, we assign 2 DOFs to each edge. Clearly, Tet-(1,1) spans the same space as the Mur type [10] elements: $\vec{N}_{ij} = \xi_i\nabla\xi_j$.

For a hexahedral grid, we denote as Hex-(1,0) elements the set of 12 vector basis functions, which are constant along the associated edges, and vary linearly in the transverse directions, e.g., $\vec{N}(x,y,z) = xy\hat{z}$ in a reference element, where $\hat{z}$ is the unit vector of z-coordinate. The Hex-(1,1) elements are obtained by adding 12 more basis functions, which vary linearly not only in the transverse directions, but also in the longitudinal direction, e.g., $\vec{N}(x,y,z) = xyz\hat{z}$. Therefore, for Hex-(1,0) elements, 1 DOF is assigned to each edge; and for Hex-(1,1) elements, 2 DOFs are assigned to each edge.

One observation is that for the tetrahedral grid, the space spanned by $\{\nabla\times\vec{N}_j, j = 1,...,12\}$ from Tet-(1,1) is the same as that spanned by $\{\nabla\times\vec{N}_j, j = 1,...,6\}$ from Tet-(1,0), which means that Tet-(1,1) can not improve the accuracy of the solutions, as long as only the magnetic field is concerned (e.g. in the static calculations). On the contrary, for the hexahedral grid, the space spanned by $\{\nabla\times\vec{N}_j, j = 1,...,24\}$ from Hex-(1,1) is larger than that spanned by $\{\nabla\times\vec{N}_j, j = 1,...,12\}$ from Hex-(1,0). Therefore, even the field representation should be improved.

III. The difficulty with oblique laminations

In the case of laminations not aligned with the mesh, the power loss computed with the lowest order Nédélec elements can be very inaccurate. This is demonstrated for an eddy current problem in a cube, refered hereafter as the cube problem.

Assume an 1m × 1m × 1m conducting cube, with homogeneous permeability $\mu = \mu_0$ and anisotropic conductivity $\bar{\bar{\sigma}}$. The magnetic field at the surface of the cube is specified as a given time-harmonic field $\hat{n}\times\vec{H} = \hat{n}\times\vec{H}_s$. We want to compute the power dissipation due to the induced current in the cube. The computational domain is $\Omega = \{(x,y,z)|(x,y,z)\in[0,1]^3\}$.

In the simplest case, the given field is homogeneous $\vec{H}_s = H_y\hat{y} = const$. If the laminations are effective so that there is little or no eddy current, the magnetic vector potential $\vec{A}$ satisfies

$$\frac{\partial A_x}{\partial z} - \frac{\partial A_z}{\partial x} = B_y = const. \tag{3}$$

If the lamination is aligned with the (hexahedral) grid, e.g.

$$\bar{\bar{\sigma}} = \sigma_0 \begin{pmatrix} 1 & 0 & 0 \\ 0 & 1 & 0 \\ 0 & 0 & 0 \end{pmatrix}, \tag{4}$$

the solution of the time-harmonic problem is a homogeneous field $\vec{H} = \vec{H}_s$, with zero eddy current. Therefore, $E_x = 0$ and $A_x = 0$. Equation (3) then shows that A_z, and consequently E_z, are linear functions of x. Such solutions can be represented exactly by the mixed order hexahedral elements Hex-(1,0).

For the oblique lamination, e.g.,

$$\bar{\bar{\sigma}} = \sigma_0 \begin{pmatrix} 0.5 & 0 & -0.5 \\ 0 & 1 & 0 \\ -0.5 & 0 & 0.5 \end{pmatrix}, \tag{5}$$

the solution is still a homogeneous field with zero current, which means $E_x = E_z$ and $A_x = A_z$. Equation (3) and $A_x = A_z$ yield

$$\frac{\partial A_z}{\partial z} - \frac{\partial A_x}{\partial x} = B_y. \tag{6}$$

Therefore, at least one of $\partial E_x/\partial x$ and $\partial E_z/\partial z$ does not vanish. Such E-field can not be represented exactly by the mixed order edge elements, where the basis functions have constant tangential components along the associated edges. The mixed order elements represent E_x (E_z) as piece-wise constant functions along x (z).

The approximation error of the power dissipation can be estimated from (6). Equation (6) implies that the eddy current $|J_x| = |0.5\sigma_0(E_x - E_z)| = |0.5\sigma_0 j\omega(A_x - A_z)| \sim \sigma_0 h\omega B_y$, where h is the mesh size. The power loss density can then be estimated as $J^2/\sigma_0 \sim \sigma_0 h^2\omega^2 B_y^2$, which is quite large even for a fine grid.

The exact power loss is zero for the problem described above. In more general cases, the eddy current does not vanish with the oblique lamination (5). Let us consider an example, when the given field $\vec{H}_s$ at the surfaces of the cube is due to an infinitely long wire, located outside the cube, with a time-harmonic current flowing in the z-direction. We compare the accuracy of power loss computations with different types of elements.

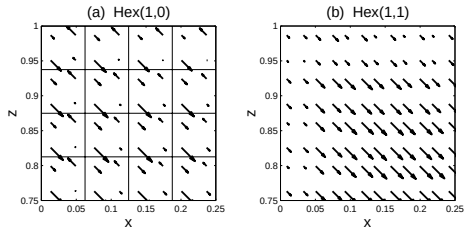

Fig. 1. Eddy current pattern of the cube problem with external field from a straight wire and oblique lamination in the xz-plane. The current is computed with (a) Hex-(1,0) and (b) Hex-(1,1), and plotted at the same plane. One quarter of the solution plane is shown.

Figure 1 shows the eddy current pattern with oblique lamination (5) in the xz-plane. The current is computed with Hex-(1,0) and Hex-(1,1) and plotted at the same plane at Gaussian quadrature points. (In this calculation 8-points Gaussian quadrature for a hexahedron is used, which gives exact integration for element matrix calculation.) Figure 1(a) shows that Hex-(1,0) elements gives a current pattern with oscillations, whereas the Hex-(1,1) elements, which approximate correctly a linear E-field along all directions, give a much more regular current pattern, as shown in Fig.1(b).

The oscillating pattern in Fig.1(a) can be understood by looking at the electric field in the conductor. Figure 2 shows the x- and z-components of the E-field, plotted along x. For Hex-(1,0) elements, E_x is piece-wise constant along x, and E_z is piece-wise linear along x. Since for this lamination, $J_x = 0.5\sigma_0(E_x - E_z), J_z = 0.5\sigma_0(E_z - E_x)$, both J_x and J_z will have oscillating characteristics along x. Obviously, both J_x and J_z are oscillating also along z, since E_x is piece-wise linear and E_z is piece-wise constant along z.

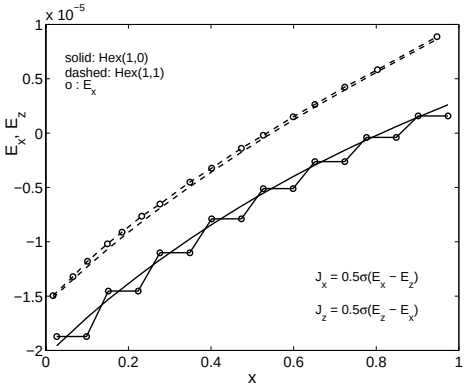

Fig. 2. The x- and z-component of the electric field along x, for the cube test problem with oblique lamination and hexahedral grids. Solid curves correspond to Hex-(1,0) elements; dashed curves correspond to Hex-(1,1) elements. Curves marked with "o" are E_x-fields, curves without makers are E_z-fields. The E-fields from Hex-(1,1) elements are shifted up by $\delta E = 0.5 \times 10^{-5}$ in the plot.

The approximation with Tet-(1,0) elements is even worse, since in this case the grid can never be aligned with any lamination in a fixed direction. The current pattern seems rather chaotic as shown in figure 3, where the same cube problem with non-uniform field is solved for the lamination (4). The analytical solution in this case again has zero eddy current, which can be obtained with Tet-(1,1) elements, even at the coarsest grid.

Figure 4 shows the convergence of the computed power loss with respect to the grid refinement, for tetrahedral and hexahedral grids. Here, we consider the cube problem with oblique lamination (5) and external field from an infinite wire. From the figure, one can see that all four types of elements give the same converged loss value. However, the accuracy is very different on finite grids. With Tet-(1,0) elements, the relative error is about 68% even on the finest grid, where the mesh size is about 30% of the skin depth. With the same number of nonzero matrix elements, the Hex-(1,0) grid gives a relative error of 57%. In contrast, the Tet-(1,1) and Hex-(1,1) give 2.9% and 4.5% error, respectively, with the same number of nonzero matrix elements

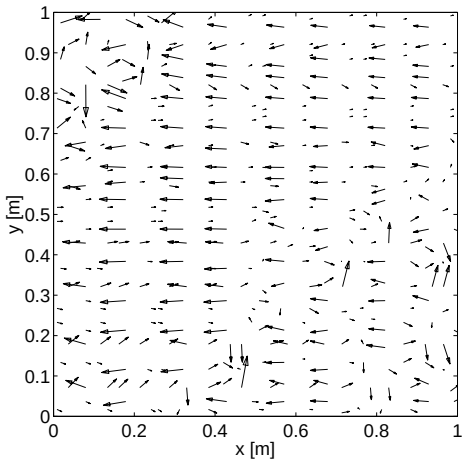

Fig. 3. Eddy current pattern of the cube problem with $\sigma_z = 0$, shown at the *xy*-plane. The lowest order Nédélec tetrahedral elements are used.

at coarser resolution.

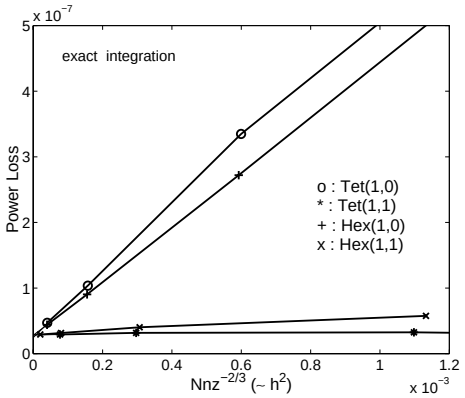

Fig. 4. Convergence of power loss with grid refinement, for the cube problem with oblique lamination and external field from an infinite wire. Different elements are used. N_{nz} is the number of non-zero matrix elements. The loss is calculated with exact integration.

Since the oscillating current pattern from Hex-(1,0) elements (see Fig.1(a)) has quite regular behavior, one would expect that some interpolation techniques could help in establishing better results [11]. We found that a suitable procedure is to apply midpoint integration to compute the dissipation. Another, similar way is to average the current over Gaussian points before computing the power dissipation. Both techniques, applying to Hex-(1,0) elements, give quite accurate power dissipation even on very coarse grids.

Figure 5 shows the convergence of the computed power loss with respect to the grid refinement. The difference with figure 4 is that here we applied midpoint integration to compute the loss.

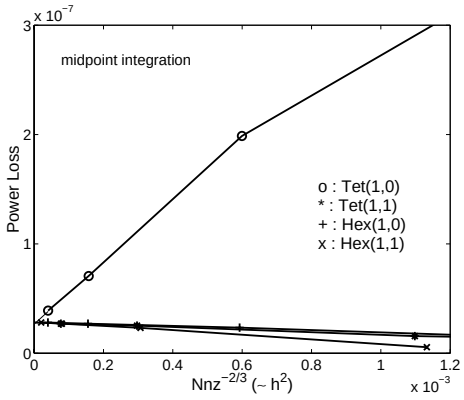

Fig. 5. Convergence of power loss with grid refinement, for the same problem as in Fig. 4, but the loss is calculated by midpoint integration. N_{nz} is the number of non-zero matrix elements.

The advantage of averaging technique for Hex-(1,0) elements is obvious: the error of power dissipation decreases from 57% to less than 1%. The averaging is not very helpful for Tet-(1,0) elements: the error decreases only from 68% to 39%, for the finest grid. The averaging does not increase the accuracy for Tet-(1,1) and Hex-(1,1) elements, for this test problem.

IV. Computations for a generator model

For the generator problem, discussed in [6][7], the simulated region contains an angular segment of the four stacks at the axial end of the hydrogenerator. In the circumferential direction of the generator, the simulation region includes a slot and half a tooth, and its physical dimensions are 50mm $\times$ 749mm $\times$ 400mm. The geometry and the material properties are described in detail in [6][7]. In this problem, both the electric conductivity and the magnetic permeability are anisotropic. Particularly, the laminated cores in the four stacks are replaced by a homogeneous material with zero conductivity along the axial direction. The boundary conditions have been prescribed as vanishing normal magnetic flux density $B_n = 0$ on certain symmetry planes Γ_B and the tangential components of the magnetic field $\vec{H}_s$, as calculated from the Biot-Savart law for the currents in the rotor coil, on the remaining surfaces Γ_H.

In this problem, there are several non-connected conducting regions Ω_σ (laminated stator cores, finger), a simply connected non-conducting region Ω_0 (air, rotor part, clamping plate), and the coil region Ω_s, where the source current $\vec{J}_s$ is specified. The coil region is separated from the conducting regions.

In the non-conducting region Ω_0, we solve an equation for the magnetic scalar potential ψ

$$-\nabla \cdot \bar{\bar{\mu}} \cdot \nabla \psi = 0, \tag{7}$$

where the permeability $\bar{\bar{\mu}}$ is in general a tensor. The magnetic field is calculated as $\vec{H} = -\nabla\psi$.

In the coil region Ω_s, where the time-harmonic source current

is specified, we solve the curl-curl equation for the magnetic vector potential $\vec{A}$

$$\nabla \times \bar{\bar{\mu}}^{-1} \nabla \times \vec{A} = \vec{J_s} \tag{8}$$

In conducting regions Ω_σ, we use the so-called ungauged *AV* formulation, which improves dramatically the convergence rate of the iterative solver, compared with gauged *A*-formulations [7].

$$\nabla \times \bar{\bar{\mu}}^{-1} \nabla \times \vec{A} + \bar{\bar{\sigma}} \cdot (j\omega\vec{A} + \nabla V) = 0, \tag{9}$$

$$-\nabla \cdot \bar{\bar{\sigma}} \cdot (j\omega\vec{A} + \nabla V) = 0. \tag{10}$$

The conductivity $\bar{\bar{\sigma}}$ is typically a tensor to model the laminations, and ω is the angular frequency. The electric field in the conductors is computed as $\vec{E} = -(j\omega\vec{A} + \nabla V)$, and the eddy current is $\vec{J_\sigma} = \bar{\bar{\sigma}} \cdot \vec{E}$.

Galerkin's method is applied to solve Eqs. (7)-(10). A scalar function ϕ is introduced in the coil region to guarantee solvability of the discretized equations [7]. The first order nodal-based elements are used to approximate all the scalar functions V, ϕ, ψ, and the first order incomplete/complete edge elements are used to approximate vector potential $\vec{A}$.

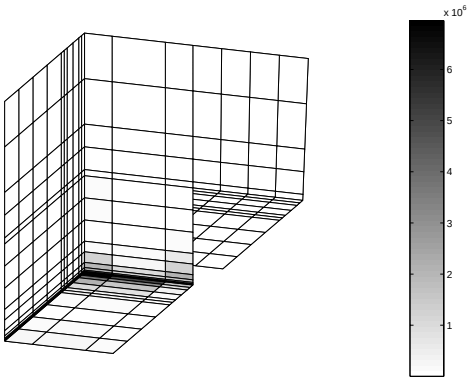

Fig. 6. Power loss distribution at the surface of the first stack of the laminated stator core, calculated for the generator problem with the lowest order Nédélec hexahedral elements.

Figure 6 shows the power loss distribution at the surface of the first stack of the laminated stator core, calculated for the generator problem with hexahedral elements Hex-(1,0). (In order to show the eddy current effect clearly, this figure, as well as figures 8 and 9, is plotted with a distorted aspect ratio along *x*, *y*, and *z* directions. Therefore, the elements could look "elongated" along certain direction.) The eddy current is distributed mainly along one of the bottom corners of the stack, as a result of the magnetic field distribution and laminations.

The eddy current in the corner region is plotted in figure 7, at the lamination plane. A regular pattern is observed. Such pattern is also obtained with Hex-(1,1) elements.

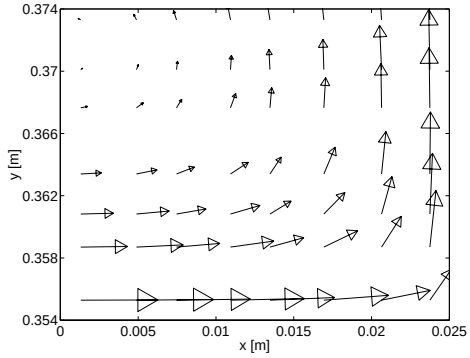

Fig. 7. Eddy current pattern in the corner region of the first stack, computed for the generator problem with Hex-(1,0) elements.

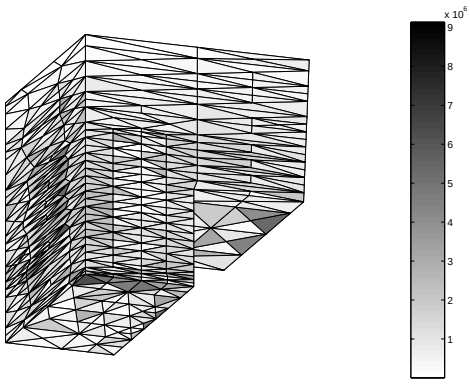

Fig. 8. Power loss distribution at the surface of the first stack of the laminated stator core, calculated for the generator problem with lowest order Nédélec tetrahedral elements.

Figure 8 shows the power loss distribution at the surface of the first stack of the laminated stator core, calculated for the same problem with tetrahedral elements Tet-(1,0). The irregular behavior of the solution is clearly seen. The computed total power loss is more than 20 times larger than that from the hexahedral grid shown in Fig. 6. Contrary to this, the complete basis Tet-(1,1) gives much better results, as shown in figure 9. The eddy current has the same density distribution as that computed with Hex-(1,0) elements (see Fig. 6). The total losses computed with Tet-(1,1) and Hex-(1,0) agree within 4%.

The current pattern at this corner shows clear differences between Tet-(1,1) and Tet-(1,0) elements. Figure 10 shows the eddy current in *xy*-plane across the corner, for both Tet-(1,0) and Tet-(1,1) elements. The current computed with Tet-(1,0) is highly oscillatory. Tet-(1,1) elements give a much more regular pattern.

Figure 11 shows B_y, computed along a line across the stator core of the generator with Tet-(1,1), Hex-(1,0), and Hex-(1,1) elements. The field from the tetrahedral grid has been smoothed in the plot. One can see that different basis functions give quite

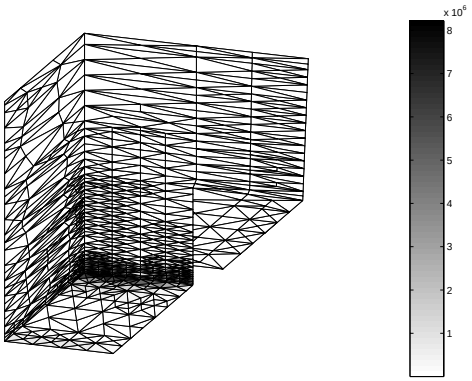

Fig. 9. Power loss distribution at the surface of the first stack of the laminated stator core, calculated for the generator problem with lowest order complete tetrahedral elements.

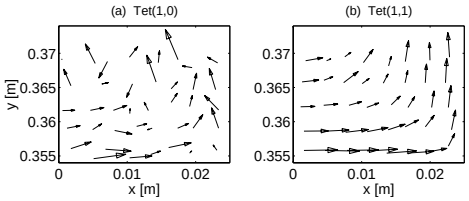

Fig. 10. Eddy current pattern at the corner of the first stack, computed for the generator problem with Tet-(1,0) and Tet-(1,1) elements.

similar results.

V. Adaptive mesh refinement

For the adaptive mesh refinement, we use an *a posteriori*, element-wise, local error estimator η_e

$$\eta_e^2 = h_e^2 \left\{ \underbrace{\frac{1}{\mu}\|\nabla\cdot\vec{B}\|_e^2}_{\Omega_0} + \underbrace{\mu\|\nabla\times\vec{H}-\vec{J}_\sigma-\vec{J}_s\|_e^2}_{\Omega_\sigma\cup\Omega_s} \right\} +$$

$$\sum_f h_f \left\{ \underbrace{\frac{1}{\bar{\mu}}\|[\hat{n}\cdot\vec{B}]\|_f^2}_{\Omega_0} + \underbrace{\frac{1}{\bar{\sigma}\omega}\|[\hat{n}\cdot\vec{J}_\sigma]\|_f^2}_{\Omega_\sigma} + \underbrace{\bar{\mu}\|[\hat{n}\times\vec{H}]\|_f^2}_{\Omega_\sigma\cup\Omega_s} \right\}$$

where $\{\vec{B},\vec{H},\vec{J}_\sigma\}$ is the FEM solution on the current grid, h_e is the characteristic dimension of the element considered, and h_f is the characteristic dimension of the element face f, $[\cdot]$ denotes the jump value across the element face, and $\|\cdot\|$ is the L_2-norm.

This estimator can be derived using the energy norm for the local residuals, following Refs. [9] and [8]. Some aspects concerning this error estimator can be noted:

- For the first order tetrahedral elements and Hex-(1,0) elements, since $\nabla\cdot\vec{B}$ as well as $\nabla\times\vec{H}$ vanishes inside each element, these two terms give no contribution to the error estimator.

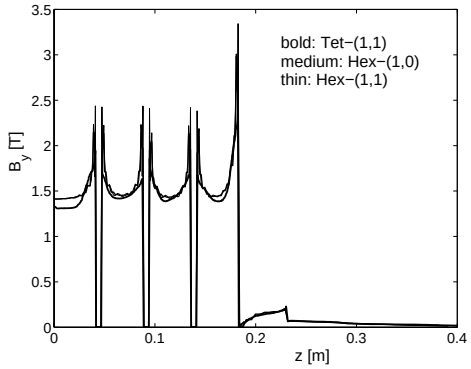

Fig. 11. B_y computed along a line across the stator core of the generator with Tet-(1,1) (solid line), Hex-(1,0) (dashed), and Hex-(1,1) (dotted) elements. The results from the two hexahedral grids are almost indistinguishable. The frequency is $f = 50$Hz.

- If two neighboring elements have different material properties μ or σ, some average value of the coefficients before the interface face integral has to be taken, we adopt the one described in Ref. [9].
- For the tetrahedral grids with isotropic refinement, the choice of the parameters h_e and h_f has little influence on the refinement process. This is not the case for the hexahedral grids and anisotropic refinement. The refinement here is more sensitive to how these parameters have been chosen. For instance, one could choose h_e as the shortest edge of the hexahedron, or the longest one, or the averaged edge lengths. According to [8], the proper choice is to set $h_e = h_{\min}$ and $h_f = h_n$, where $h_{\min}$ is the minimum distance inside the local element, and h_n is the dimension of the element along the direction, perpendicular to the face f. We found that this choice does restore the $O(h^2)$ convergence rate for the power dissipation.
- Since we are using conforming hexahedral grids, local refinement is not possible. Instead, we use global refinement for hexahedral grids, based on "global" error estimators computed as the sum of local ones along certain directions. For anisotropic refinement of hexahedral grids, we adopted the following procedure.

The local error estimator η_e can be rewritten as

$$\eta_e^2 = \eta_{ee}^2 + (\eta_{ef}^x)^2 + (\eta_{ef}^y)^2 + (\eta_{ef}^z)^2,$$

where η_{ee} represents the contribution from the volume integrals, $\eta_{ef}^{x,y,z}$ represent the contributions from the surface jump integrals at surfaces which have normal vector along x,y,z directions, respectively. Thus, each local estimator is splitted into three parts:

$$(\xi_e^x)^2 = \eta_{ee}^2 + (\eta_{ef}^x)^2,\ (\xi_e^y)^2 = \eta_{ee}^2 + (\eta_{ef}^y)^2,\ (\xi_e^z)^2 = \eta_{ee}^2 + (\eta_{ef}^z)^2.$$

The global error estimator along x direction is defined as

$$\zeta_x(x) = \sum_e [\alpha\xi_e^x + \beta(\xi_e^y + \xi_e^z)],$$

where the sum is taken over all elements e whose center has the same x-coordinate. The parameters α and β are defined such that

$$\alpha + 2\beta = 1, \qquad \beta = C_a\alpha.$$

The estimators along y and z directions, $\zeta_y(y)$ and $\zeta_z(z)$, are defined in a similar manner. Finally, the grids are refined according to the global indicators $\zeta = \{\zeta_x, \zeta_y, \zeta_z\}$. The refinement is anisotropic if the parameter $C_a \neq 1$.

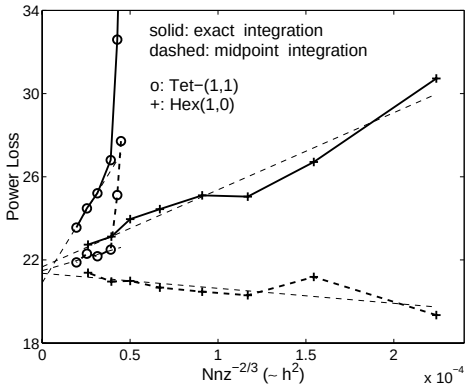

Fig. 12. Convergence of power loss with grid refinement, for the generator problem, using different elements and different integration schemes.

The convergence of the power loss with grid refinement for the generator problem is shown in Fig. 12, both for exact and midpoint integration in the laminated region. The problem has been solved with Tet-(1,1) and Hex-(1,0) elements. Also Hex-(1,1) elements were tested but always gave worse convergence than both Tet-(1,1) and Hex-(1,0). For the tetrahedral grids, we did isotropic refinement; for the hexahedral grids, we used anisotropic refinement with $h_e = h_{\min}$ and $h_f = h_n$. The best choice of parameter C_a we found for the generator problem is $C_a = 2$ for Hex-(1,0) elements. The nominal $O(h^2)$ convergence rate can be easily recovered with local refinement, as shown for tetrahedral grids. With global refinement (for hexahedral grids), it is still possible, but more difficult to recover $O(h^2)$ convergence for the power dissipation. Nevertheless, the values extrapolated to zero grid size for these schemes agree within 4%. Figure 12 shows that Hex-(1,0) elements give much more accurate results, with the same number of non-zero matrix elements (hence approximately the same computation effort). Midpoint integration improves the convergence slightly for the Hex-(1,0) elements. For Tet-(1,1) the improvement from midpoint integration is considerable, and this solution gives almost as good convergence as the Hex-(1,0) elements aligned with the laminations. Similar differences between the different bases are found for the convergence of the magnetic energy, but here the converged values agree within 1%.

Figure 13 shows the refined hexahedral mesh for the generator problem at 50Hz, after 5 steps of anisotropic refinement. Shown also the 2-D geometry (bold lines) of the generator in *xy* and *yz* planes.

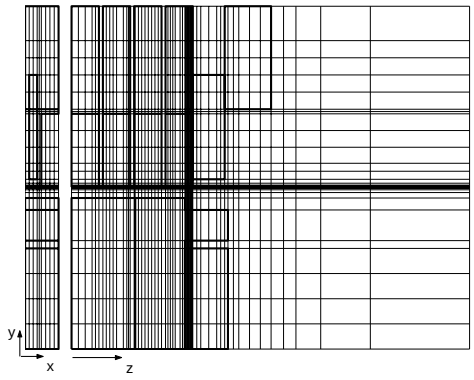

Fig. 13. The refined hexahedral mesh for the generator problem at 50Hz. Anisotropic mesh refinement is used to recover $O(h^2)$ convergence.

VI. Conclusion

For anisotropic conductivity, we found that the first order Nédélec elements on tetrahedral grids give very inaccurate results, for the power dissipation from conduction currents. In practice, this type of elements can not be used for realistic problems, such as the generator problem considered in this paper. The hexahedral elements give much better results, even on quite coarse grid, when the grid is aligned with the laminations. If this is not possible, good convergence is found for the currents at the midpoints of the hexahedral elements and the Hex-(1,0) basis.

The complete first order Nédélec elements give significant improvement on tetrahedral grids, at the expense of almost doubled number of DOFs in the conducting regions. When combined with midpoint integration, they perform almost as well as the Hex-(1,0) elements.

The main conclusion is that for laminated eddy current computations, the lowest order hexahedral element is the best choice, in the sense of both accuracy and efficiency. Furthermore, midpoint integration is generally favorable in regions of laminated materials.

When the grid is aligned with the laminations,we found it is possible to recover the $O(h^2)$ nominal convergence rate for the power dissipation with conforming hexahedral grids, by using anisotropic adaptive refinement techniques. For this kind of calculations, non-conforming hexahedral grids with local anisotropic refinement may be more efficient and we plan to implement such schemes in the future.

Acknowledgments

We would like to thank Thomas Rylander for very useful discussions and providing a routine of Gaussian quadrature rules.

References

[1] V.C. Silva, G. Meunier, A. Foggia, "A 3-D finite-element computation of eddy currents and losses in laminated iron cores allowing for electric

and magnetic anisotropy", *IEEE Trans. Magn.*, vol.31, no.3, pp.2139-2141, May 1995.

[2] V.C. Silva, G. Meunier, A. Foggia, "A 3D finite-element computation of eddy currents and losses in the stator end laminations of large synchronous machines", *IEEE Trans. Magn.*, vol.32, no.3, pp.1569-1572, May 1996.

[3] T. Tokumasu, S. Doi, K.Ito, M. Yamamoto, "An electric vector potential method approach for 3-D electromagnetic field in turbine generator stator core end", *IEEE Trans. on Power App. and Systems*, vol.103, no.6, pp.1330-1338, June 1984.

[4] A.G. Jack, B.C. Mecrow, "A method to calculate turbogenerator end region fields and losses and validation using measured results", *IEEE Trans. on Energy Conversion*, vol.2, no.1, pp.100-107, March 1987.

[5] K. Hollaus and O. Bíró, "A FEM formulation to treat 3D eddy currents in laminations", *IEEE Trans. Magn.*, vol.36, no.4, pp.1289-1292, July 2000.

[6] M. Tuoma Holmberg, "Three-dimensional Finite Element Computation of Eddy Currents in Synchronous Machines", *PhD Thesis*, Tech. Rep. 350, Dept. Power Eng., Chalmers Univ. Tech., 1998.

[7] Yueqiang Liu, A. Bondeson, R. Bergstrm, C. Johnson, M.G. Larson, and K. Samuelsson, "Eddy current comutations using adaptive grids and edge elements", *IEEE Trans. Magn.*, vol.38, no.2, March 2002.

[8] Kunibert G. Siebert, "An a posteriori error estimator for anisotropic refinement", *Numer. Math.* vol.73, pp.373-398, 1996.

[9] R. Beck, R. Hiptmair, R. H. W. Hoppe, B. Wohlmuth, "Residual based a posteriori error estimates for eddy current computation", *ESAIM-Mathematical Modelling and Numerical Analysis*, vol. 34, pp. 159-182, January-February 2000.

[10] G. Mur and A.T. de Hoop, "A finite-element method for computing three-dimentional electromagnetic fields in inhomogeneous media", *IEEE Trans. Magn.*, vol.21, no.6, pp.2188-2191, November 1985.

[11] Thomas Apel, "Interpolation of non-smooth functions on anisotropic finite element meshes", Math. Modeling Numer. Anal. vol. 33, pp. 1149-1185, 1999.

Paper VII

FEM ALGORITHMS FOR MAXWELL'S EQUATIONS

T. Rylander[1], R. Bergström[2], M. Levenstam[2], A. Bondeson[1], C. Johnson[2]
[1]Department of Electromagnetics, [2]Department of Mathematics
Chalmers University of Technology, Göteborg

1 Introduction

Although the FDTD (Finite-Difference Time-Domain) scheme [1, 2] has been very successful for electromagnetic problems, its connection to structured grids makes it difficult to use in applications with complicated geometry. For complex geometry, which frequently arises in technical applications, unstructured grids are generally needed, and in such cases FEM is the method of choice. Unstructured tetrahedral grids allows the use of powerful grid generators [3].

This is the basis for a collaborative project started early 1998 at Chalmers University of Technology between the Department of Electromagnetics and the Department of Mathematics. The project is connected to the Chalmers Finite Element Centre Φ and involves two graduate students under the NGSSC program. The aim of the project is to implement FEM schemes for Maxwell's equations in 3D that are accurate, efficient and flexible for multi-purpose applications and can deal with complex geometries.

2 Choice of elements

Several FEM schemes have been developed for solving Maxwell's equations, both in the frequency [4–8] and time [9] domains. Early approaches mainly used Galerkin formulations and nodal elements for the scalar and vector potentials [4, 5]. However, we prefer formulations in terms of the physical fields $\vec{E}$ and $\vec{H}$ because they are more accurate for the fields and should be easier to couple to calculations involving other physical phenomena or to other methods for solving Maxwell's equations.

There are well known difficulties in solving Maxwell's equations using finite elements [7, 8, 10]. Straightforward application of nodal elements for $\vec{E}$ and $\vec{H}$ in frequency-domain calculations gives rise to "spurious solutions", which are rapidly varying spatially, yet have low frequencies. The occurrence of such spurious solutions can be understood by means of "numerical dispersion relations" [10–13]. Paulsen and Lynch [10] added a penalty term $\propto (\nabla \cdot \epsilon\vec{E} - \rho)^2$ to the variational form to eliminate the spurious solutions. This approach can be used to turn Maxwell's equations into a vector Helmholtz equation. Unfortunately this procedure introduces other extra solutions for which $\nabla \cdot \vec{E} \neq 0$. (Quite obviously, the solutions of the Helmholtz and Maxwell equations are not identical.)

A FEM approach, that is well suited to high frequency applications, uses the Galerkin method with the edge elements of Nédélec [6, 7]. In fact, the lowest order edge elements on a cubic grid together with mass lumping leads to the FDTD. Edge elements avoid spurious solutions and have mixed order. For the lowest order edge elements, this means that in any direction, the component transverse to that direction is a linear function, while the longitudinal component is constant inside one cell. At the cell boundaries the tangential components are continuous (the elements are curl-conforming), while the normal component is discontinuous.

It may be thought therefore that edge elements cannot deal correctly with space charge and cannot be used for an electrostatic problem. However, as will be shown in the following section, the edge elements work well also for almost electrostatic problems. A disadvantage of the edge elements on tetrahedrons compared with the FDTD is that "mass lumping" leads to a mass matrix that is not guaranteed to be positive definite, so that explicit timestepping cannot in general be used [9].

The other approach that we are pursuing is a node-based scheme for both $\vec{E}$ and $\vec{H}$ in the time-domain which permits mass lumping and explicit time-stepping. Although a frequency-domain analysis of such elements together with the strict Galerkin method show spurious eigenmodes, these can be avoided in time-domain calculations by adaptive grid techniques. We have carried out tests of such node-based elements and find good performance in the time-domain. We will study the stabilization of the spurious modes by means of the combined Galerkin/least squares method [14].

We plan to test higher order finite elements and time-stepping and the resulting schemes will be compared for accuracy, efficiency, stability and the absence of spurious solutions. We are also examining the possibilities of implementing different forms of boundary conditions and of matching the solutions to those of other schemes for Maxwell's equations (the FDTD and the Method of Moments), as well as to FEM modeling of other physical processes coupled to the electromagnetic fields. Adaptive mesh generation based on *a posteriori* error estimates will be applied to optimize the computational work required to reach a certain accuracy.

3 Edge elements

Edge elements are constructed for solving the electromagnetic problem

$$\nabla \times \left(\frac{1}{\mu} \nabla \times \vec{E} \right) + \left(j\omega\sigma - \omega^2 \epsilon \right) \vec{E} = 0. \tag{1}$$

The edge elements contain a null space for the operator $\nabla \times \nabla \times$, ("electrostatic" components). Furthermore, there are solutions whose eigenvalues converge towards those of the correct "physical" solutions as the resolution is increased and there are no spurious solutions at low frequencies [7, 8]. We have verified that this holds true on a 2D rectangular region with perfectly conducting boundaries. The eigenvalues converge quadratically with the grid spacing h, and the convergence can be both from below and above.

It is not well known how edge elements handle space charge, and we therefore decided to test the elements in a capacitance problem at low frequency $\omega/2\pi$. Because of the null space for the $\nabla \times \nabla\times$ operator, the frequency cannot be chosen as exactly zero. The test case is an idealized problem from the field of lossy dielectrics: calculate the effective dielectric constant of a dielectric medium containing small particles with finite conductivity. Specifically, Eq. (1) is solved in the two dimensional computational domain shown in Figure 1. In the dielectric medium (domain I) the dielectric constant is $\epsilon_r^I = 4$, and the conductivity $\sigma^I = 0$. In the cylindrical conducting regions (domain II) the dielectric constant is the same $\epsilon_r^{II} = 4$, and the conductivity $\sigma^{II} = 10^{-5}$ S/m. The simulation domain is 1 m $\times$ 1 m and the radius of subdomain II is 0.309019 m. The upper and lower boundary

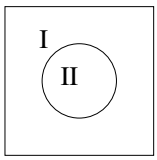

Figure 1: Computational domain with two different materials.

of the square are perfect electrical conductors. The simulation domain is discretized using triangular elements and the electric field is expressed in terms of the standard linear edge elements. The electric field is forced to be periodic in the horizontal direction and we apply Galerkin's method to Eq. (1). The voltage between the plates is prescribed as $V = \int \vec{E} \cdot \vec{dl}$ along the vertical boundaries and this is imposed by means of a Lagrange multiplier. (As a consequence, Maxwell's equations are not strictly satisfied on the vertical boundaries.) The resulting system of equations is solved for 7 frequencies from 200 Hz to 2 MHz. Figure 2 shows the electric field for the frequency 15.4 kHz.

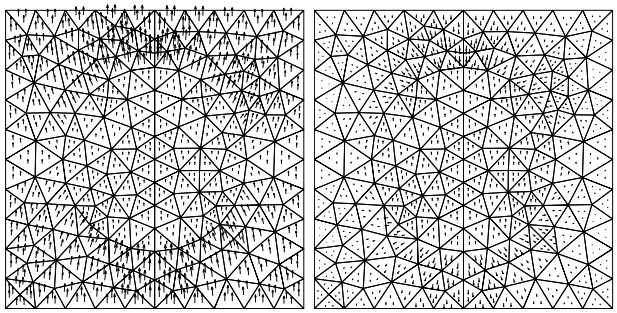

Figure 2: The real and the imaginary part of the solution, to the left and right respectively.

We have computed solutions for discretizations with 322 triangles and then doubled the linear resolution twice to make a convergence study for the resulting complex capacitance per unit length, $C(\omega, h) = c_0 + c_1 h^{\alpha} + \ldots$. There are different ways to extract the capacitance from the solution and the order of convergence is affected by this definition. A simple definition is $C = Q/V$, where the charge $Q = \int \epsilon E_n dl$, for example along the conducting plates. With this definition, the order of convergence α is typically between 1 and 1.5. By contrast, we find clearly quadratic convergence when C is computed from the quadratic form

$$C|V|^2 = \int_{I+II} \left(\epsilon - \frac{j\sigma}{\omega}\right) |E|^2 dS.$$

Convergence is worst at the frequency where the imaginary part of C maximizes. For this case, the relative error on the coarsest mesh with 322 triangles is about 4 per mille. The real and imaginary part of the effective permittivity ϵ_r^{eff} are shown in Figure 3 as circles.

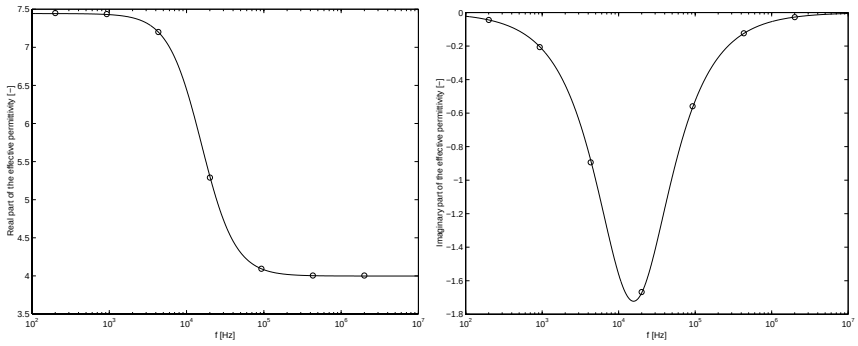

Figure 3: Left - real and right - imaginary part of the effective permittivity.

An excellent approximation to $C(\omega)$ can be obtained as the complex conductance of a circuit consisting of the high frequency capacitor $C_0 = 4\epsilon_0$ in parallel with the series combination of a resistor R and a capacitor C_1 giving

$$C = C_0 + \frac{C_1}{1 + j\omega R C_1} \tag{2}$$

This gives a Padé approximation for C and for our particular test case $R = 333.6$ kΩ and $C_1 = 30.46$ pF. The low frequency limit agrees with the result of a Boundary Element analysis at zero frequency. The fit (2) is shown as the curve in Figure 3. If we exclude the highest frequency 2 MHz (where finite wavelength, or electromagnetic, effects are nonnegligible) and the lowest frequency 200 Hz (where convergence is uncertain because of an ill-conditioned matrix) the relative error of the fit (2) is less than 0.3 per mille.

We conclude that the lowest order edge elements converge as $O(h^2)$ in an integral sense (although the local field components tend to converge as $O(h)$) and handle space charge

correctly. Furthermore, although edge elements cannot be used in strictly static problems, they work well at surprisingly low frequencies.

4 Node-based Schemes

When using node-based elements we solve the Maxwell's equations directly. For time dependent problems we apply the Lee-Madsen formulation [15, 16]

$$\left(\epsilon\vec{E}_t,\vec{\phi}\right)+\left(\sigma\vec{E},\vec{\phi}\right)-\left(\nabla\times\vec{H},\vec{\phi}\right) = \left(\vec{J},\vec{\phi}\right) \quad (3)$$

$$\left(\mu\vec{H}_t,\vec{\psi}\right)+\left(\vec{E},\nabla\times\vec{\psi}\right) = 0 \quad (4)$$

for $0 < t \leq T$ and with initial conditions $\vec{E}(0) = \vec{E}_0$ and $\vec{H}(0) = \vec{H}_0$ where $\vec{H}_0$ satisfies $\nabla\cdot(\mu\vec{H}_0) = 0$ in Ω and $\vec{H}_0\cdot\vec{n} = 0$ on Γ. The boundary condition $\vec{n}\times\vec{E} = 0$ on $\Gamma\times(0,T)$ is then fulfilled in a weak sense which simplifies the implementation. If not the whole of the boundary consists of perfect conductors, a boundary integral has to be added in Eq. (4).

In two dimensions this formulation has been tested successfully. Problems with spurious eigenmodes in reflected waves could effectively be avoided by resolving the reflecting objects and only eight nodes per wavelength were needed to get the phase velocity within one per cent of the correct one.

We have now tested this in three dimensions with promising results. In Figure 4 we show an electromagnetic wave in three dimensions, interacting with a complex object. The mesh consisted of approximately 1.1 million elements. In this particular case an implicit time stepping algorithm was used but, as mentioned above, mass lumping and explicit methods can be used.

For magneto- and electrostatic problems we have used the least squares finite element method [17]. In this formulation the equations are solved in primitive variables and the divergence constraint is included in the formulation. In this approach the boundary conditions are fulfilled by imposing them in a strong sense. The solution strategy is based on an adaptive multigrid solver. In figure 5 an example of a magnetostatic problem can be seen. It is the resulting magnetic field produced by a constant current in a solenoidal wound around a core. Both the surrounding air and the inside of the coil and core have been meshed using an advancing front mesh generator. This mesh has then been adaptively refined by the solver. In figure 5 isolines of the magnitude of the magnetic field can be seen in a plane. In fig 6 an isosurface of the same quantity is shown.

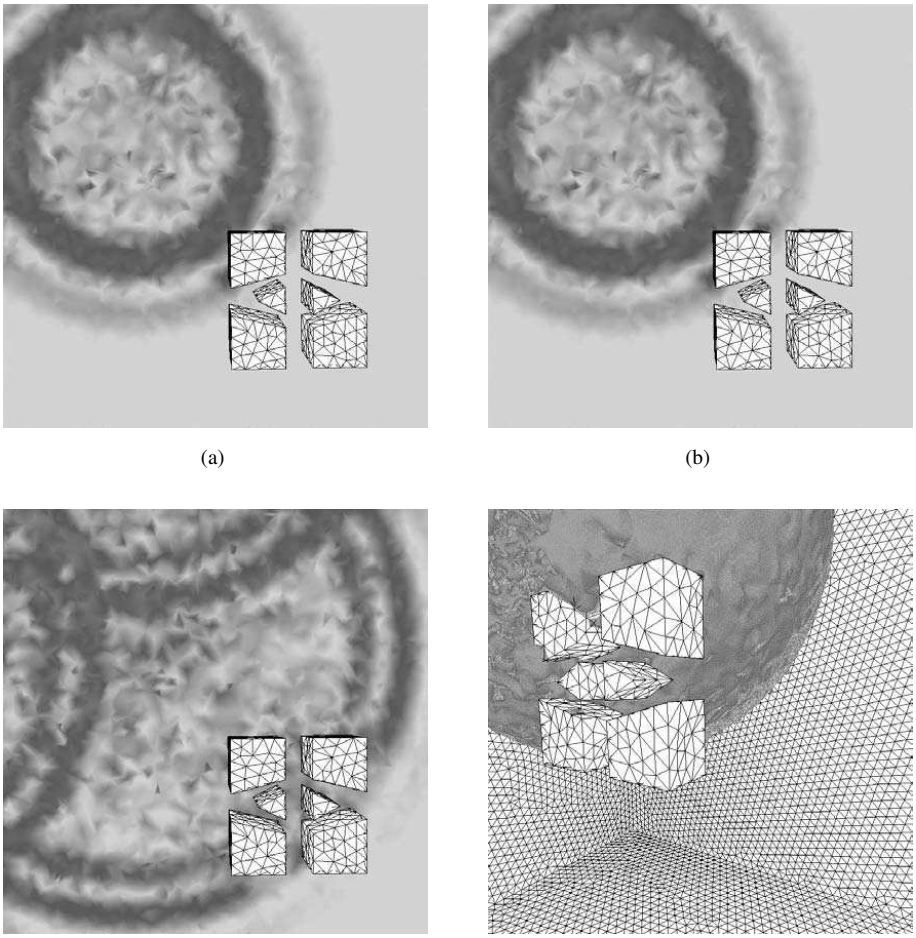

(a) (b)

(c) (d)

Figure 4: Time evolution of the magnitude of the electric field. In 4(d) the wavefront in 4(b) is shown.

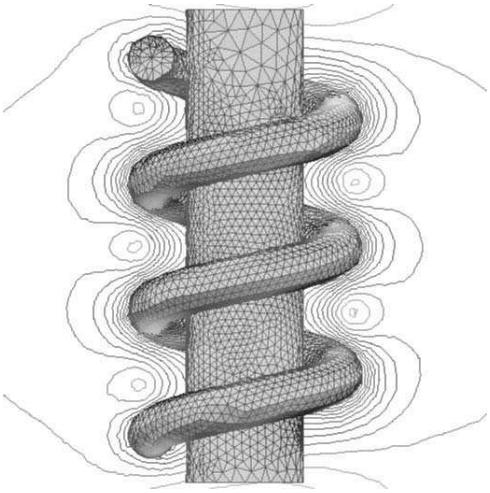

Figure 5: Magnitude of the magnetic field around a coil

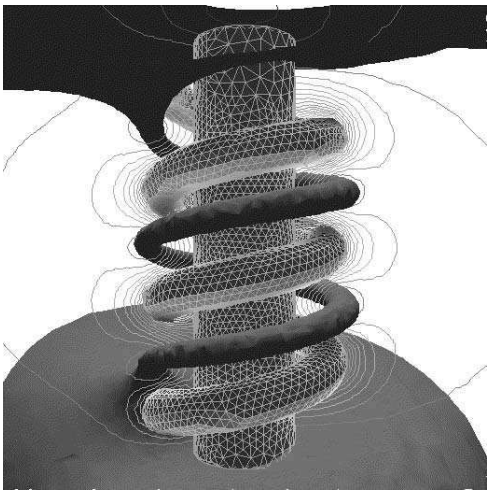

Figure 6: Isosurface of the same quantity as above

References

[1] K. S. Yee, IEEE Trans. Antennas Propagat. **14**, 409 (1966).

[2] A. Taflove, *Computational Electrodynamics: the finite-difference time-domain method* (Artech House, 1995).

[3] P. Möller and P. Hansbo, Int. J. Numer. Methods Eng. **26**, 61 (1995);
J. Frykestig, "Unstructured mesh generation and CAD coupling", Technical Report 1996:1, Swedish Institute of Applied Mathematics, S-412 88 Göteborg, Sweden 1996.

[4] P. P. Silvester and R. L. Ferrari, *Finite Elements for Electrical Engineers* (Cambridge University Press, 1983).

[5] K. J. Binns, P. J. Lawrenson, C. W. Trowbridge, *The Analytical and Numerical Solution of Electric and Magnetic Fields* (Wiley, 1994).

[6] J. Nédélec, Numer. Math. **35**, 315 (1980).

[7] J. Jin, *The Finite Element Method in Electromagnetics* (Wiley, 1993).

[8] A. F. Peterson, S. L. Ray, R. Mittra, *Computational Tools for Electromagnetics* (IEEE Press, 1998).

[9] J. F. Lee, R. Lee and A. Cangellaris, IEEE Trans. Antennas Propagat. **45**, 430 (1997).

[10] K. D. Paulsen and D. R. Lynch, IEEE Trans. Microwave Theory Tech. **39**, 395 (1991).

[11] G. S. Warren, W. R. Scott, IEEE Trans. Antennas Propagat. **42**, 1502 (1994).

[12] P.B. Monk, A.K. Parrott, SIAM J. Sci. Comput. **15**, 916 (1994)

[13] J. Y. Wu, R. Lee, IEEE Trans. Antennas Propagat. **45**, 1431 (1997).

[14] C. Johnson, *Computational Differential Equations* (Cambridge University Press, 1996).

[15] R.L. Lee and N.K. Madsen, J. Comp. Phys. **88**, 284 (1990).

[16] P.B. Monk, J. Sci. Statist. Comp. **13**, (1992)

[17] B.-N. Jiang, J. Wu and A. Povinelli, J. Comp. Phys. **125**, 104 (1996).

Paper VIII

Dispersion Analysis of Galerkin Least Squares Approximations of Maxwell's Equations *

Rickard Bergström† Mats G. Larson†

Abstract

The Galerkin Least Squares (GLS) finite element method is obtained by interpolation between the standard Galerkin method and the usual least squares method for the time-harmonic Maxwell's equations. A dispersion analysis of the GLS method is presented and it is shown that by choosing a scalar interpolation parameter properly a method with an improved discrete dispersion relation is obtained.

1 Introduction

In this note we introduce a Galerkin Least Squares (GLS) finite element method for Maxwell's equations by interpolating, or simply taking a linear combination, between the standard Galerkin method and the least squares finite element method. For details on the least squares method see, for instance Monk and Wang [5] and the book [1], by Jiang.

One motivation for introducing the GLS method is to improve the numerical dispersion relation. As is well known the phase error in the standard Galerkin method always have the same sign, independent of the propagation direction of the wave, see for instance Monk [6]. Here we extend the dispersion analysis to the GLS method, and as a special case, the least squares method. We find that in the least squares method the phase error also have the same sign independent of the direction, but with opposite sign compared with the standard Galerkin method. Further we show that by choosing the parameter in the interpolation between the standard Galerkin and the least squares method we may improve the dispersion relation. In particular, the phase error may have different sign depending on the direction of the wave. This property is believed to be desirable for computations on unstructured grids where cancellations of phase errors with different signs may occur, see the discussion in Wu and Lee [7].

2 The Galerkin Least Squares Method

For the dispersion analysis we consider the time-harmonic Maxwell's equations in $\mathbf{R}^d$, with $d = 2, 3$: find the electric and magnetic fields, E and H, such that

$$
\begin{aligned}
-i\omega E - \nabla \times H &= 0, \\
-i\omega H + \nabla \times E &= 0, \\
\nabla \cdot E = \nabla \cdot H &= 0,
\end{aligned}
\tag{1}
$$

*In the printed proceedings, this papers starts on page 748.

†Chalmers Finite Element Center and Department of Mathematics, Chalmers, University of Technology, Gothenburg, Sweden.

where ω is the frequency.

To discretize this system of equations we introduce a triangulation of $\mathbf{R}^d$ and the corresponding finite element space $\mathcal{V}$ of piecewise linear continuous vector polynomials. The Galerkin least squares (GLS) method is obtained by interpolation between the standard Galerkin method and the least squares method and takes the form: find $U = [E, H] \in \mathcal{V}$, such that

$$(1-\alpha)A_G(U,\overline{U}) + \alpha A_{LS}(U,\overline{U}) = 0 \quad \text{for all } \overline{U} \in \mathcal{V}, \tag{2}$$

where $\alpha \in [0,1]$ is a parameter. Further $A_G(\cdot,\cdot)$ is the bilinear form associated with the standard Galerkin method

$$A_G(U,\overline{U}) = -(i\omega E,\overline{E}) - (\nabla \times H,\overline{E}) - (i\omega H,\overline{H}) + (\nabla \times E,\overline{H}), \tag{3}$$

and $A_{LS}(\cdot,\cdot)$, is the form associated with the least squares method

$$\begin{aligned} A_{LS}(U,\overline{U}) = {} & (i\omega E + \nabla \times H, i\omega\overline{E} + \nabla \times \overline{H}) \\ & + (i\omega H - \nabla \times E, i\omega\overline{H} - \nabla \times \overline{E}) \\ & + (\nabla \cdot E, \nabla \cdot \overline{E}) + (\nabla \cdot H, \nabla \cdot \overline{H}). \end{aligned} \tag{4}$$

Note that for $\alpha = 0$ we obtain the standard Galerkin method and for $\alpha = 1$ the least squares method. For all $\alpha \in [0,1]$ we obtain a scheme with optimal order of convergence. The dispersion relation may however be improved by choosing the proper α. We now turn to this topic.

3 The Dispersion Analysis and Examples

To compute the numerical dispersion we consider a uniform triangulation of $\mathbf{R}^d$ and assume a plane wave solution propagating in the $\hat{k}$ direction ($|\hat{k}| = 1$), of the form

$$E(x) = E_0 e^{ik\hat{k}\cdot x} \qquad \text{and} \qquad H(x) = H_0 e^{ik\hat{k}\cdot x} \tag{5}$$

where E_0 and H_0 are constant vectors and k is the wave number. For the continuous equations, this assumption yields the following dispersion relation between ω and k:

$$\omega = |k|, \qquad \omega = -|k|, \qquad \omega = 0, \tag{6}$$

independent of the direction $\hat{k}$.

If we instead insert (5) into the GLS finite element formulation (2) we get an eigenvalue problem for each node in the triangulation, which determines the numerical frequency $\tilde{\omega}$ in terms of k and $\hat{k}$. Solving these eigenvalue problems for a range of k and $\hat{k}$ gives the numerical dispersion relation $\tilde{\omega}(k,\hat{k})$.

Here we consider two different triangulations, one with equilateral triangles and one with right angled, see Figure 1. For each triangulation, we use symmetry to conclude that the eigenvalue problems associated with the nodes are identical. Thus, we obtain only one (small) eigenvalue problem for each triangulation.

In Figures 2 and 3 the numerical dispersion relation is plotted for the standard Galerkin and the least squares methods respectively. The contour lines are 0.02 apart, and the quantity plotted is $|\tilde{\omega}/k|$, which should, of course, be 1. Thus the plots give an easy visual way to study the dependence of the error in the phase speed on the wavenumber k and propagation direction $\hat{k}$.

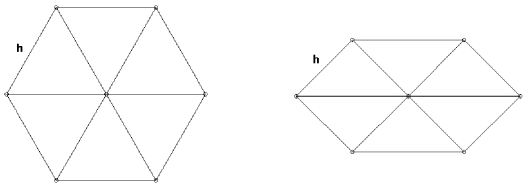

(a) *Part of an equilateral triangulation*

(b) *Part of a right angled triangulation*

FIG. 1. *The two triangulations used in this study*

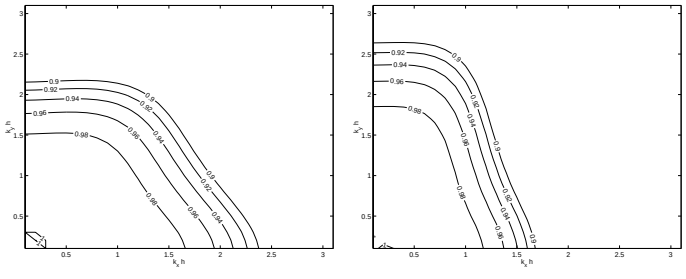

(a) *Equilateral triangulation*

(b) *Right angled triangulation*

FIG. 2. *Contour maps of the phase speed error as a function of* $\xi = kh\hat{k}$ *for the standard Galerkin method, where* h *is the length of the side of a triangle in the triangulation.*

We can see that for the least squares method, the phase speed will become larger than the exact value for increasing k, while for the standard Galerkin method we instead get a smaller phase speed. We can also see the dependency of $\hat{k}$, which is slightly favourable for the least squares method, at least on the equilateral triangulation.

The different behaviours of the standard Galerkin and least squares method suggest that a properly chosen α in the GLS method (2) should produce a method with an improved dispersion relation. In Figure 4 we show the dispersion relation for the GLS method with $\alpha = 0.4$. This particular value of α is somewhat arbitrarily chosen and we plan on studying the choice of α in a future work.

We can see that the region $|\tilde{\omega}/k| \approx 1$ is larger for both triangulations compared with the other two methods. In particular, in Figure 5 we compare the regions for the standard Galerkin and least squares methods where the phase speed error is less than 4%. In addition, for the GLS method we also obtain a phase speed that is larger than the exact value in some regions and smaller in other. This property is considered important when using unstructured triangulations, since in that case, the phase error may cancel as the wave propagates from element to element. See Wu and Lee [7] for further discussions of this topic.

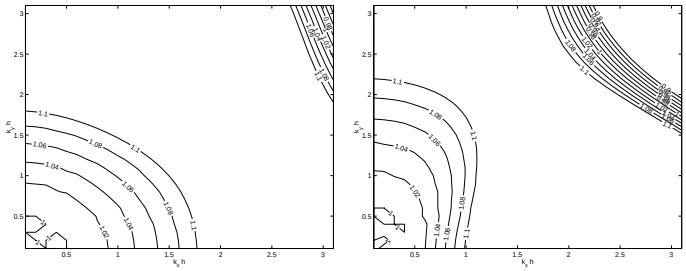

(a) *Equilateral triangulation* (b) *Right angled triangulation*

FIG. 3. *Contour maps of the phase speed error as a function of* $\xi = kh\hat{k}$ *for the least squares method, where* h *is the length of the side of a triangle in the triangulation.*

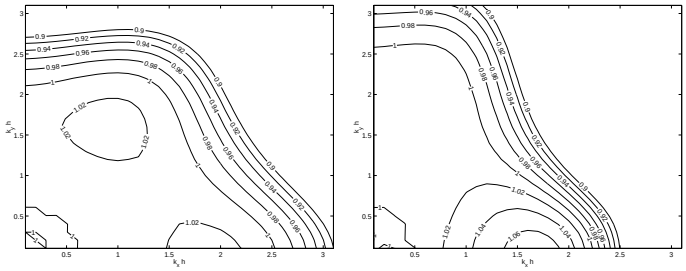

(a) *Equilateral triangulation* (b) *Right angled triangulation*

FIG. 4. *Contour maps of the phase speed error as a function of* $\xi = kh\hat{k}$ *for the GLS method with* $\alpha = 0.4$*, where* h *is the length of the side of a triangle in the triangulation.*

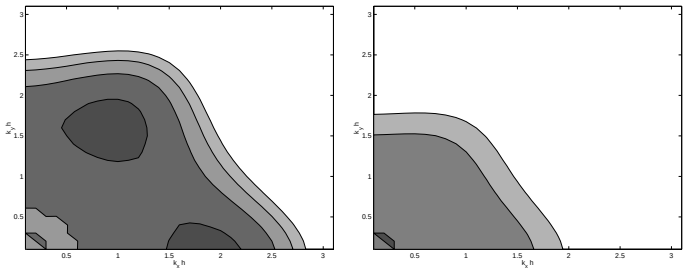

(a) *Galerkin least squares method* (b) *Standard Galerkin method*

FIG. 5. *The coloured zone indicates the region where the phase speed error is less than 4%, for an equilateral triangulation.*

References

[1] B.-N. Jiang. *Least-squares finite element method : Theory and applications in computational fluid dynamics and electromagnetics.* Springer-Verlag, 1998.

[2] B.-N. Jiang, J. Wu, and L.A. Povinelli. The Origin of Spurious Solutions in Computational Electromagnetics. *J. Comput. Phys.*, 125:104-123, 1996.

[3] P.B. Bochev and M.D. Gunzburger. Finite Element Methods of Least-Squares Type. *SIAM Rev.*, 40(4):789-837, 1998.

[4] F.H. Hu, M.Y. Hussaini, and P. Rasetarinera. An Analysis of the Discontinuous Galerkin Method for Wave Propagation Problems *J. Comput. Phys.* 151:921-946, 1999.

[5] P. Monk and D.-Q. Wang. A least-squares method for the Helmholtz equation. *Comput. Metods Appl. Mech. Engrg.*, 175:121–136, 1999.

[6] P.B. Monk and A.K. Parrot. A dispersion analysis of finite element methods for Maxwell's equations. *SIAM J. Sci. Comp.*, 15(4):916–937, 1994.

[7] J.-Y. Wu and R. Lee. The advantages of triangular and tetrahedral edge elements for electromagnetic modeling with the finite-element method. *IEEE Trans. Antennas Propagat.*, 45(9), 1997.

Paper IX

Object Oriented Implementation of a General Finite Element Code

Rickard Bergström

Abstract

We present the framework of a finite element code, written with the explicit aim of being as general and as close to the mathematical viewpoint as possible. Due to the object oriented programming paradigm, the weak form of the mathematical model is easily implemented in a style close to the mathematical formula, and element types and quadrature rules can quickly be changed or easily implemented. This work only concerns the discretization of the problem, and does not consider mesh generation or solvers for the linear system.

1 Introduction

The finite element method (FEM) is a general framework for solving several classes of PDE:s and ODE:s, and there are several program packages that have implemented the method, both commercial and free. Many of these implementations are however written for a certain engineering application in, e.g., solid mechanics, and it may be difficult to adapt the code to a specific need. This paper describes a code which instead tries to stay close to the mathematical framework of FEM. The benefits include an accessible problem formulation and easy extension with new element types etc.

This implementation is made in C++, a language gaining popularity in the numerical society. Advances in compilers and programming techniques have made efficiency comparable to that of simpler structural languages such as Fortran. The possibility of creating new types, called objects, and specify their properties makes it possible to write programs which are highly readable and with the same notations as in the literature on the subject.

There are similar object oriented code projects with different generality and level of abstraction. In solid mechanics, large scale design is described in e.g. [11] and [21] and a smaller "idea testing" design is presented in [25]. A more general approach can be found in [13]. Also SIFFEA [15] is

close to this projects but is written for 2D calculations. Another inspiration for this code has been the Norwegian commercial package DiffPack [1], also described in [18].

2 Aim of the code

When this coding project started, there was a need for a flexible finite element code for research purpose. Different research projects imposed the necessity for an easy change of the weak form in which the problem was posed, as well as the possibility of implementation of different types of elements. Multiphysics with coupled equations or hybrid methods was also a possible extension. Moreover, the different applications made it necessary to have a large range of algebraic solvers to use.

These specifications have to a large extent been met by the implementation presented in this paper. The weak form is isolated and easily readable. This makes the change of finite element formulation or the implementation of a new equation straightforward. Several different types of elements have been incorporated, including standard nodal elements of various polynomial order and the Nédélec edge elements.

Many different projects have started with the core of this code and later been transformed to more specific, and thus more fine tuned and efficient, codes. The applications include least-squares FEM for interface problems [8], discontinuous LSFEM [6][9], magnetostatic computations with coupled scalar and vector potentials [14], eddy current computations with edge elements [19][20] , hybrid FEM-FDM for the wave equation [5], and incompressible flow in porous media [23], as well as smaller in-house projects concerning, e.g., error estimators for higher order polynomial finite elements and eddy current/heat transfer coupled problems. A parallel version of the code has also been developed.

3 The abstraction of FEM

The strength of object oriented programming is that it is possible to implement abstractions of the underlying problem, which make the code easy to read, understand, and maintain. The code can be written in a way that makes the coupling to the underlying problem direct and apprehendable.

In the case of scientific computing, it is natural to use the objects that are present in the mathematical or physical formulation of the problem. On the highest level, it is the *equation* (or rather the weak form when it

concerns finite element methods) together with *boundary conditions*, the *domain* and possibly algebraic or constitutive relations that further define the computational problem.

In the finite element method the *element* is the centerpoint. We will adapt to the definition of Brenner and Scott [12] for this, i.e. a finite element consists of

- a *subdomain* for the element,
- a function space defined on the domain, the *shape functions*,
- the *degrees of freedom*.

This is a general definition that includes all types of elements and methods.

Furthermore the concept of inner products, or *integration*, is needed to form the weak form.

3.1 Implementation issues in object oriented numerical programming

In scientific computing the efficiency of the code is an important issue. A high level of abstraction in the code may impede performance greatly. It is therefore necessary to compromise to get a code that is both general and readable as well as efficient. To keep inner loops free of time consuming function calls or other constructions, some of the abstract objects mentioned above have been collected into the same class to facilitate numerically efficient code. The different concepts are however clearly present.

4 Code details

The components described in this section have been used directly in the main function of a C++ program. To hide details even further and make the usage cleaner, it would of course be possible to wrap the objects together in problem modules. One might thus see the program described in Section 5 as one part of a larger code.

The notation used in describing the code is based on that of Rumbaugh *et al.* [22]. To represent a class, we use a box divided in three sections. The first contains the class name, the second shows the class attributes, while the third lists the methods in the class. Object relationship is shown with lines connecting the class objects. A symbol on the line indicates the type and number of relationships: no symbol identify only one object, a solid circle

termination means zero to many objects, diamonds indicate aggregation, i.e. the class is *made-up-of* the attached classes, and finally, triangles are used to indicate inheritance with the base of the triangle towards the derived class and the tip towards the parent class.

4.1 Extent of the code

In this paper, we are only concerned with finding the discrete finite element solution on a given geometry and mesh. Thus, no routines to generate meshes or post-processing (except for adaptive mesh refinement) are included. In practise, we have used either meshes from a separate program package (such as ProEngineer or Matlab) or written routines to generate meshes for a specific problem. Post-processing has been handled in the same way. Most of the classes to handle the meshes have been provided through another code project, related to DiffPack [1][18] and partly described in [7], while some have been developed for this project. For self-containment a brief description of the code used for grids, geometry and adaptivity is provided.

Furthermore, to have a large library of solvers to choose from, we have used the software package PETSc [4][24]. This package is written in object oriented C, and provides a nice interface to work with sparse matrices and vectors and the solution process of matrix problems. For the parallel version we used the METIS-package [2][16][17] to decompose the problem.

4.2 General structure

4.2.1 Basic objects

Some basic mathematical objects are essential when numerically solving PDEs: matrices and vectors. We have chosen to use the implementation in PETSc. It provides a basic *Matrix* type which is the interface to different implementations, i.e. storage formats, of sparse matrices such as the traditional row oriented *MatSeqAIJ* or the blocked version *MatSeqBAIJ*. Parallel versions are also provided, e.g. *MatMPIAIJ* and *MatMPIBAIJ*. The *Vector* object is analogous.

4.2.2 Element

An *Element* object contains all three parts of the definition of a finite element cited above, following the discussion in Section 3.1. The parts are however separated in the class. The object includes one part containing the grid information concerning this particular element, i.e. the nodes and their

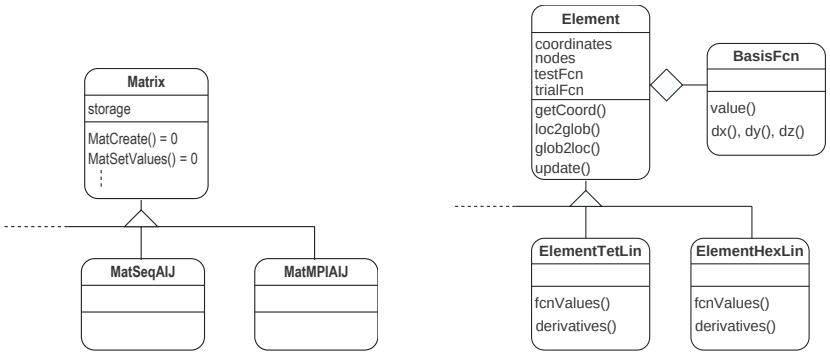

(a) *Matrix class.* (b) *Element class*

Figure 1: Description of the *Matrix* and *Element* classes. Vectors are handled analogously to *Matrix*.

coordinates. Note that there is not an *Element* object for each element in the grid, but the information in *Element* is continuously updated with geometrical information.

There is a *Basis function* object corresponding to the shape functions mentioned above. However, objects of this type are only used as an interface when communicating with the *Equation* class, the actual description of the function space is implemented in different instances of *Element*, such as quadratic polynomials on tetrahedrons, *ElementTetQuad*, or edge elements on hexahedrons, *ElementEdgeHex*. The shape functions are implemented for a reference element and operations on the functions are performed through the *Mapper*. Finally, a map for going from local to global degrees of freedom is needed.

4.2.3 Equation

In objects of this class, we include the weak form and routines to perform the integration needed to form these functionals. For some applications it would have been advantageous to isolate the integration, with the possible problem of time consuming function calls or overloaded operators in the inner loops. We have mainly considered integration by numerical quadrature and this construction has been flexible enough.

Using information from an element and a quadrature rule, the *Equation* has functionality to compute the element matrices by numerical integration.

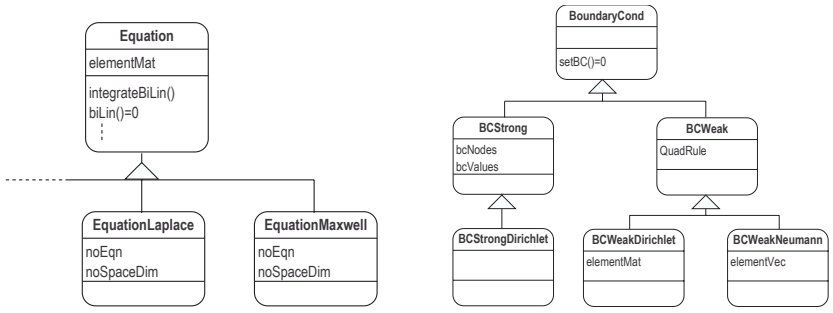

(a) *Equation class.* (b) *BC class*

Figure 2: Description of the classes for the equation and boundary conditions.

In order to do this, also element neighbor information is needed. Furthermore, the mapping from local to global degrees of freedom, provided by the element, is used to compute global matrix indices for the element matrix terms.

Different problems have been implemented in instances of *Equation*, e.g. *EquationLaplace* or *EquationHarmonicMaxwell*, in a form very similar to the analytical variational formulation, see the example in Section 5.

4.2.4 Boundary condition

Essentially, there are two methods implemented for boundary conditions. The first is a direct implementation of Dirichlet conditions, *BCStrong*. In this case we have chosen to keep the structure of the system matrix and not eliminate the unknowns corresponding to degrees of freedom on the Dirichlet boundary. In the case of a scalar Dirichlet condition, this consists of zeroing rows in the matrix and inserting ones in the diagonal and data values in the right hand side vector. When the condition involves normal or tangential traces, a local coordinate transformation has been implemented to be performed before operating on the matrix.

The second method, *BCWeak*, includes inhomogeneous natural boundary conditions and weakly imposed conditions. Then additional integrals are added to the weak form in a procedure identical to the one in *Equation*. For interface problems or the discontinuous Galerkin method, there are classes corresponding to *BCWeak* performing the same integration.

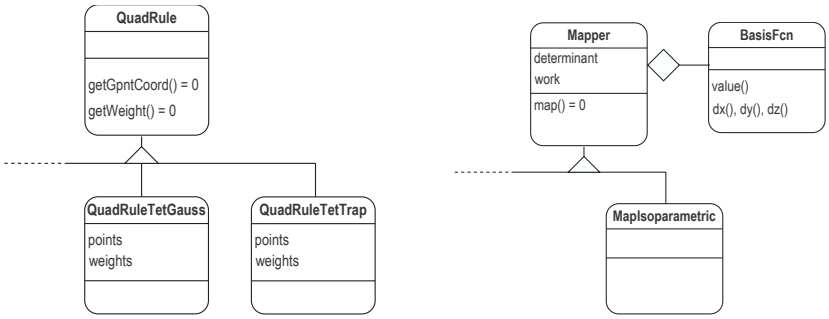

(a) *QuadRule class.* (b) *Mapper class*

Figure 3: Description of the *Quadrature rules* and *Mapper* classes.

4.2.5 Quadrature rule

This class a straightforward implementation of the quadrature rules used. It isolates the implementation of the points for the quadrature rule and their corresponding weights.

4.2.6 Mapper

The *Mapper* takes care of the transformation from the actual element in the grid to a reference element. For a parametric mapping it uses an *Element* object to define the mapping and to update the values of the shape function in the quadrature points.

4.2.7 Discretiser

This is where the different parts are put together to assemble the system matrix. The *Element* is updated for each element in the grid, new function values are computed by the *Mapper*, element matrices are integrated in *Equation* and assembled into the *Matrix*. In the case of the parallel version of the code, this is also where partitioning of the problem is handled.

4.2.8 Solver

The *Solver* class we use is picked from the PETSc package. It contains a large range of Krylov subspace methods, together with different preconditioners. They are also implemented for parallel computations. We refer to the manual of PETSc [3] for more details.

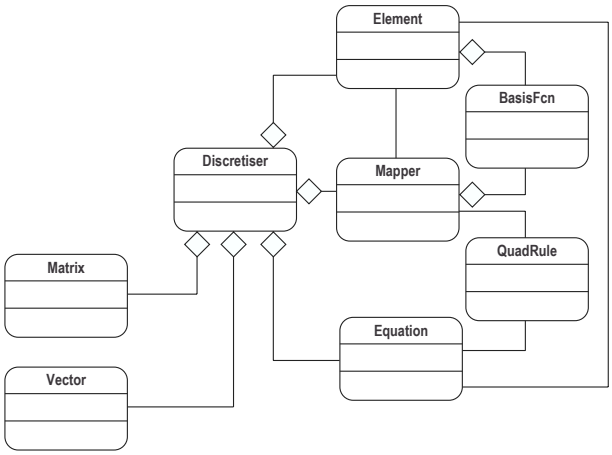

Figure 4: The relation between the *Discretiser* and other classes.

Apart from the PETSc solvers, a multigrid solver has been implemented and tested, see [10].

4.2.9 Grid and geometry

A *Grid* object contains the elements, nodes, and coordinates of the nodes of the computational mesh. Elements and nodes are not implemented as separate classes but are represented as arrays in *Grid*. Derived from the base class is, e.g., objects to handle nested adaptively refined meshes, *GridFEHier*, and meshes for discontinuous/interface problems, *GridDiscont*. There is also a class for surface meshes to handle boundary conditions, *GridSurface*.

The geometry description is handled by NURB curves and surfaces, and collected into *GridGeometry*. The *GridGeometry* is used to compute correct normals on boundary and interface surfaces, and to make sure that a refined mesh respects the geometry by projecting new nodes onto the geometrical surface.

5 An example: the Poisson problem

To get a better conception of how these classes interact in a code, we will present a computation of the Poisson problem, written in pseudo C++ language.

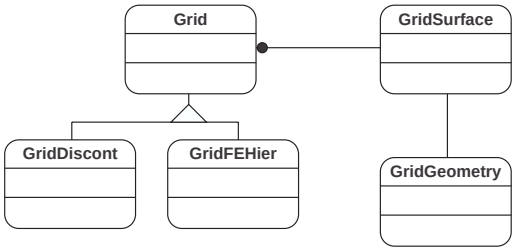

Figure 5: The relation between the classes that handle geometry and meshes.

The starting point is to model the problem,

$$-\nabla \cdot A\nabla u = f \quad \text{in } \Omega, \tag{5.1a}$$
$$n \cdot A\nabla u = g_N \quad \text{on } \Gamma_N, \tag{5.1b}$$
$$u = g_D \quad \text{on } \Gamma_D. \tag{5.1c}$$

For simplicity we choose $f(x) = A(x) = 1$, $\Gamma_D = \partial\Omega$, and $g_D(x) = 0$. The variational formulation of the problem is then: find $u \in \mathcal{V}_0$ such that

$$(\nabla u, \nabla v) = (f, v), \quad \forall v \in \mathcal{V}_0, \tag{5.2}$$

or, writing out the functionals explicitly,

$$\int_\Omega \frac{\partial u}{\partial x}\frac{\partial v}{\partial x} + \frac{\partial u}{\partial y}\frac{\partial v}{\partial y} + \frac{\partial u}{\partial z}\frac{\partial v}{\partial z}\, dx = \int_\Omega f v\, dx \tag{5.3}$$

This is implemented in the class *EquationPoisson* as

```
real f(){
  return 1.;
}

EquationPoisson:: biLin() {
  BasisFcn v = *testFcn
  BasisFcn u = *trialFcn

  biLin = u.x()*v.x()+u.y()*v.y()+u.z()*v.z()

}
```

```
EquationPoisson:: load() {
  BasisFcn v = *testFcn

  load = f()*v()

}
```

In the main function, the domain is loaded into the *Grid* and *GridGeometry* classes. Then equation, element, and quadrature rule are chosen before the *Discretiser* is called to create the linear system of equations. Finally the *Solver* generates the approximate solution by solving the matrix problem. This will look like

```
main(){

  // Set up the problem
  int quadOrder = 4;
  int noSpaceDim = 3;
  Grid                grid;
  GridGeometry        geom;
  QuadRuleTetGauss    quad(quadOrder);
  ElementTetLin       element;
  EquationPoisson     equation(noSpaceDim);
  BCStrongDirichlet   bc;
  MapIsoparametric    mapper(noSpaceDim);
  Discretiser         discrete;
  SolverGMRES         solver(discrete);
  Vector              U;

  // Read mesh and geometry
  geom.scan('geom.file');
  grid.getSurface().attachGeom( geom );
  grid.scan('grid.file');

  // Create and assemble the system matrix and rhs vector
  discrete.createSeqProblem( grid, equation );
  discrete.discretise( equation, bc, mapper, element, quad, grid );
```

```
  // Solve the matrix problem
  U=solver.solve();

}
```

As we can see, the *Discretiser* is the kernel of this program. The member function `discretise` performs the actual assembling of the problem and looks like

```
Discretiser:: discretise( Equation eq,
                          BC bc,
                          Mapper map,
                          Element elm,
                          QuadRule quad,
                          Grid grid){

  for( el=0; el < grid.getNoElms(); el++ ){
    elm.update( el, grid );
    map.map( quad, elm );
    eq.integrateBiLin( quad, elm, elmMat );
    MatSetValues( elmMat, A );
    eq.integrateLoad( quad, elm, elmVec );
    VecSetValues( elVec, b );
  }
  bc.setBC( A, b )

}
```

Acknowledgements

We would like to thank Dr. Klas Samuelsson for providing the grid classes and the multigrid solver, and Dr. Mårten Levenstam for interesting discussions and helpful suggestions.

This work is supported by ABB Corporate Research, Sweden, and the Swedish Foundation for Strategic Research.

References

[1] Diffpack home page. `http://www.nobjects.com/Products/Diffpack`.

[2] Metis home page. `http://www-users.cs.umn.edu/~karypis/metis/`.

[3] S. Balay, W.D. Gropp, L.C. McInnes, and B.F. Smith. PETSc 2.0 users manual. Technical Report ANL-95/11 - Revision 2.0.28, Argonne National Laboratory, 2000.

[4] S. Balay, W.D. Gropp, L.C. McInnes, and B.F. Smith. PETSc home page. `http://www.mcs.anl.gov/petsc`, 2000.

[5] L. Beilina, K. Samuelsson, and K. Åhlander. A hybrid method for the wave equation. Preprint 14, Chalmers Finite Element Center, Chalmers University of Technology, 2001.

[6] R. Bergström. Least-squares finite element method with applications in electromagnetics. Preprint 10, Chalmers Finite Element Center, Chalmers University of Technology, 2002.

[7] R. Bergström, A. Bondeson, C. Johnson, M.G. Larson, Y. Liu, and K. Samuelsson. Adaptive finite element methods in electromagnetics. Technical Report 2, Swedish Institute of Applied Mathematics (ITM), 1999.

[8] R. Bergström and M.G. Larson. Discontinuous least-squares finite element methods for the Div-Curl problem. Preprint 12, Chalmers Finite Element Center, Chalmers University of Technology, 2002.

[9] R. Bergström and M.G. Larson. Discontinuous/continuous least-squares finite element methods for elliptic problems. Preprint 11, Chalmers Finite Element Center, Chalmers University of Technology, 2002. To appear in Math. Models Methods Appl. Sci.

[10] R. Bergström, M.G. Larson, and K. Samuelsson. The $\mathcal{LL}^*$ finite element method and multigrid for the magnetostatic problem. Preprint 2, Chalmers Finite Element Center, Chalmers University of Technology, 2001.

[11] J. Besson and R. Foerch. Large scale object-oriented finite element code design. *Comput. Methods Appl. Mech. Engrg.*, 142:165–187, 1997.

[12] S.C. Brenner and L.R. Scott. *The Mathematical Theory of Finite Element Methods.* Springer-Verlag, 1994.

[13] P. Donescu and T.A. Laursen. A generalized object-oriented approach to solving ordinary and partial differential equations using finite elements. *Finite Elements in Analysis and Design*, 22:93–107, 1996.

[14] M. Fontana. Adaptive finite element computation of 3D magnetostatic problems in potential formulation. Preprint 8, Chalmers Finite Element Center, Chalmers University of Technology, 2001.

[15] X. Jiao, X.Y. Li, and X. Ma. SIFFEA: Scalable integrated framework for finite element analysis. In S. Matsuoka, R.R. Oldehoeft, and M. Tholburn, editors, *Computing in Object-Oriented Parallel Environments*, pages 84–95. Springer-Verlag, 1999.

[16] G. Karypis and V. Kumar. A fast and high quality multilevel scheme for partitioning irregular graphs. *SIAM J. Sci. Comput.*, 20(1):359–392, 1998.

[17] G. Karypis and V. Kumar. Parallel multilevel k-way partitioning scheme for irregular graphs. *SIAM Rev.*, 41(2):278–300, 1999.

[18] H.P. Langtangen. *Computational Partial Differential Equations.* Springer-Verlag, 1999.

[19] Y.Q. Liu, A. Bondeson, R. Bergström, M.G. Larson, and K. Samuelsson. Edge element computations of eddy current in laminated materials. Submitted to IEEE Trans. Magn., 2002.

[20] Y.Q. Liu, A. Bondeson, K. Samuelsson, R. Bergström, M.G. Larson, and C. Johnson. Eddy current computations using adaptive grids and edge elements. *IEEE Trans. Mag.*, 38:449–452, 2002.

[21] B. Patzák and Z. Bittnar. Design of object oriented finite element code. *Advances in Engineering Software*, 32:759–767, 2001.

[22] J. Rumbaugh, M. Blaha, W. Premerlani, F. Eddy, and W. Lorensen. *Object-Oriented Modeling and Design.* Prentice Hall, 1991.

[23] N.H. Sharif and N.-E. Wiberg. Adaptive ICT-procedure for non-linear seepage flows with free surface in porous media. *Communications in Numerical Methods in Engineering*, 18:161–176, 2002.

[24] G. Smith, P. Bjørstad, and W. Gropp. *Domain Decomposition.* Cambridge University Press, 1996.

[25] T. Zimmerman, P. Bomme, D. Eyheramendy, L. Vernier, and S. Commend. Aspects of an object-oriented finite element environment. *Computers and Structures*, 68:1–16, 11998.